FEDERAL UNIVERSITY OF ITAJUBÁ
POST GRADUATION PROGRAM ON MATERIALS FOR ENGINEERING - DOCTORATE

DEVELOPMENT OF TRIDIMENSIONAL CARBON FIBER/EPOXY COMPOSITES REINFORCED THROUGH THE THICKNESS AND THE MECHANICAL CHARACTERIZATION OF INTERLAMINAR FRACTURE TOUGHNESS AND VIBRATION PROPERTIES

DANIEL BRIGHENTI BORTOLUZZI

Itajubá/MG - Brazil
2022

UNIVERSIDADE FEDERAL DE ITAJUBÁ
PROGRAMA DE PÓS-GRADUAÇÃO EM MATERIAIS PARA ENGENHARIA

DESENVOLVIMENTO DE COMPÓSITOS TRIDIMENSIONAIS DE FIBRA DE CARBONO/EPÓXI REFORÇADOS ATRAVÉS DA ESPESSURA E AVALIAÇÃO DE SUAS PROPRIEDADES DE TENACIDADE À FRATURA INTERLAMINAR E VIBRAÇÕES MECÂNICAS

DANIEL BRIGHENTI BORTOLUZZI

Itajubá/MG - Brasil
2022

FEDERAL UNIVERSITY OF ITAJUBÁ
POST GRADUATION PROGRAM ON MATERIALS FOR ENGINEERING - DOCTORATE

DANIEL BRIGHENTI BORTOLUZZI

DEVELOPMENT OF TRIDIMENSIONAL CARBON FIBER/EPOXY COMPOSITES REINFORCED THROUGH THE THICKNESS AND THE MECHANICAL CHARACTERIZATION OF INTERLAMINAR FRACTURE TOUGHNESS AND VIBRATION PROPERTIES

Doctoral thesis submitted to the Post Graduation Program of Materials for Engineering (PPG-EM) in fulfillment of the requirements to obtain the degree of Doctor of Science in Materials for Engineering.

Concentration Area: Non-Metals.

Advisor: Prof. Dr. Antonio Carlos Ancelotti Junior
Co-advisor: Prof. Dr. Guilherme Gomes Ferreira

Itajubá/MG - Brazil
2022

AKNOWLEDGMENTS

To my parents for all their support, encouragement and trust throughout this time.

My sister and brother-in-law for their support and aid at all times.

To my Advisor Prof. Dr. Antonio Carlos Ancelotti Junior for the friendship, for the opportunity to supervise me and allow me to continue my studies and to be part of Composite Technology Center (NTC) and also for the knowledge transmitted, guidance, availability, trust and assistance in this work.

To my Co-advisor Prof. Dr. Guilherme Ferreira Gomes for friendship, transfer of knowledge, supervising and great contribution in the accomplishment of the present work.

To CAPES for the Doctorate scholarship.

The author is also grateful to the Technicians and Professors of the Physics and Chemistry Institute - IFQ and Mechanical Engineering Institute - IEM at UNIFEI.

And to my colleagues at NTC for collaboration and also the good and funny times during these last years.

"*Persistence is the shortest path to success."*

Charles Chaplin

ABSTRACT

This study is focused on the assessment of the interlaminar fracture toughness in mode II and vibration mechanical properties of composites reinforced through the thickness with rectangular z-pinned manufactured by VARTM (Vacuum-assisted resin transfer molding) process. The influence of z-pinning in the mechanical properties of laminated structures is carried out and for the specimens with different z-pins sizes and pin areal densities are manufactured after Design of Experiment (DOE) matrix determination. For the composites fabricated without a polymeric mold, vibration properties z-pins reinforced composites demonstrated that the size and density of insertion of z-pins has a direct influence on the natural frequency of vibration, on the damping, or loss, and the amplitude of vibration. With the optimization made by the method of response surface (MSR), in a mono-objective analysis, it was demonstrated that it is possible to obtaining reductions in the maximum amplitude of forced vibration of 115%, and in an analysis multi objective has been shown that with a given insertion density and size of z-pins 81% reductions in maximum forced vibration amplitude and increases of 25% and 11% can be achieved damping factor and natural frequency of vibration, respectively. For the composites manufactured with polymeric mold, the fracture toughness in mode II was investigated and the results showed that pinning in composites improved the fracture resistance for all pinning proposals built. For the NPC (Non-precracked) step, the highest (G_{IIc})value achieved was for a 0.50 mm with a 2% pin density insertion, being 106% higher than the unpinned specimen. For the PC (Precracked) step, the thicker pins 1.00 mm and 1.10 mm acted again as a positive influence to mitigate the delamination and achieved elevated values of (G_{IIc}), 77.5% and 78.3% higher than the unpinned specimen, respectively. The statistical results pointed that for the NPC case, the increase in density of pins always generates an increase in the fracture toughness and the contribution of the pin size to increase the fracture toughness. From there, increasing the size of the pin has little influence in NPC. For PC case, was shown that the pin size increasing decreases the fracture resistance, except for low pin density. Furthermore, the Artificial Neural Networks (ANN) trained with part of these experimental data showed excellent predictive capacity of fracture toughness. The modal responses of the laminates fabricated with a polymeric mold the experimental results indicated that, in most cases, there was an increase in the natural frequency and highlights the reduction, from approx. 60% to 70%, in the amplitude of vibration for all specimens with z-pin reinforcement in comparison to the unpinned. Furthermore, the experimental data compared the statistical results pointed that z-pins had a positive influence increasing and decreasing natural frequency and forced vibration amplitude, respectively, of z-pinned composites compared to the non-reinforced and the trained ANN with the experimental data presented a very good agreement with experimental tests carried out in this investigation for predicting modal response.

Keywords: Z-pinned Composites; Modal Responses; Facture Toughness in Mode II; Design of Experiments; Artificial Neural Networks

RESUMO

Este estudo tem como objetivo analisar a influência da inserção de *z-pin*s retangulares com diferentes tamanhos e densidades de inserção, determinados pela matriz de experimentos de um Planejamento de Experimentos (DOE), nas propriedades mecânicas de tenacidade à fratura interlaminar em modo II e de vibrações de compósitos reforçados através da espessura fabricados por VARTM (*Vacuum-assisted resin transfer molding*). Para os compósitos fabricados sem molde polimérico, as propriedades de vibração dos compósitos reforçados com *z-pins* demonstraram que o tamanho e a densidade de inserção têm influência direta na frequência natural de vibração, no amortecimento e na amplitude de vibração. Com a otimização feita pelo método de superfície de resposta (MSR), em uma análise monoobjetiva, foi demonstrado que é possível obter reduções na amplitude máxima de vibração forçada de 115%, e em uma análise multiobjetiva foi demonstrado que com uma determinada densidade de inserção e tamanho dos *z-pins* têm-se 81% de redução na amplitude máxima de vibração forçada e aumentos de 25% e 11% podem ser alcançados no fator de amortecimento e na frequência natural de vibração, respectivamente. Para os compósitos fabricados com molde polimérico, a tenacidade à fratura em modo II foi investigada e os resultados mostraram que a inserção de *z-pins* aumentou a resistência à delaminação para todas os corpos de prova. Para a etapa NPC (*Non-precracked*), o maior valor de (G_{IIc}) foi para o pino de 0,50 mm com inserção de 2%, sendo 106% superior ao corpo de prova sem reforço através da espessura. Para a etapa PC (*Precracked*), os pinos maiores com 1,00 mm e 1,10 mm atuaram novamente como uma influência positiva para mitigar a delaminação e atingiram valores elevados de (G_{IIc}), 77,5% e 78,3% maiores que o corpo de prova sem pino, respectivamente. Os resultados estatísticos apontaram que para o caso NPC, o aumento da densidade de inserção sempre gera um aumento na tenacidade à fratura. A partir disto, aumentar o tamanho do pino tem pouca influência no NPC. Para a etapa PC foi demonstrado que o aumento do tamanho do pino diminui a resistência à fratura, exceto para baixa densidade de inserção. Além disso, as Redes Neurais Artificiais (Artifial Neural Network - ANN) treinadas com parte dos dados experimentais mostraram excelente capacidade preditiva das propriedades de tenacidade à fratura interlaminar. Para as respostas modais dos laminados fabricados com molde polimérico, os resultados experimentais indicaram que, na maioria dos casos, houve um aumento na frequência natural e houve uma redução, entre 60% a 70%, na amplitude de vibração para todos os corpos de prova reforçados com *z-pins* quando comparados aos sem reforço através da espessura. Além disso, os dados experimentais comparados com os resultados estatísticos apontaram que os *z-pins* tiveram uma influência positiva aumentando a frequência natural e diminuindo a amplitude de vibração forçada dos compósitos reforçados com *z-pins*, além disso, a ANN treinada com os dados experimentais apresentou concordância com os resultados dos testes experimentais realizados neste trabalho para se prever as respostas modais.

Palavras-chave: Compósitos Reforçados com *Z-pins*; Tenacidade à Fratura em Modo II; Análise Modal; Planejamento de Experimento; Redes Neurais Artificiais

TABLE OF CONTENTS

LIST OF FIGURES

LIST OF TABLES

LIST OF ABBREVIATIONS

ANOVA	Analysis of Variance
ANN	Artificial Neural Network
ASTM	American Society for Testing and Materials
CAI	Compression After Impact
CC	Compliance Calibration
CCD	Central Composite Design
CFRP	Carbon Fiber Reinforced Plastics
CNT	Carbon Nanotube
DOE	Design of Experiments
ENF	End-notched Flexure
EVA	Ethylene Vinyl Acetate
FE	Finite Element
FEA	Finite Element Analysis
FFT	Fast Fourier Transform
FRF	Frequency Response Function
MWCNT	Multi-walled Carbon Nanotube
NPC	Non-precracked
PC	Precracked
PS	Polystyrene
QI	Quasi-isotropic
RSM	Response Surface Methodology
UAZ	Ultrassonically Assisted Z-fiber
UD	Uni Directional
2D	Two Dimensional
3D	Three Dimensional

LIST OF SYMBOLS

R^2_{adj}	Adjusted coefficient of determination
β	Constant coefficients
ξ	Damping ratio
ω_d	Damped natural Frequency
x_i	Design factor i
y	Displacement
α	Distance from center point
E_1	Elasticity modulus direction longitudinal
E_2	Elasticity modulus direction transverse
ΔE	Energy lost per radian
f	Function
R^2	Indicator of model fit
G_{IIc}	Interlaminar Fracture Toughness in Mode II
η	Loss factor or loss coefficient
$\Delta\eta$	Loss factor shift (%)
A_{max}	Maximum vibration amplitude in forced vibration
ΔA_{max}	Maximum amplitude shift (%)
β	Model constant
ω_n	Natural frequency
$\Delta\omega_n$	Natural frequency shift (%)
k	Number of design parameters
x_d	Pin area density
x_p	Pin size
υ_{12}	Poisson ratio
U_{max}	Potential energy at maximum displacement
e	random error term

ε	Random error term or noise
Y	RSM response
ω_r	Resonance frequencies
y	Response variable
G_{12}	Shear modulus plane 12
ρ	Specific mass
x_1	Variable of factor 1
x_2	Variable of factor 2
y'	Velocity
a_i	Vibration amplitude a
b_i	Vibration amplitude b

CHAPTER 1: INTRODUCTION

Carbon fiber reinforced composite laminates are extensively used in many structural applications due to their excellent in-plane specific stiffness and strength, fatigue properties, chemical properties, lightness. Also, the development of polymer science, which has improved the performance and durability of composite materials, made their application drastically increase in aerospace, sports equipment, automotive and naval structures, where stiffness, strength and lightness are key factors in the materials selection and design process to replace metallic structures (CUI *et al*., 2011; PARK *et al*., 2012; FRANCESCONI *et al*., 2018). Composites are known as bidirectional (2D) structures and are usually manufactured by stacking layers of unidirectional or bidirectional fabrics and resin impregnation. Since the layers of conventional composites are free from the adjacent ply and are cured with a resin, of relatively lower strength than the fibers, the lack of reinforcement in the thickness direction provides out-of-plane properties lower than in-plane properties and making these structures prone to delamination and debonding when subject to impact and transverse loads (PARDINI, 2000; LI & CHEN, 2019).

Delamination is a long-standing problem and one of the most dominant failure modes and this limits the applications of laminates in the specific environment, for example, impact of high velocity or through-thickness tensile load (CHENGU *et al*., 2012). A potential solution to improve the delamination resistance in carbon fiber reinforced composites is to insert a mechanical bond between the different plies of the composite laminate by means of through-thickness reinforcement several techniques have been developed such as 3D braiding, 3D woven, stitching, tufting and z-pinning (CARTIÉ *et al*.; 2006a; BIANCHI & ZHANG, 2011).

Among these reinforcement techniques, z-pinning is a very versatile process since it involves the insertion of pins made of Carbon/Epoxy, Carbon/BMI, S-Glass/epoxy, titanium, stainless steel materials with 0.25 mm to 1.0 mm in diameter and typically areal density insertion from 0.5% to 5% and can be applied either in prepreg materials or in dry fabrics stacks followed by liquid compression molding, resin transfer molding (RTM) and vacuum assisted resin transfer molding (VARTM) processes (CHANG *et al*., 2007; HUANG & WAAS, 2009; CHENGU *et al*., 2012).

The z-pinning insertion process was idealized and developed Aztex Inc. (Foster Miller) and is knowns as an ultrasonically assisted Z-fiber insertion (UAZ^{TM}) process

(DANTALURI *et al*., 2007). Before the insertion, a collapsible foam (known as Z-pin preform) containing the z-pins quantified in terms of size and of percent reinforcement is placed upon the surface of the prepreg or a stack of dry fabric lay-up and the insertion can be either orthogonally or in angles. Placing the z-pin foam on the part to be reinforced, the insertion occurs aided by an ultrasonic hammer that with its high-frequency sonic action excites the pins and they penetrate through the thickness of the prepreg or dry fabric preform. In the case of prepregs, due to the hammer frequency and the pin vibration, there is localized heating that softens and reduce the resin viscosity and facilitate the z-pin insertion. When the pin achieves the defined depth or length the foam is removed and the pin excess is sheared off and discarded. The Figure 1.1 summarizes the UAZ technique.

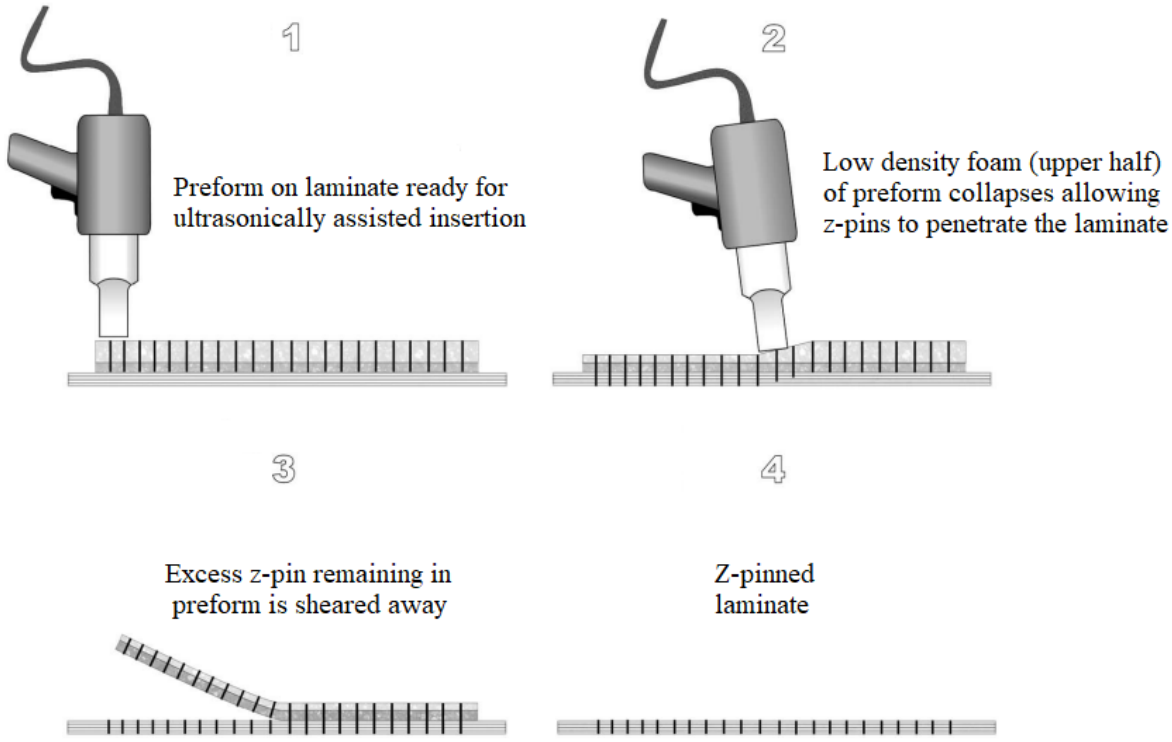

Figure 1.1 – Scheme of UAZ Z-pinning insertion technique (Adapted from MOURITZ et al., 2011).

Although the UAZ technique is the most popular and used method to insert z-pins, especially for prepregs, alternative methods have been created for insertions in prepregs and dry fabric preforms. An example is “Caul Plate” insertion where the z-pin foam preform is placed in the prepreg preform, the Caul Plate is positioned above the foam preform, the whole system is vacuum bagged and submitted to pressure and temperature in an autoclave. The temperature lowers the resin viscosity and facilitate the reinforcement insertion (BARRETT,

1996; MARTINS, 2018). Vaidya *et al*. (2000) developed a device capable to insert z-pins with different sizes and length in prepreg and dry fabric preforms, for the later the manufacture of the through the thickness reinforced composite was by vacuum assisted resin transfer molding (VARTM) process.

The original and most commonly used z-pins are cylindrical rods made of unidirectional carbon fiber polymer composite, however, Knaupp & Scharr, 2014 used a method for dry fabrics developed in the Rostock University to create reinforced composites with rectangular z-pins. The fabric plies were manually stacked and impregnated and aluminum plate drilled holes (with a predefined pin-to-pin distance) is placed on the top of the impregnated fabric preform. After that, the z-pins are inserted in the holes and pushed through the thickness using a metallic rod, then the aluminum plate is replaced by mold, to compress the composite, and the compressing and cure step occurred in a pneumatic molding press. In another study, through the thickness reinforced composite laminates were fabricated using a wet hand-layup process. To this, a z-pin foam carrier was placed in the impregnated fabric top surface, a balsa wood was positioned on the top of the setup and then the whole system was subjected to high pressure of 350kPa in a hydraulic press (LADANI *et al*., 2016; RAVINDRAN *et al*., 2019a).

Regarding the effect and mechanical performance of z-pinned composites, many authors have investigated the interlaminar fracture toughness properties and delamination toughening mechanisms under mode I, mode II and impact damage resistance mechanical properties improvements of composite laminates (MOURITZ, 2020).

Zhang *et al*. (2016) showed that z-pinned laminates fracture toughness in mode I was 8 kJ/m2 and 10 kJ/m2 for Carbon fiber reinforced polymers (CFRP) and glass fiber reinforced polymers (GRFP) respectively whilst unpinned was about 0.3 kJ/m2 for CFRP and 0.2 kJ/m2 for GFRP and also reported that a 0.5% z-pin density insertion can increase the fracture toughness by at least one order of magnitude in comparison to not reinforced composites. Knaupp *et al*. (2014a) investigated composites reinforced with circular and rectangular pins to quantify the increase in interlaminar fracture toughness in Mode I. When comparing the same areal density rectangular z-pins, independently of their orientation, provided higher interlaminar fracture toughness than circular pins and comparing the same quantity of z-pins and when comparing the same number of pins, the parallel oriented pins have a slightly higher

fracture toughness and the perpendicular oriented pins have lower fracture toughness than the control with round pins.

In impact and post-impact investigation, Zhang *et al.* 2006 tested z-pinned composites with different thicknesses and obtained reduction from 19% to 64% in the impacted damage area, depending on the specimen thickness and impact energy, and achieved significantly increase the compression-after-impact (CAI) strength at about 45% compared to the unpinned composites. Knaupp *et al.* (2014b) studied the impact properties carried out in different impact energy levels of rectangular and circular z-pins with 0.5% and 1.0% areal density insertion in composite laminates. For all the tests, the best performance was for the rectangular z-pinned composites with reduced delaminated areas up to 60% and 20% CAI improvement compared to unpinned composites.

Experimental studies regarding end-notched flexure (ENF) test method have achieved the mode II delamination resistance and pointed out the toughening mechanisms of z-pinned carbon-epoxy laminates and the positive influence of z-pins in the interlaminar fracture toughness (MOURITZ, 2020).

Yan *et al*. (2004) studied the behavior of composite laminates reinforced with 0.28 mm diameter z-pin in a 1% areal density insertion and the obtained result for mode II fracture toughness was 190% higher than the non-reinforced composite. Cartié *et al*. (2006b) investigated the mode II performance of 3D reinforced composites with 0.28mm diameter z-pin inserted in an areal density of 0.5%, 2.2% and 4.0% and achieved the increase in the interlaminar fractures toughness in mode II (G_{IIc}) values of 150%, 590% and 975%, respectively, compared to the unpinned composites.

Yasaee *et al*. (2017) evaluated the properties of interlaminar fracture toughness, in mode II, of 0.28mm diameter z-pin reinforced composites with a density of insertion of 2% and described an increase of 294% concerning composites not reinforced. Ravindran *et al*. (2019a) studied the behavior under mode II loading of composites reinforced through the thickness with circular z-pins of different diameters, 0.28mm and 0.51mm, with an insertion density of 2%. The results obtained for the interlaminar fracture toughness showed an increase, compared to those without 3D reinforcement, of 248% and 370% for the 0.28mm and 0.51mm z-pins, respectively.

As well as the static properties in 3D reinforced composites, it is worth highlighting the performance of through the thickness reinforced composites concerning their vibration

properties in modal analysis and in a certain way try to correlate them with the static properties.

Studies show that the modal properties of composites change according to the amount and orientation of layers and the addition of reinforcements in the matrix.

Mishra & Sahu, (2014) investigated the free vibration response glass fiber/epoxy composites with different thickness, with $[0]_8$, $[0]_{12}$ and $[0]_{16}$ plies, and different stacking sequences, $[(0/0)_2]_s$, $[(30/-30)_2]_s$, $[(45/-45)_2]_s$, and it was achieved that in thicker composites the natural frequency of vibration increases due to bending-stretching coupling and the natural frequency of the woven composite plates decreases with the increase of fiber orientation. Rafiee *et al*. (2019a) investigated the epoxy modification with carbon nanotubes (CNTs), from 0.075% to 0,3% in weight (wt.%) concentration, for glass fiber/epoxy composites in forced vibration responses and achieved damped natural frequencies in the nanocomposites increased with an increase in nanoparticle loading confirming the beneficial effect of high content nanofillers on the damping ratio of nanocomposites.

Equally important, 3D reinforcement techniques tend to modify the natural frequencies, damping and amplitude, thus the dynamic response is also changed. Regarding 3D composites, Pei *et al.* (2015) described the natural frequency obtained in experimental tests is related to the fiber volume fraction and the angle variation of 3D braided composites. With equal fiber volume fraction, the natural frequency improves when the 3D braiding angles decrease. When the surface braid angle is the same, the natural frequency enhances when the fiber volume content increases. Equally important, Fan *et al.* (2019) Investigated the damping coefficient and variation of vibration amplitude in different composites laminates fabricated of 3D and 2D fabrics. The damping coefficient of the 3D composite is higher than that of the 2D multilayer composite as well as the decreasing on vibration amplitude, implying that the Z-binders (stitched yarn) in the 3D-reinforced structures can transmit vibration energy to the middle or lower layer, speeding up the energy dissipation process.

To date, the approach to reinforce composites through the thickness is still used mostly to improve the interlaminar fracture toughness and delamination mitigation properties and there are few studies regarding modal responses in 3D composites structures.

Thus, because few studies related to mode II and vibrations reinforced in the thickness direction with rectangular z-pins (which in most cases presented better properties in comparison to circular z-pins) have been published and found in the database researched, it

favors the study of their behavior. Therefore, this research involves an original study to investigate the interlaminar fracture toughness in mode II and vibration mechanical properties of composites reinforced through the thickness with rectangular z-pinned, manufactured by VARTM process, using the Design of Experiments to pursue the optimization of z-pins sizes and density insertions parameters which can innovate, bring benefits, and help in the composite manufacture decision making and in the property's improvement. Also, this research can contribute to further research, scientific publications, technology improvement and, besides the later mentioned improvements and contributions, the insertion technique and the composite laminates manufacturing processes presented in this work are suitable to be used in a laboratory and industry scale as an alternative and a more affordable way to the most used fabrication methods.

Considering different sizes and areal density insertion parameters obtained by Response Surface Methodology (RSM) analysis, in Chapter 2 is carried out a study of 3D reinforced composites modal responses such as natural frequency, damping or loss factor and maximum vibration amplitude in forced vibration.

Moreover, Chapter 3 the interlaminar fracture toughness in mode II is evaluated Response and a Surface Model and Analysis of Variance are used to support a detailed statistical discussion of the experimental results and the generated data are used to training an Artificial Neural Network, to predict the influence of the pin size and density configuration in the interlaminar fracture properties of z-pinned composites structures.

In Chapter 4 The modal responses of composite laminates reinforced through the thickness with rectangular z-pins sizes and areal density insertion design variables generated from Design of Experiments (DOE) are studied with free and forced vibration tests being carried out to assess and predict the modal responses of z-pinned composites.

Chapter 5 gives a conclusion of this work and analyzes each characterization test used and contributes to the validation of this process development.

1.1 Research Objective

The aim of this work is the development and fabrication of composites manually reinforced through-thickness based on the z-pinning technique and to evaluate the mechanical properties of interlaminar fracture toughness and vibrations.

This is carried out by pursuing several activities addressing the manufacturing, mechanical behavior response of z-pinned laminates. These can be summarized in the following objectives:

- Design of Experiments (DOE) to determine the dimensions and areal density insertion of the 3D reinforcements (z-pins) for further optimization of the manufacturing process;
- Materials selection of polymeric molds and for the composites manufacturing;
- Define the layers' quantity and orientation of the laminates to be machined to manufacture the z-pins;
- Through the thickness reinforced composites manufacturing by VARTM;
- Interlaminar Fracture Toughness Test in mode II (ENF) and Modal Analysis experimental tests;
- Data analysis.

(Intentionally left in blank)

1.2 Methodology of the Research

The flowchart in Figure 1.1 presents the methodology used in the development of this work, thus the following Ph.D. thesis is organized into five chapters with a final chapter with the general conclusions.

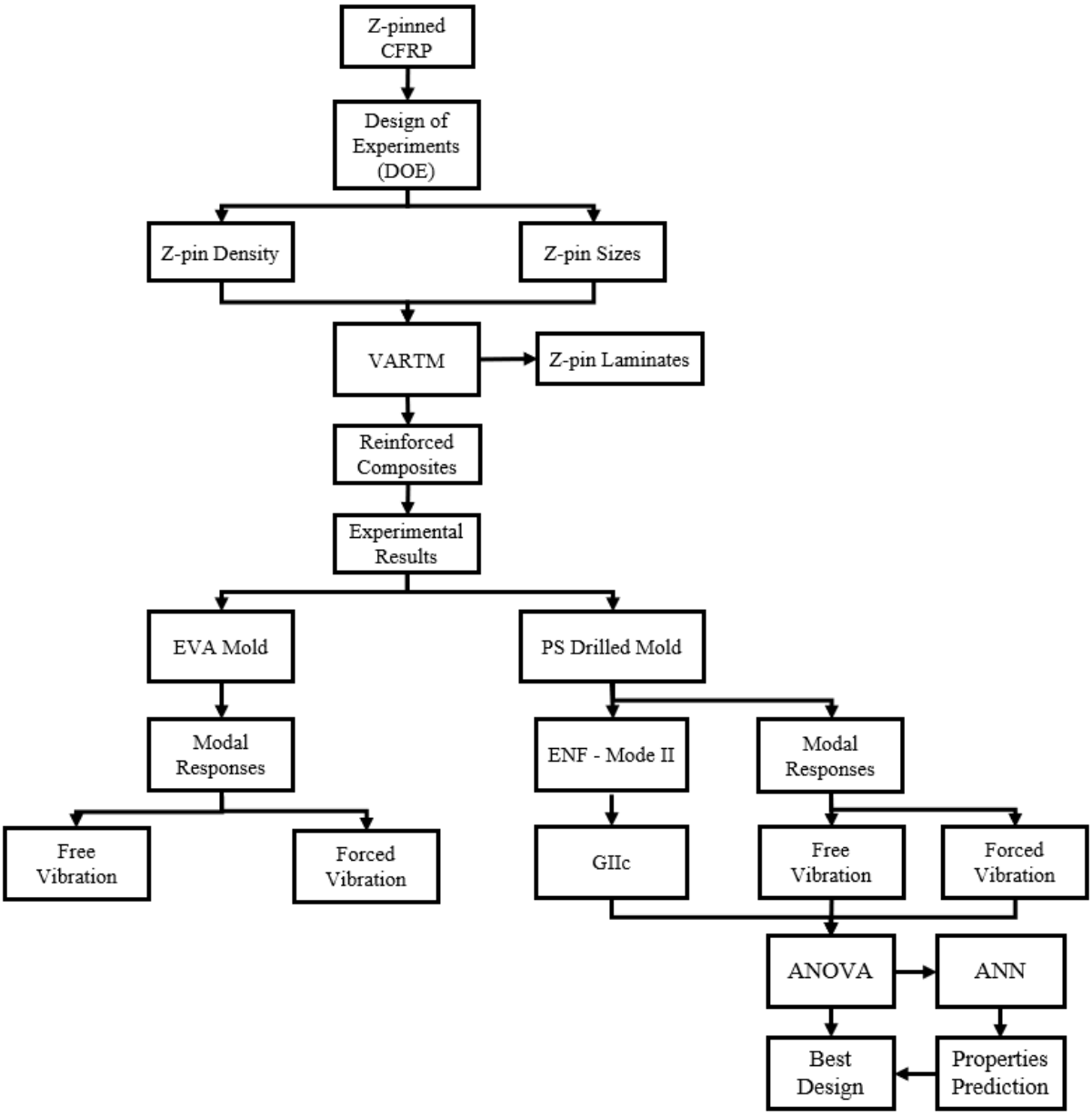

Figure 1.2 – Flowchart of the methodology used for optimum manufacturing conditions of z-pinned CFRP specimens in the Ph.D. thesis work.

- In Chapter 2, an experimental study was conducted in order to understand the modal responses analysis behavior and analyze the experimental results;
- In Chapter 3, an experimental study was conducted to achieve the experimental and statistical results, and the behavior prediction for fracture toughness in Mode II;
- In Chapter 4, the free and forced vibration were investigated, the experimental results were obtained, statistically analyzed and the modal responses behavior were predict;
- In Chapter 5, the thesis terminates with an overview of the main conclusions obtained for each covered subject and, the perspectives for the future works.

(Intentionally left in blank)

CHAPTER 2: AN EXPERIMENTAL DYNAMIC ANALYSIS OF Z-PINNED UNIDIRECIONAL CFRP BEAMS

This chapter aims to evaluate the influence of z-pinning on the modal responses. The z-pinning process was made considering machined rectangular carbon fiber/epoxy z-pins with different dimensions at different insertion spacing densities on the structure. Both the insertion density and the dimensions of the pin were obtained by RSM analysis to evaluate the influence on the mechanical modal properties (natural frequency, loss factor and vibration amplitude) and to obtain an ideal value of insertion area density and pin width.

2.1 Introduction

The extensive application of polymeric matrix composite materials in several fields (aerospace, civil construction, medicine, etc.) is not only related to the excellent mechanical performance, but also the lightweight of this type of structure compared to metallic alloys (GNABA *et al.*, 2018). Conventional composite laminates are one of the most widely used composite materials in the manufacture of structural parts due to their ability to withstand high in-plane loads. These materials, known as bidirectional (2D) composites, are usually processed in the classic way of stacking individual layers of unidirectional or bidirectional fabrics previously impregnated with thermoplastic or thermoset matrices (PARDINI, 2000).

The stacking arrangement of the reinforcement makes each layer free from the adjacent layer and, consequently, the bonding between the layers is provided only by the matrix. The interlaminar region (between fabric layers and matrix) is, therefore, subject to damage due to the lower interlaminar fracture toughness of the matrix (Wisnom, 2012). Interlaminar fracture, or delamination between layers, is the most frequent failure mode in thermoset and thermoplastic matrix composites (GOMES *et al.*, 2018; BARBOSA *et al.*, 2019). Fractures of this type occur even under low out-of-plane mechanical loading, which, in turn, compromise the structural integrity of the component. Due to this limitation, applications of composites are restricted.

Regarding the delamination in composites laminates, Bruno & Greco (2001 a,b), presented an improvement on the technique of energy release rates evaluation, with the

introduction of a simple linear interface model that the constitutive relation connecting opening and sliding displacement jumps to normal and shear interlaminar stresses acting on the interface. The study allowed investigating the singular behavior of interlaminar stresses close to the delamination tip and the modelling is able to detect the effects of shear stresses and their interaction. It was proposed an analytical solution procedure of the relevant governing equations, linked with a limit process that is employed to obtain the fracture energy fraction of mode I and mode II, necessary to predict the delamination growth behavior in composite laminates.

Greco *et al*. (2002) proposed an interface model, aiming the analyses of delamination and bridging phenomena in composite laminates. The analytical approach used was capable to identify the interlaminar resistance behavior of a composite laminate, avoiding the notable underestimation of the resistance got with simplified delamination models. The accuracy of this model is found through comparisons with results from continuum analysis generated by finite element (FE) proceedings. The effectiveness of the model was shown by the solution of a two-layered plate scheme subjected to pure and mixed mode loading conditions and to fiber bridging stresses and proved to be a useful tool and a low computational cost tool as efficient as a more complex FE analyses to predict delamination and bridging behavior in composite laminates.

Bruno *et al*. (2009) provided an analytical investigation on the dynamic behavior composite laminates. The model is developed within a steady state delamination crack growth. The study provided a closed form expressions for simple cases involving mode I and mode II loading conditions. A parametric study on the energy release rate as a function of the crack tip speed, the shear deformability and the crack growth conditions were developed and comparisons with numerical results obtained by the use of FE approach involving pure mode I and mode II showed the reliability of the proposed formulation of the model.

Driven by the need to mitigate or suppress delamination, increase the resistance to impact damage and the mechanical properties through the thickness, different techniques to manufacture composites reinforced through thickness have been developed and studied. The main reinforcement techniques through thickness include tridimensional weaving (3D weaving), 3D braiding, simple sewing (stitching), tufting and z-pinning. These techniques cause an increase in the properties of interlaminar fracture toughness and impact resistance in composite laminates (Partridge & Hallett, 2016; Bortoluzzi *et al.*, 2019).

In this scenario, a 3D reinforcement technique deserves to be highlighted, the Z-pinning process. Z-pinning is a technique originally developed for the application of pins, circular or rectangular, in the thickness direction, or in Z, in structures made with prepregs (carbon fiber fabrics pre-impregnated with resin), and these z-pins can be of different materials including steel, titanium and carbon fiber/epoxy resin and carbon fiber/bismaldeide (BMI) resin and are inserted in a stage prior to the curing process of the composite laminate (BIANCHI, 2012). In the same way, 3D reinforcement techniques promote improvements in the out of plane properties, while the in-plane properties, such as: tensile and compressive strength, suffer a decrease when compared to the properties of two-dimensional composites. For these reasons, it is necessary to have a relevant study of the region of application of the reinforcement and take into account how much can be gained with the increase of properties out of plane, to the detriment of in-plane properties loss (DECONINCK *et al.*, 2014; OSMIANI *et al.*, 2016).

Recently, FE models have been created to predict and evaluate the delamination crack growth and behavior and bridging mechanisms of single Z-pins or including different parameters such as rods diameter, insertion angle, and density pattern. Li & Chen (2019) developed a FE damage model to study the mixed-mode bridging mechanisms of single pins in quasi-isotropic laminates using a zero-thickness cohesive element. In the study, resin damage, rupture and splitting, debonding from the composite, frictional pull-out of the Z-pins were included in the FE model. The FE model predicted bridging laws and damage modes of the Z-pin under Mode I, Mode II and mixed-mode loading and followed the experimental results.

Li & Chen (2020) also proposed a new FE model to assess the influence of Z-pin parameters including diameter, insertion angle, and density pattern on the longitudinal tensile strength of a UD composite plate. The unit cell model includes features of fiber waviness, resin-rich zone, Z-pin, and unaffected laminate. The FE results were found to be in better agreement with the experimental data than the conventional model. The FE parametric results showed that the changing trend on tensile strength with Z-pin parameter is nonlinear and is related to the change of damage mode or microstructure.

The dynamic response is also changed by 3D reinforcement techniques, natural frequencies, damping and amplitude tend to be modified. Several studies which identify those parameters and characterize the dynamic response are published, highlighting the importance

of such analyses. Fouad *et al.* (2020) developed and characterized three different composites as candidates for dental posts, vibration modal analysis is performed to obtain frequency responses and aid in choosing the best candidates.

In the same way, Sinha *et al.* (2020) investigated numerically and experimentally the natural frequencies of laminated glass fiber reinforced polymer stiffened plates. The authors showed an increase in non-dimensional fundamental frequencies as the number of stiffeners increased. Experimental analysis used to characterize the vibration and damping properties of graphene nanoplatelets-modified epoxy composites, exhibits a decrease in damped natural frequencies with addition of graphene nanoplatelets (RAFIEE *et al.*, 2019b).

Another study presents the vibration damping enhancement offered by using composites made up of carbon fibers with liquid methyl methacrylate thermoplastic resin (BHUDOLIA & JOSHI, 2017). Vibration analysis used for evaluating the effect of porosity in a graphene-reinforced composite demonstrates an increase of the resonance frequency as the porosity increased (POURJABARI *et al.*, 2019).

These examples justify the effort to perform modal analysis on the composite beams with z-pinning reinforcement. It is expected enhancements on dynamic characteristics just as those obtained in previous studies involving reinforced composites.

As an illustration, 3D reinforcements have been applied to structural parts in the aerospace, automobile and naval industries, which are subject to impact (PARTRIDGE & HALLETT, 2016) in sandwich composites to mitigate and suppress the delamination between layers of fabric and polyurethane foam (HENAO *et al.*, 2015) and in tests to replace the use of metal rivets for fixing stringers (MILLS & JONES, 2010). Nevertheless, to the best of the authors' knowledge, very few efforts have been devoted to the development of a Response Surface Method (RSM) for composite structures with z-pinning.

In this paper, a detailed study on the influence of z-pinning on the modal response of laminated structures is carried out. For this, beams considering different geometries and pin area densities are manufactured based on a planning carried out using design of experiment and response surface model strategies. Thus, in the present work the focus is inquiring the suitable configuration for z-pinned composites structures, taking the pin size and density insertion of pins on the structure surface (density of area) as the design variables. The aim is to verify the relation of these variables in the laminated behavior with z-pinning regarding the

modal responses such as natural frequency, damping or loss factor and maximum vibration amplitude in forced vibration.

The work presented here, assesses the potential of this technique as the main tools in structural and manufacturing optimization for laminated composites structures with z-pinning. To the authors' best knowledge, there are very scarce studies in the literature investigating the influence of z-pinning on the modal responses in laminated structures.

More specifically, the major contributions of this article are summarized as follows: *i)* manufacture of CFRP with insertion of rectangular z-pinning. *ii)* development of an RSM considering different geometries and pin quantities; *iii)* detailed statistical analysis on the effect of manufacturing variables, *iv)* experimental modal analysis of CFRP with pins and *v)* optimization of the manufacturing process.

The paper is disposed as follows: In Section 2, a global background is presented. In Section 3 the methodology is discussed, showing the modeling using RSM and the experimental design. In Section 4, the results are demonstrated. Finally, in Section 5 draws the conclusions.

2.2 Theoretical Background

2.2.1 Z-Pinning

Z-pinning is considered an innovative technique for through the thickness reinforcement developed to increase the delamination resistance, or fracture toughness, damage tolerance and impact resistance of structures made of composite materials. This technique involves the manual or automatically insertion of pins, or z-pins, in the thickness direction of preforms (HOFFMANN *et al.*, 2019; FERT, 2016).

In addition, Z-pins of high stiffness and small dimensions (diameters vary between 0.28 - 1.00 mm), are manufactured with metal (titanium alloys, copper and steel) and carbon fibers and pultruded glass. They are mechanically introduced through the thickness after increasing the temperature and decreasing the viscosity caused due to the ultrasonic vibrations of the equipment (FERT, 2016; HOFFMANN & SCHARR, 2018a). The z-pins can be inserted either orthogonal or inclined to the upper surface of the preform (M'MEMBE *et al.*, 2019). This technique was developed by Aztex Inc, being called UAZ (Ultrasonically

Assisted Z-Fiber) and is the most used in the insertion of reinforcements through preforms made in prepreg and cured in autoclave (MOURITZ, 2007).

In the Z-pinning process there is a foam in which the pultruded carbon fiber pins are contained, these pins can have different patterns of spacing, or areal density, generally corresponding to 0.5 - 4.0% in areal density (FRANCESCONI & AYMERICH, 2018; HOFFMANN & SCHARR, 2018b). The foam is positioned at the reinforcement site and with the aid of an ultrasonic hammer, the pins are inserted into the preforms, made from prepreg. The pins inserted in the thickness direction give the composite an increased toughness to the interlaminar fracture. As the other three-dimensional reinforcement methods, this one also presents distortion and waviness of the fibers and the presence of regions with excess resin, causing the in-plane properties to decrease (MOURITZ, 2007; HOFFMANN & SCHARR, 2018b; CUI *et al.*, 2019). The Figure 2.1 illustrates the UAZ insertion method in a prepreg preform.

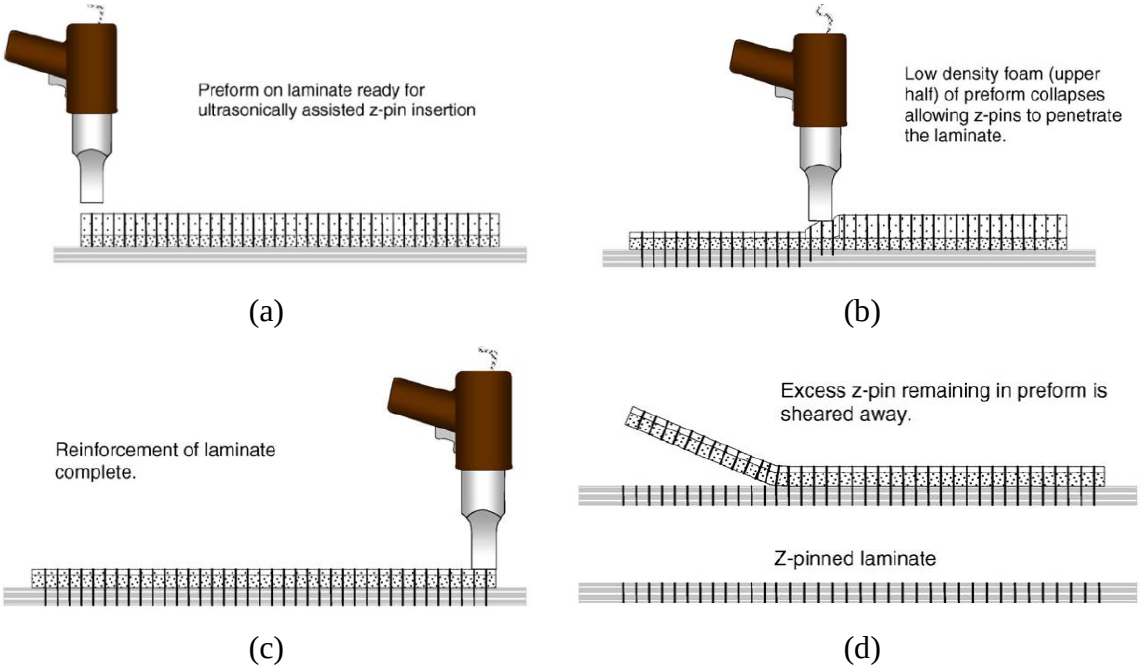

Figure 2.1 – Schematic of the UAZ process (MOURITZ, 2007).

An alternative and low-cost z-pinning method for dry fabrics, instead of prepeg laminates, was developed in the Rostock University. The purpose of the invention was to create pin-reinforced composites with rectangular pins. The fabric plies are manually stacked

and impregnated with the resin using a brush. On top of the laminate, an aluminum plate is placed. This plate has holes in it with a predefined pin-to-pin distance according to the z-pin areal density needed. Thereafter, the z-pins are placed in the holes and pushed through the thickness of the perform using a metallic rod. The next step is to replace the holed aluminum plate by a die to compress the composite. The Compressing and curing occur in a pneumatic molding press (KNAUPP & SCHARR, 2014).

An approach to reinforce fiber composites that are produced in a liquid composite molding (LCM) process was presented by Hexcel and refined by EADS (HOFFMANN *et al*., 2019). In this Z-pinning technique developed by EADS Innovation Works to reinforce dry performs, the Z-pins insertion occurs with a vibrating hollow needle containing the Z-pin inside. The needle is pushed through the thickness of a dry perform and when the right depth is reached, the needle is pulled leaving the Z-pin inside the preform. The excess of the pins are cut and then the preform can be injected using a resin transfer moulding (RTM) system (VAZQUEZ *et al*., 2011).

Vaydia *et al*. (2000) designed, manufactured and implemented a device to reinforce through the thickness dry fabric and prepreg system based performs with Z-pins and the equipment was capable to insert different pin diameters, pin types and pin lengths. The insertion device allowed the manufacture of damage tolerant Z-pin reinforced glass/epoxy composite laminates using the affordable vacuum assisted resin transfer molding (VARTM) process.

Efforts to make z-pinning economically attractive were performed in this work where the z-pins were manufactured in house, inserted manually in dry fabric preforms and the composite laminates were manufactured using the VARTM process.

2.2.2 Experimental Modal Analysis

Structures are exposed to static and dynamic loads determined by their operating conditions. They will respond to these excitations, and this response must be quantified and analyzed in order to ascertain whether design conditions are met. The dynamic characteristics of a structure or system are natural frequency, damping and mode shapes. Observing the dynamic response as a whole may not provide enough information to understand the structure or system behavior, modal analysis comes as a better way to interpret dynamic behavior.

Avitable (2018) defines modal analysis as the study of the dynamic characteristics of a system defined in an independent way from the loads applied and the respective response of the structure or system. For each mode, the system has a frequency, a damping, and a specific deformation.

Natural frequency is the frequency at which a system will vibrate on its own, without external forces, after an initial disturbance (RAO, 2018). The number of degrees of freedom of a system has, determines the number of natural frequencies. Mode shapes are the deformation that the component would show when vibrating at the natural frequency. The decay observed in an oscillating system happens due damping. The nondimensional coefficient ζ, called the damping ratio, describes the oscillations' capacity after a disturbance. Damping causes loss of energy in the system and the most commonly used quantity to describe the energy lost is the loss factor or loss coefficient, denoted by η. Loss factor represents the energy lost (ΔE) per radian divided by the potential energy at maximum displacement (U_{max}) (INMAN, 2014), and is given by Equation 2.1. At resonance, the loss factor equals two times the damping ratio.

$$\eta = \frac{\Delta E}{2\pi \cdot U_{max}} \tag{2.1}$$

When performing modal analysis, the response of the structure can be measured with an accelerometer, obtaining data of acceleration over time, or with a laser vibrometer, obtaining data of velocity over time. Using the fast Fourier transform (FFT), time data is transformed to the frequency domain in order to compute the frequency response function (FRF).

The frequency response function is the ratio between the output response of the structure and the applied load which caused the response. Due to the use of the FFT, the FRF possesses real and imaginary components. Phase and magnitude components can also be obtained and provide useful information for obtaining the dynamic parameters.

There are various methods available for analyzing the FRF. The Peak-Amplitude Method assumes all the response can be assigned to one mode while disregarding any effects by other modes (EWINS, 2000). This method works properly for structures with well-separated modes in the FRF. Natural frequencies are obtained by detecting peaks ($|H|$) on the FRF magnitude plot which are confirmed to be resonance frequencies (ω_r) by observing a 180^o variation on the phase plot in the same value of frequency of the peak. The local maximums are used to determine two points ('a' and 'b') called half-power points, obtained

by dividing the response value by √2. After obtaining the half-power points, the loss factor (η_r) of this particular mode can be estimated by Equation 2.2.

$$\eta_r = \frac{\omega_a^2 - \omega_b^2}{2 \cdot \omega_r^2} \tag{2.2}$$

Another procedure is the Least-squares time domain method, which is based on the model of free decay vibration response for a multi-degree of freedom system (He & Fu, 2004). It consists of using a curve-fitting algorithm in order to derive the modal parameters. The free vibration response of the multi-degree of freedom system is known to be Equation 3.

$$x(t) = \sum_{i=1}^{N} e^{-n_i t} \cdot [a_i \cdot \sin(\omega_{di} t) + b_i \cdot \cos(\omega_{di} t)] \tag{2.3}$$

The coefficients a_i and b_i describe the vibration amplitude, ω_{di} represents the damped natural frequency and n_i relates to the damping ratio. Therefore, adjusting the response obtained experimentally to Equation 2.3 allows all the modal parameters to be identified.

In this study, vibration is taken through the velocity response. In this case, the FRF assessed is known as Mobility. In order to obtain the structural modal response results, the natural frequencies were extracted considering the peak-to-peak method and the structural damping value (loss factor), extracted by the curve fitting method of the SDOF model. More details will be discussed in the following sections.

2.3 Methodology

2.3.1 Composites Manufacturing

For the manufacture of laminates used to machine the z-pins, according to the specifications and dimensions obtained by a design of experiments (DOE), 4 layers of 6K Unidirectional fabric (UD) with a areal weight of 167 g/m², supplied by Hexcel, and stacked in the [0/±45/0] directions in a flat metallic mold. The plies quantity and stacking sequence were chosen so that it was possible to carry out the machining process, facilitate the laminate handle (avoiding it to brake and separate in the 0º direction) and so one of the reinforcement dimensions (thickness of the composite laminate) could be maintained. Also, the [0/±45/0] stacking sequence were chosen because these z-pins will be used in further studies where the specimens are going to be subjected to shear loadings (End-notched flexure (ENF) - mode II tests).

After stacking and positioning the fabric plies in the flat metal mold, the composite was manufactured using the VARTM resin infusion method. The resin used for molding the composites was the AMPREG AR21 epoxy system and A21 SLOW hardener. The VARTM process was carried out at room temperature and with a vacuum pressure of 28 mmHg. At the end of the infusion, the mold was placed inside an oven and was subjected to four (4) hours curing cycle at 80°C. After the cure process the z-pins were machined on a computerized numerical controlled (CNC) Router according to calculated widths. After machining and before the z-pins insertion, the rods were sonicated in an ultrasonic cleaner bath and then dried.

The test specimens were manufactured considering 18 plies oriented at 0°, i.e., in a stacking sequence $[0]_{18}$ by using same materials and process as used to obtain the carbon/epoxy Z-pins. Prior to the VARTM process, the machined z-pins were manually inserted in the preforms with the right areal density and z-pin widths. To achieve the right position to insert the z-pins, a template was designed on a 2 mm thick ethylene-vinyl acetate (EVA) sheet. The z-pins insert positions were marked using a pen attached to a CNC Router. The Figure 2.2 shows the template during the assembling and finished.

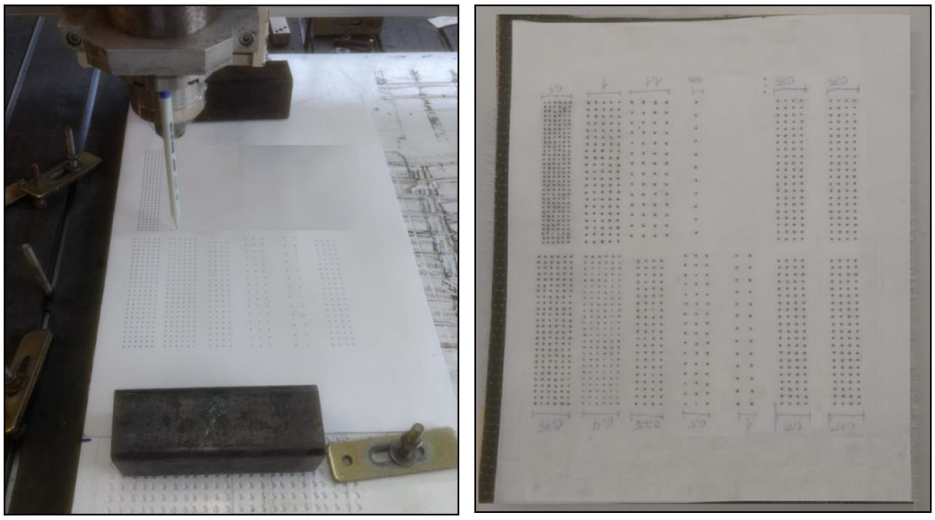

(a) (b)

Figure 2.2 – (a) EVA template during the manufacturing and (b) finished.

Later, the EVA sheet was placed on the top surface of the perform and the z-pins were inserted aided by a hollow needle. The rods were placed inside of the holed needle and the needle was pushed through the thickness of the perform. Thereafter, the needle was pushed

back, the rods stayed inside the perform and the rod excess was cut. The Figure 2.3 shows the steps inserting the needle and the rod and then cutting the excess. When the z-pinning process was finished, the composite laminate was manufactured. The VARTM process was carried out at room temperature and with a negative vacuum pressure of 28 mmHg. At the end of the resin infusion, the composite laminate had a room temperature cure for six (6) hours, and, after that, the mold was placed inside an oven and was subjected to a four (4) hours post-cure cycle at 80°C.

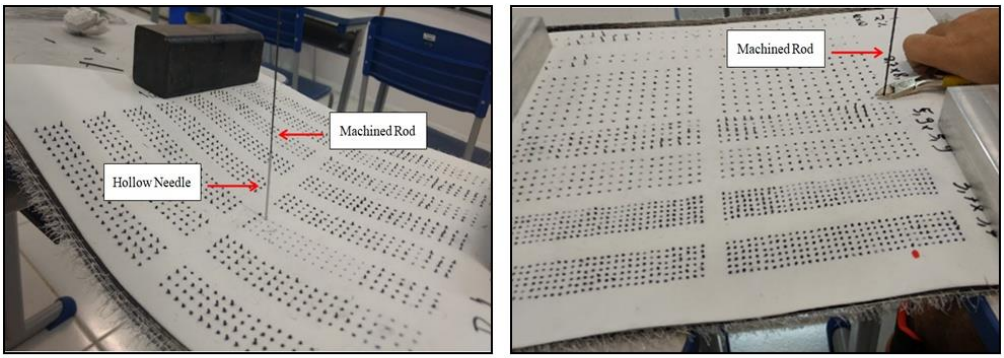

Figure 2.3 – (a) Hollow needle insertion through the thickness of the preform with the rod placed on top and (b) cutting the rod.

The Figure 2.4 elucidates the scheme of the specimens with reinforcement through the thickness. Finally, Figure 2.5 shows the manufactured specimen with and without pinning reinforcement.

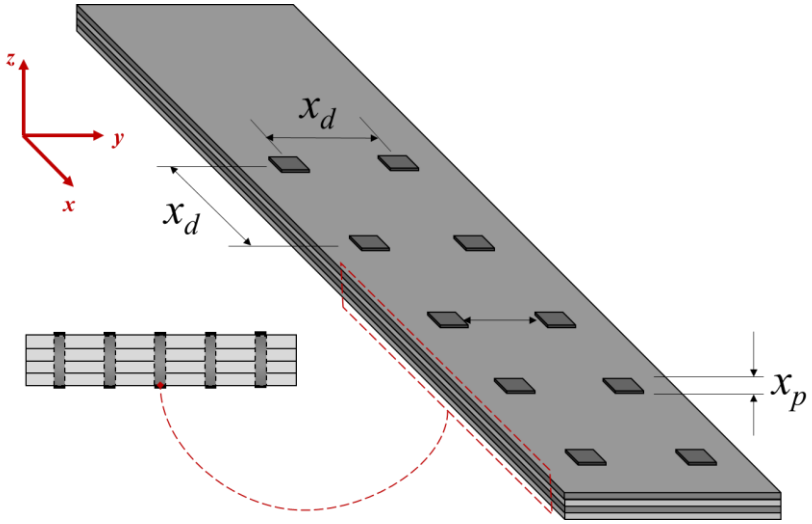

Figure 2.4 – Scheme of the specimen with reinforcement through thickness (z direction) and the design parameters xd and xp.

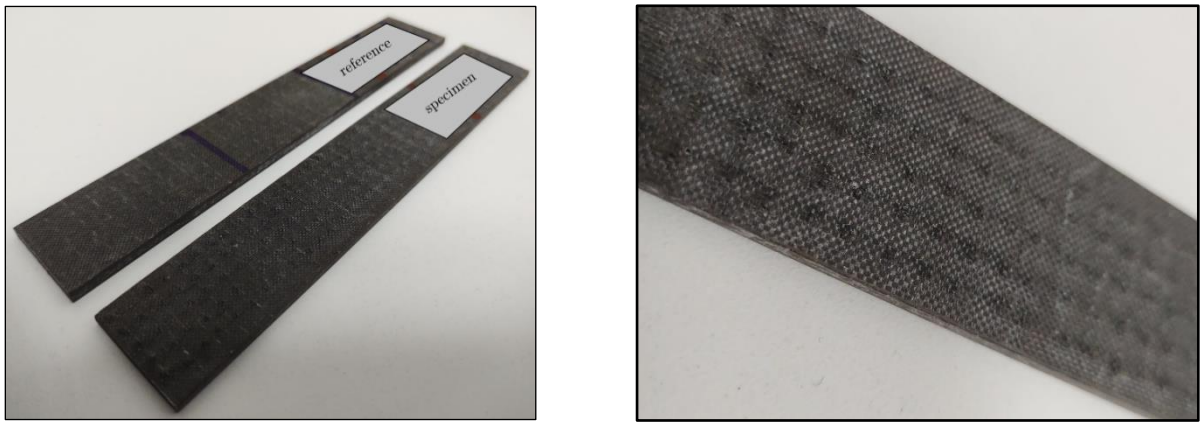

(a) (b)

Figure 2.5 – Example of the composite manufactured with and without pinning (a) and detail in surface quality in the presence of reinforcements (b).

The focus of this work is the analysis of the modal responses of composite laminates with the insertion of z-pins. For this, a design of experiments was carried out considering two main variables in the project *i)* pin density (i.e., number of pins per unit area) and *ii)* pin size (edge). Table 2.1 shows the evaluated configurations. It was defined a maximum and minimum size of the pin edge and a maximum and minimum allowed density. All these values will be used in the design of experiments following the study.

Table 2.1 - Bounds of manufacturing variables considering the pin areal density and pin width.

Specimen	Pin density x_d (%)	Pin width x_p (mm)
Reference	no reinforcement	
#1	0.50	0.50
#2	0.50	1.00
#3	2.00	0.50
#4	2.00	1.00
#5	1.25	0.40
#6	1.25	1.10
#7	0.20	0.75
#8	2.31	0.75
#9	1.25	0.75
#10	1.25	0.75
#11	1.25	0.75
#12	1.25	0.75
#13	1.25	0.75

With the insertion of z-pins through a composite laminate, additional volume will be introduced, and the laminate will increase in the z-pinned areas. Also, there will be the breakage of fibers, separation and deflection causing waviness in the fibers and free areas surrounding the z-pins which will collaborate to the thickness' increase and will form resin pockets. The Figure 2.6 (a) shows the fiber breakage during the insertion of the needle and the z-pins in the specimen #8, Figure 2.6 (b) shows the resin-rich zones, or resin pockets, formed after the resin infusion for the specimen #1 and Figure 2.6 (c) shows the waviness (eyelet shape) caused due to the insertion of the z-pin for the specimen #2.

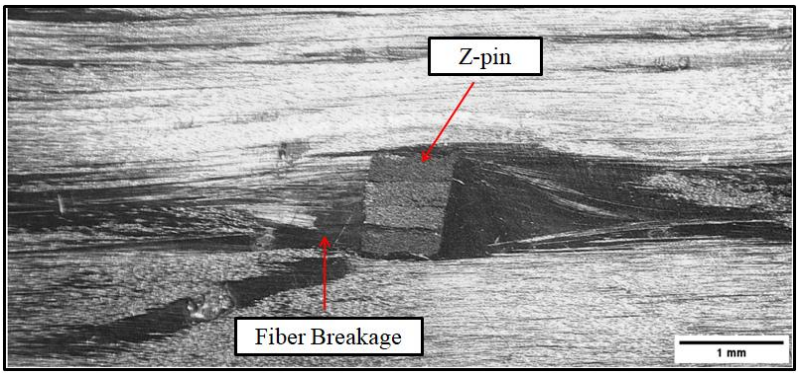

(a)

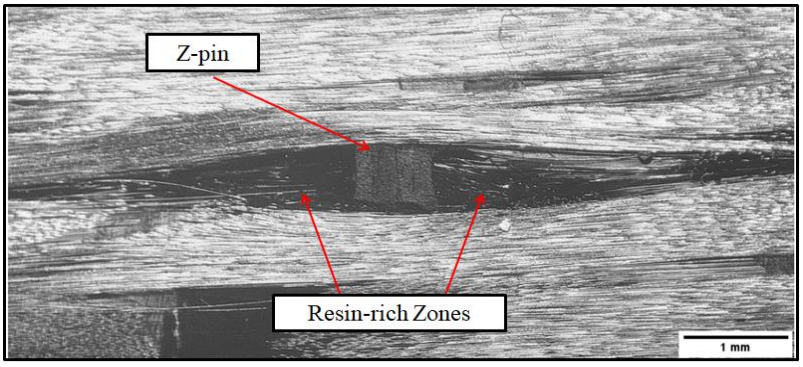

(b)

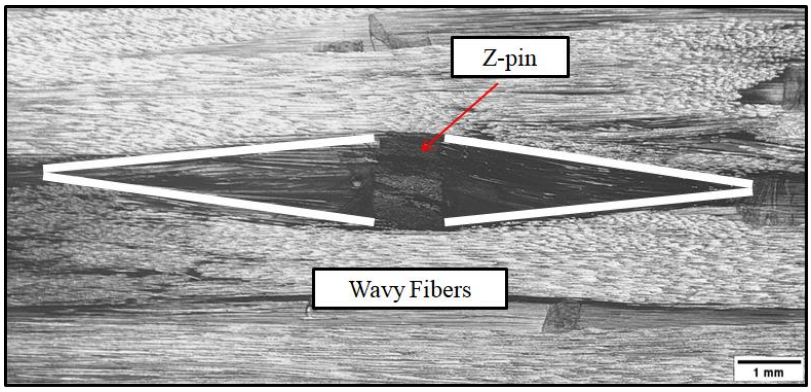

(c)

Figure 2.6 – (a) Example of fiber breakage, (b) resin-rich zones and (c) wavy fibers (eyelet shape) after the z-pin insertion and VARTM process manufacturing.

The difference in the weight and thickness are due to the quantity, density and width of z-pins fully embedded and inserted through the thickness. The z-pins' excess, after cut and prior to resin infusion, on the top surface, induce the z-pins misalignment (Appendix B), work against the compaction during the process (KNOPP & SCHARR, 2020; MOURITZ, 2007) and also creates resin accumulation on the top surface of the composite laminate after the VARTM manufacturing process.

The Table 2.2 shows the measures for the thickness and weight of the specimens' combinations considering the pin areal density and pin described in the Table 2.1.

Table 2.2 – Thickness and weight of the specimens.

Specimen	Thickness (mm)	Weight (g)
Reference	3.77	25.67
#1	4.19	27.79
#2	4.70	30.66
#3	4.63	26.10
#4	4.69	29.37
#5	3.86	26.15
#6	4.06	28.82
#7	3.93	25.85
#8	4.99	31.77
#9*	4.22	27.77

*Average for the 5 specimens with same insertion and z-pin sizes (from #9 to #13 cited on Table 2.1)

(Intentionally left in blank)

The Figure 2.7 and Figure 2.8 show the thickness and weight increase, respectively, comparing the reference specimens (not reinforced) to the specimens reinforced through the thickness.

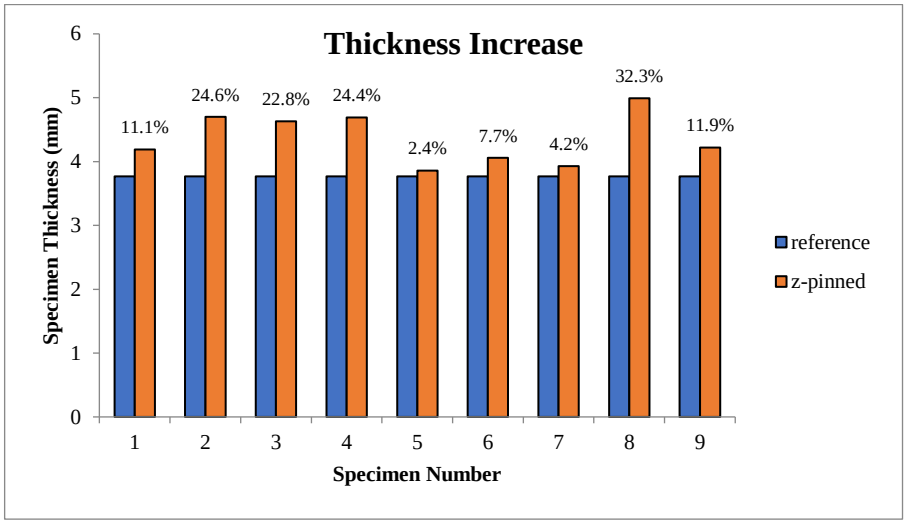

Figure 2.7 – Thickness increase for the z-pinning reinforced specimens compared to reference specimen (not reinforced).

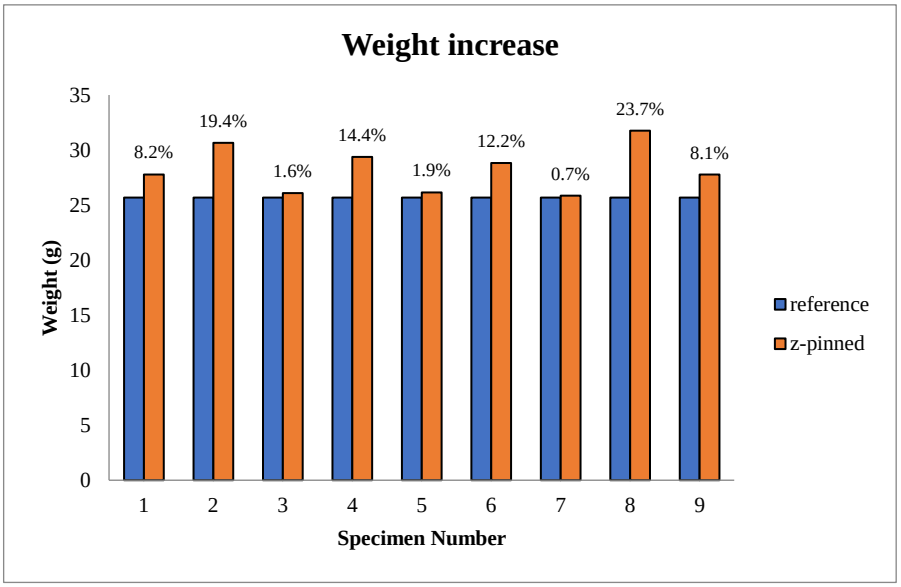

Figure 2.8 – Weight increase for the z-pinning reinforced specimens compared to reference specimen (not reinforced).

2.3.2 Experimental Planning and Design of Experiments

The Response Surface Method is a mathematical and statistical technique based on the fit of a second order equation to the experimental data, which must describe the behavior of a data set.

Thus, firstly is necessary to obtain the suitable approximation between response and variables generated an approximation function of first order, however, if the system reveals a curvature, it is necessary to use a second-order model, that describe the RSM, as shown in Equation 2.4 (Montgomery, 2017).

$$Y = \beta_0 + \sum_{i=1}^{k} \beta_i x_i + \sum_{i=1}^{k} \beta_{ii} x_i^2 + \sum_{i<j} \sum \beta_{ij} x_i x_j + \varepsilon \tag{2.4}$$

Assuming that, the Equation 2.4 demonstrate the response surface model considering the curvature in the system, where k represents the number of design parameters. A typical RSM use this model, the Figure 2.9 (a) represents a central composite design (CCD) that is a type of design used in response surface suitable to generate complete quadratic model using the two design factors related to the pin area density and size (x_d and x_p). Figure 2.9 (b) shows a plot in a 3-D space, where the factors are plotted depending on a response often aiming a fitted surface.

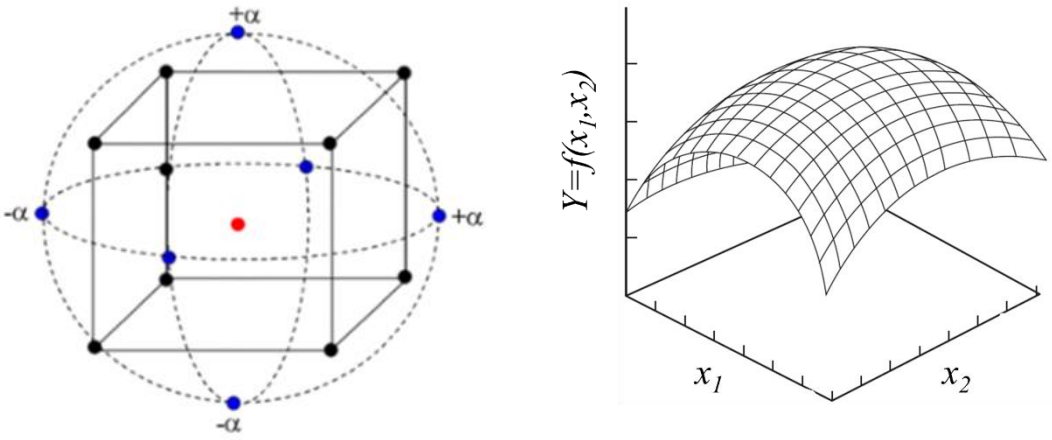

(a) (b)

Figure 2.9 – Typical response surface: (a) Central composite design (adapted from Kumar & Prasad, 2019) and (b) three-dimensional (adapted from MONTGOMERY, 2017).

Therefore, in this study the independent variables are the pin size and the number of pins per area considering three responses (frequency, damping and amplitude shifts). The RSM was used to indicate the optimal manufacturing condition considering mono and/or multi objective optimization. In this study, the optimum condition refers to obtaining optimal manufacturing parameters in order to minimize the amplitude of vibration, for example. For this reason, a central composite design (CCD) using RSM was developed considering the bounds for the two main manufacturing variables as shown in Table 2.3. In addition, Table 2.4 presents the full range of experiments, i.e., 13 manufactured specimens.

Table 2.3 – Input factors and their levels for α = 1.4142.

Control variables	**Symbol**	**Level**				
		$-\alpha$	-1	0	+1	$+\alpha$
Pin areal density	x_d	0.1893	0.50	1.25	2.00	2.3106
Pin size	x_p	0.3964	0.50	0.75	1.00	1.1035

Table 2.4– Response surface model considering two manufacturing (design) factors.

Standard Order	**RunOrder**	**Type**	**Blocks**	**Size**	**Density**
1	1	1	1	0.50	0.50
2	2	1	1	1.00	0.50
3	3	1	1	0.50	2.00
4	4	1	1	1.00	2.00
5	5	-1	1	0.40	1.25
6	6	-1	1	1.10	1.25
7	7	-1	1	0.75	0.19
8	8	-1	1	0.75	2.31
9	9	0	1	0.75	1.25
10	10	0	1	0.75	1.25
11	11	0	1	0.75	1.25
12	12	0	1	0.75	1.25
13	13	0	1	0.75	1.25

2.3.3 Experimental Modal Testing Setup

In order to obtain the results, it was necessary to carry out a quality experimental arrangement. The experimental arrangement was divided into two parts: the first step for the analysis of free vibrations, without the presence of external forces. These tests were fundamental for the acquisition and characterization of the modal behavior of the evaluated structures. In a second step, forced vibration tests were conducted. The external force was applied by a shaker. The entire experimental apparatus is shown in Figure 2.10.

For the experimental tests, a cantilevered beam configuration was selected. Figure 2.10 presents the experimental set-up, which is integrated with sensor, shaker, data acquisition and signal analysis. The instruments used in the experiment include LabVIEW programming, Data Acquisition (DAQ) board, laser sensor and shaker.

The DAQ board used was a model Photon+ by Brüel&Kjær. The laser vibrometer, model VQ-500-D by Ometron, was used to measure the vibration displacement at a specific point. For the free vibration analysis, an impact hammer, Brüel&Kjær, was used in the modal experimental test. The shaker, model 4808 by Brüel&Kjaer, was driven by the voltage signal from the power amplifier, model 2712 by Brüel&Kjaer. The RT Pro Photon software was used for analysis of all obtained signals. Due to the low reflective characteristic of the carbon/epoxy skin, a reflective adhesive tape was used in the sample to avoid losses of signal. The use of a laser vibrometer is better considered than accelerometer since the laser does not influence the total mass of the system and consequently it also does not influence the vibration results.

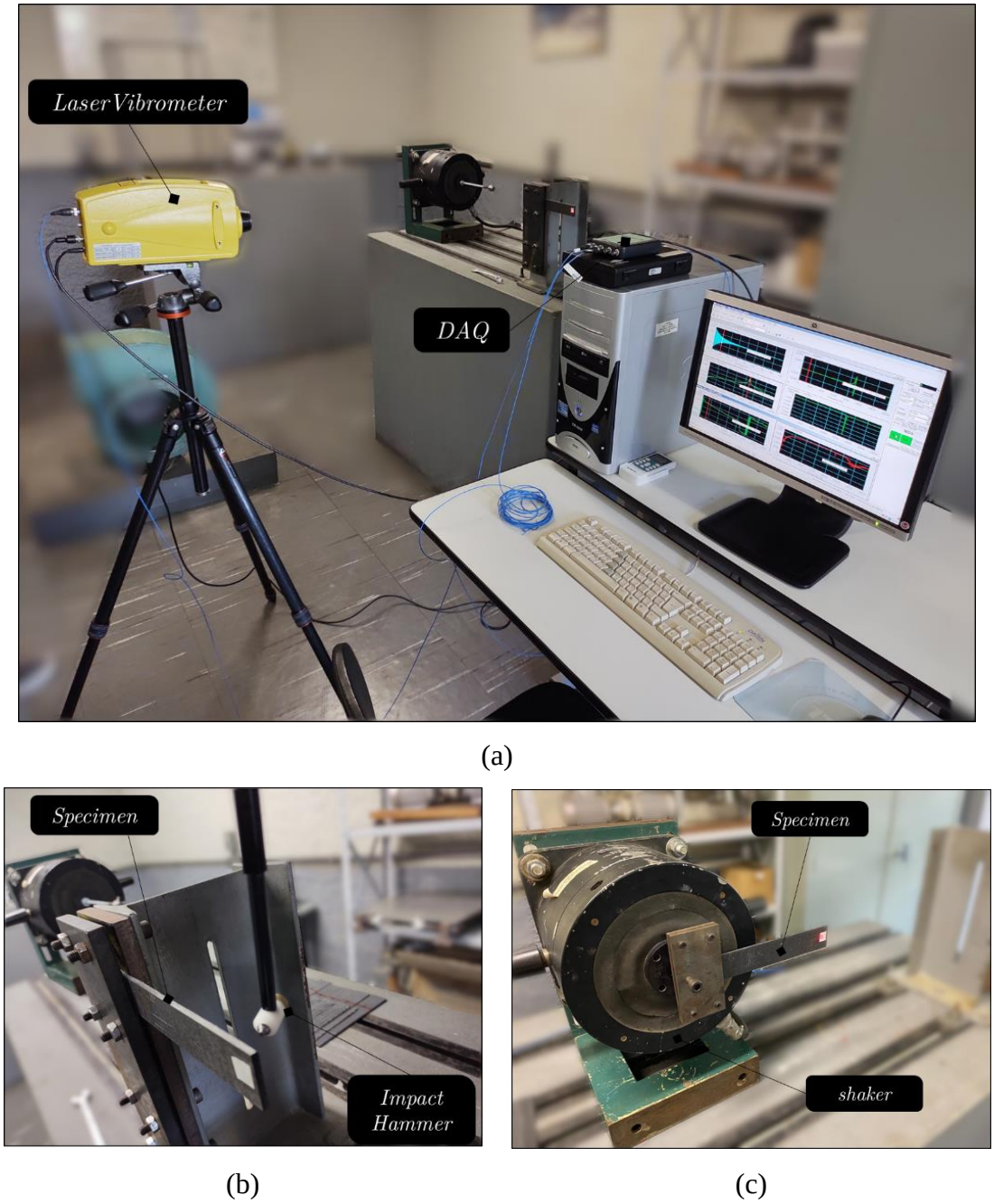

Figure 2.10 – General experimental setup (a) and details for (b) free and (c) forced vibration.

2.4.1 Free Vibration Results

First, experimental analyses were performed for a free-vibration test. Then, the setup presented in Figure 2.10 was used, except by the use of the shaker. By means of this test, it was possible to know the variation of the natural frequencies and damping/loss factor as a function of the manufacturing factors of z-pinning laminated composites. Figure 2.11 shows the main time response results for all the different configurations obtained by the CCD/RSM

in contrast with the reference specimen (without z-pinning process). The stiffness of the pinned specimens is increase since transversal reinforcement is included in the manufacturing. As can be seen, the peak velocity decreases with respect to the reference one.

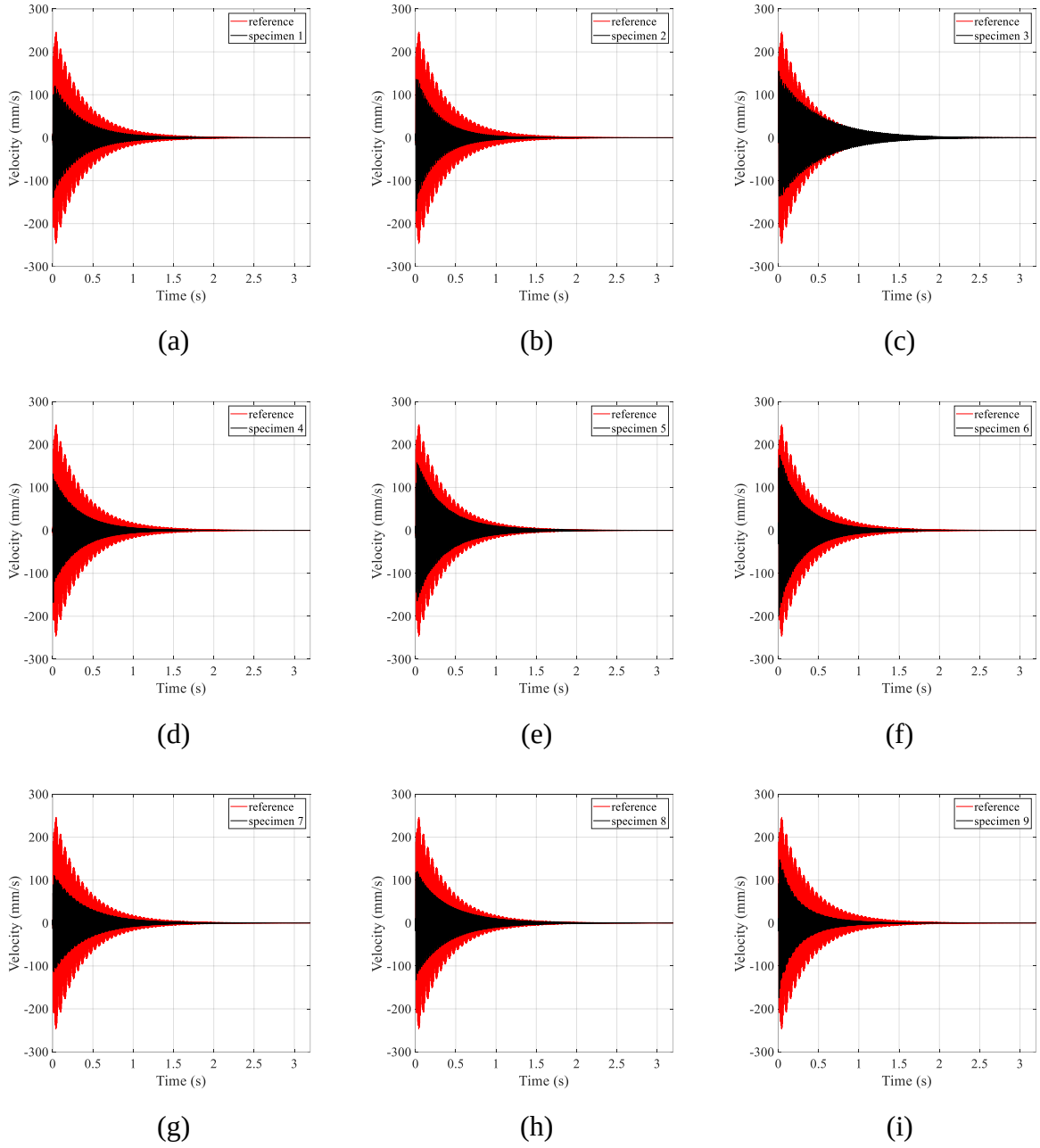

Figure 2.11 – Free vibrations analysis considering the time response for the pinned and reference (no pin) specimens.

In addition, Figure 2.12 shows the frequency spectrum (mobility) highlighting the first mode of vibration for the pinned beams tested. It can be seen, from this Figure, that the insertion of the pins displaces the original natural frequency of the structure (reference). In all cases, there was an increase in the value of the natural frequency (except for Figure 12h).

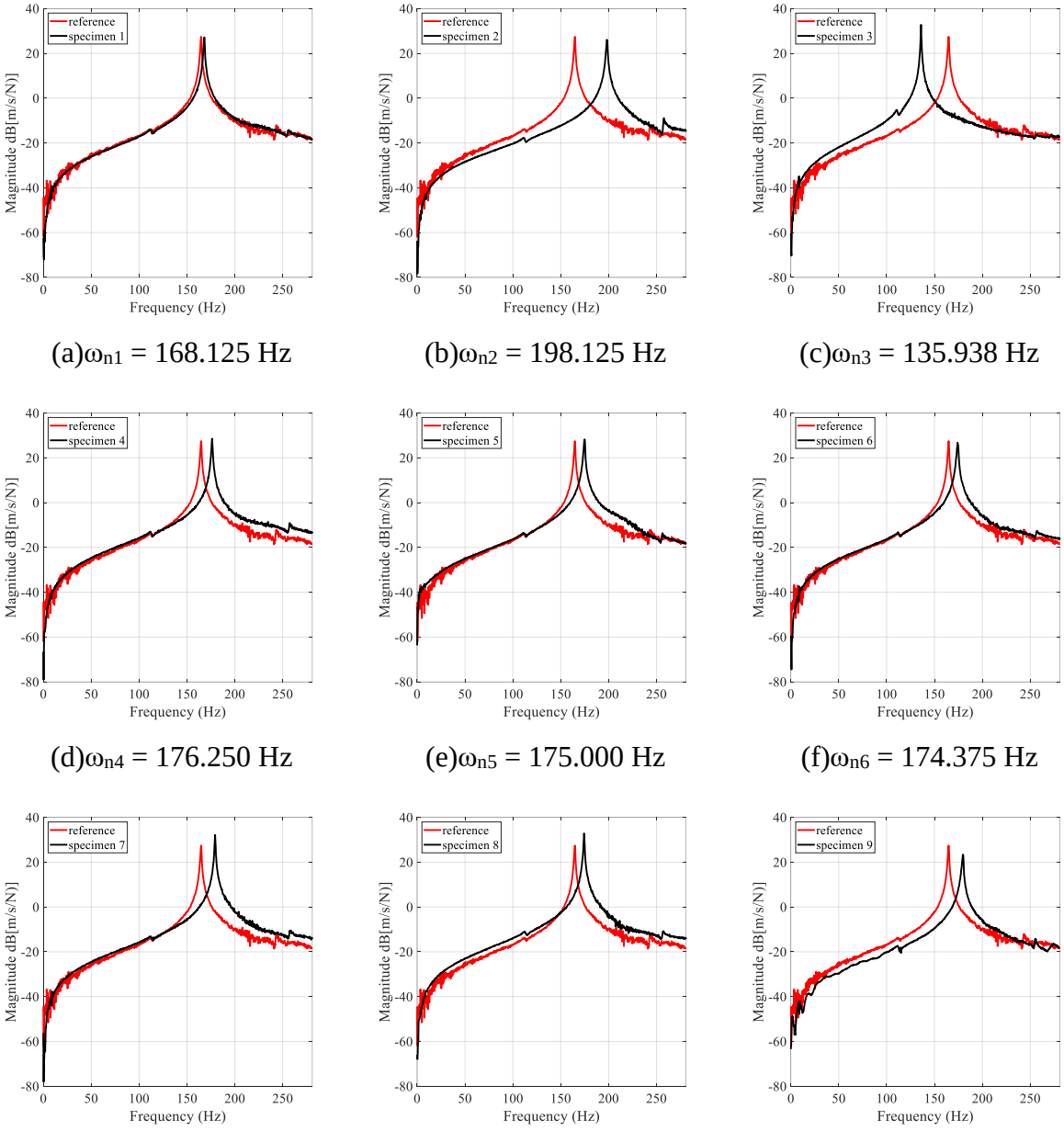

(a)ω_{n1} = 168.125 Hz (b)ω_{n2} = 198.125 Hz (c)ω_{n3} = 135.938 Hz

(d)ω_{n4} = 176.250 Hz (e)ω_{n5} = 175.000 Hz (f)ω_{n6} = 174.375 Hz

(g)ω_{n7} = 179.375 Hz (h)ω_{n8} = 179.688 Hz (i)ω_{n9} = 179.915 Hz

Figure 2.12 – Free vibrations analysis considering the mobility frequency response function for the pinned and reference (no pin) specimens (ωref = 164.687 Hz).

The insertion of the pins leads to a small increase in structural mass; however, the stiffness portion is more significantly affected, since the frequency depends on the stiffness/mass ratio, as shown in Table 2.5.

Table 2.5 – Response surface model considering two factors with responses.

Experiment	Pin Size (mm)	Pin Density (%)	ω_n(Hz)	η	A (mm/s)	$\Delta\omega_n$	$\Delta\eta$	ΔA_{max}
Reference	unpinned		164.69	0.0052	51.17	-	-	-
1	0.50	0.50	168.13	0.0057	8.70	2.08	8.59	82.98
2	1.00	0.50	198.13	0.0057	12.97	20.30	8.79	74.64
3	0.50	2.00	135.94	0.0045	28.19	-17.45	-12.92	44.89
4	1.00	2.00	176.25	0.0054	7.84	7.02	3.36	84.66
5	0.40	1.25	175.00	0.0054	10.73	6.26	3.89	79.02
6	1.10	1.25	174.06	0.0059	8.03	5.69	13.25	84.29
7	0.75	0.20	179.38	0.0047	11.36	8.91	-9.47	77.78
8	0.75	2.30	174.38	0.0051	10.15	5.88	-1.62	80.14
9	0.75	1.25	179.69	0.0066	10.25	9.10	25.52	79.95
10	0.75	1.25	179.92	0.0067	10.26	9.24	28.84	79.93
11	0.75	1.25	180.83	0.0067	10.30	9.79	28.84	79.85
12	0.75	1.25	179.57	0.0066	10.15	9.21	26.92	80.14
13	0.75	1.25	178.13	0.0065	10.22	9.37	25.00	80.02

Equally important, in order to determine the damping factor of the curves, an adjustment by the nonlinear least squares' method was performed. For this, Equation 2.5 (HARRIS & PIERSON, 2002; DE SOUZA ELOY *et al.*, 2018) was used as the answer to the analytical solution. Equation 5 concerns the equation in displacement and Equation 6, in velocity, of a system in free vibration damped with a degree of freedom, assuming damping factors less than 1. x_p

$$y(t) = e^{-\xi\omega_n t}\left[A\cos(\omega_d t) + B\sin(\omega_d t)\right] \tag{2.5}$$

$$\dot{y}(t) = -\xi\omega_n\left[\frac{A\cos\left(\omega_d t\right) + B\sin\left(\omega_d t\right)}{e^{\xi\omega_n t}}\right] - \left[\frac{A\omega_d \sin\left(\omega_d t\right) - B\omega_d \cos\left(\omega_d t\right)}{e^{\xi\omega_n t}}\right] \tag{2.6}$$

where ω_n represents the natural frequency(rad/s), ω_d is the damped frequency and ξ is the damping factor.

An example of a velocity curve response over time is shown in Figure 2.13. With these responses in graphic form, it became possible to determine the damping/loss factors of the laminated beams as a function of the different z-pinning configuration which will be described in sequence.

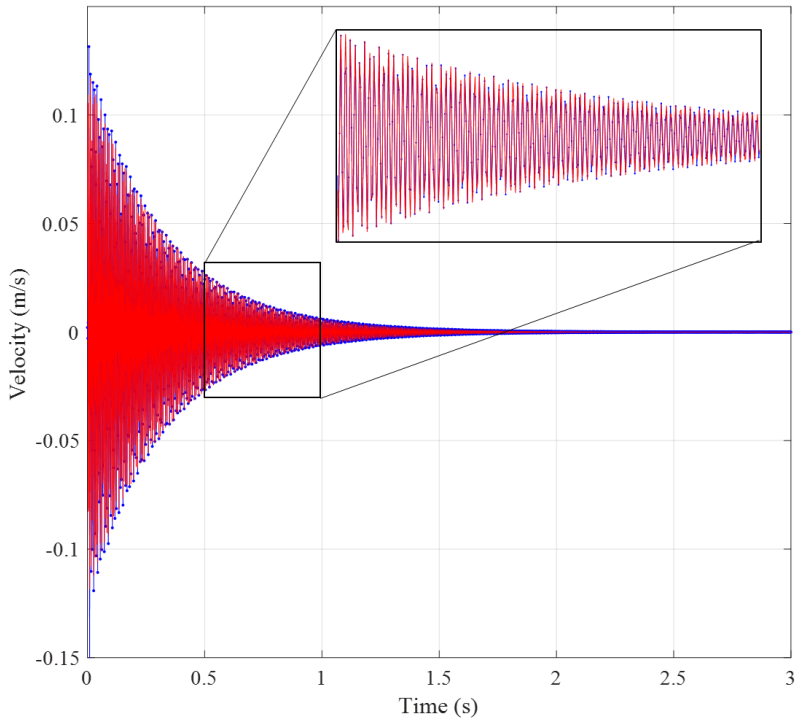

Figure 2.13 – Velocity response and response adjustment using least squares method to obtain damping factors (legend: ▬ experimental and ▬ adjusted curve).

Table 2.6 shows the values of the loss factors obtained by the proposed adjustment. It can be seen that in general the damping of the structure is very low, which was already expected by the type of material studied. It can be noted that the damping factor, although low, is directly related to the type of pin configuration, with positive and negative variations in relation to the reference. Therefore, an optimal manufacturing parameter maximizes/minimizes, for example, the loss factor. Finding this point is only possible through the methodology proposed through RSM.

Table 2.6 – Free vibration results for natural frequency and loss factor.

Experiment	ω_n	η	Experiment	ω_n	η
Reference	164.687	0.0052	**7**	179.375	0.0047
1	168.125	0.0057	**8**	174.375	0.0051
2	198.125	0.0057	**9**	179.688	0.0066
3	135.938	0.0045	**10**	179.915	0.0067
4	176.250	0.0054	**11**	180.825	0.0067
5	175.000	0.0054	**12**	179.565	0.0066
6	174.063	0.0059	**13**	178.125	0.0065

2.4.2 Forced Vibration

The second part of the modal analysis consists of performing the forced vibration test to check the vibration amplitude. The support used in the free vibration test is different from that used in the forced vibration test, since the shaker was not used in the first one. All beams were excited according to their characteristic natural frequencies (Table 2.6) and observed their response over time. Figure 2.14 shows the results of the time vibration tests for the 1stmode as a function of the different manufacturing designs.

The Figure 2.14 shows as a comparison the results of forced vibration in the natural frequency characteristic of each beam. The maximum amplitude of resonance vibration (A) for the beam without pins was 51.1690 mm/s. The results indicate that there was a significant reduction in this amplitude when considering composite materials with z-pinning. For example, beam #4 (Figure 14d) had a maximum amplitude of 7.8463 mm/s, which means a reduction of approximately 85% of the vibration level.

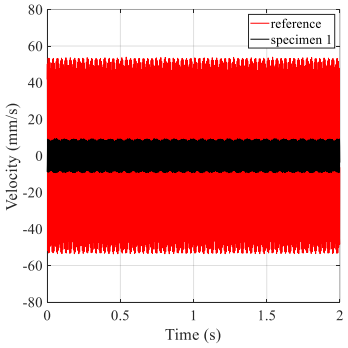

(a)A_1 = 8.7042 mm/s

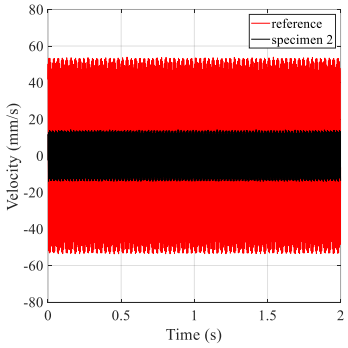

(b)A_2 = 12.9731 mm/s

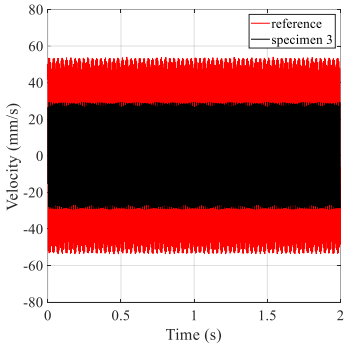

(c)A_3 = 28.1909 mm/s

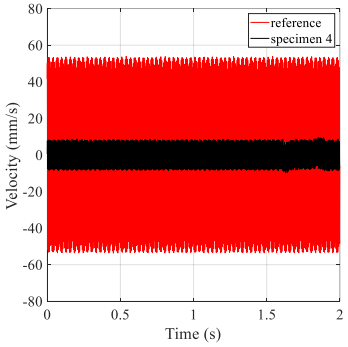

(d)A_4 = 7.8463 mm/s

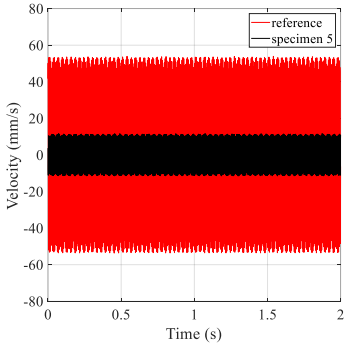

(e)A_5 = 10.7308 mm/s

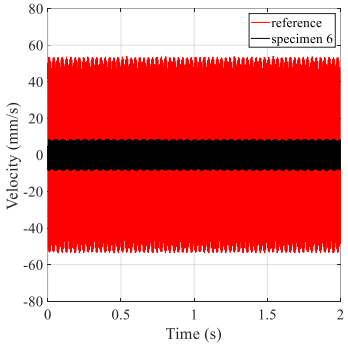

(f)A_6 = 8.0371 mm/s

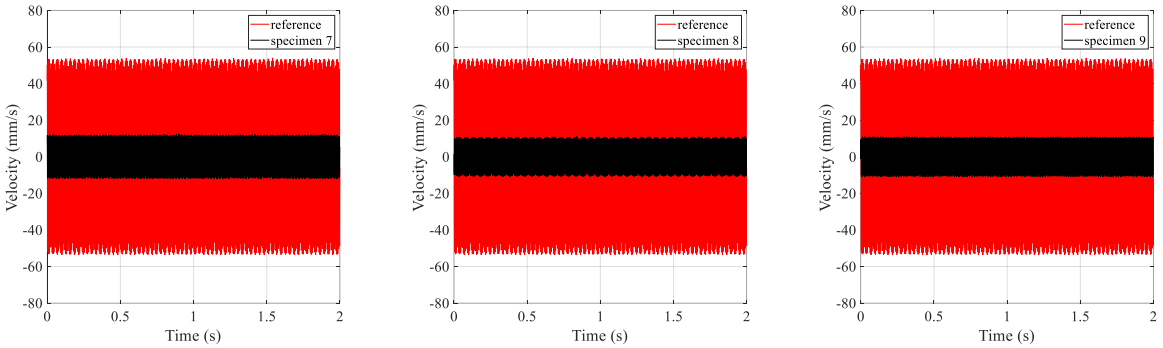

(g)A_7 = 11.3681 mm/s (h)A_8 = 10.1592 mm/s (i)A_9 = 10.2555 mm/s

Figure 2.14 – Forced vibrations in time domain for the pinned and reference (no pin) specimens

2.4.3 Statistical Results

This study has as main objective the dynamic characterization of laminated composites structures with z-pinning. The results were conducted from an experimental planning using RSM, where the parameterization of the manufacturing process was carried out according to two decision variables considering three modal responses, that is, natural frequency, loss factor and maximum amplitude of vibration. For the analysis of the statistical results, the modal responses were normalized by analyzing the percentage variation, as shown in Equation 2.7 to Equation 2.9. Table 2.5 summarized the overall results of this study, with the experimental arrangement and responses.

$$\Delta\omega_n = \left(1 - \frac{\omega}{\omega_{ref}}\right) \times 100 \tag{2.7}$$

$$\Delta\eta = \left(1 - \frac{\eta}{\eta_{ref}}\right) \times 100 \tag{2.8}$$

$$\Delta A = \left(1 - \frac{A}{A_{ref}}\right) \times 100 \tag{2.9}$$

Figure 2.15 represents the result obtained by means of an analysis of variance (ANOVA) of the responses as a function of the manufacturing factors. For all three modal responses evaluated, it is clear that the construction parameters directly impact their results.

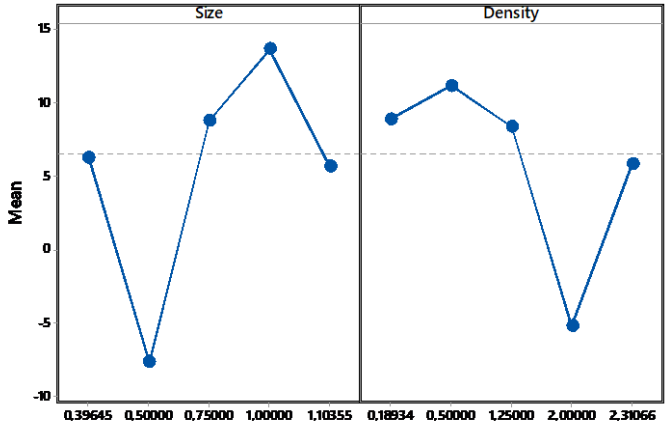

(a)Δω

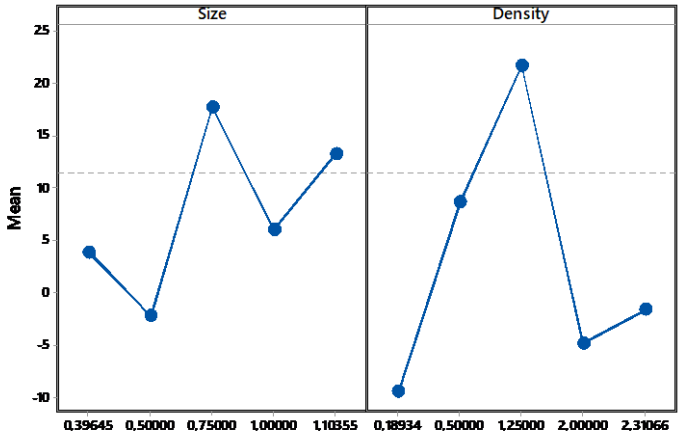

(b)Δη

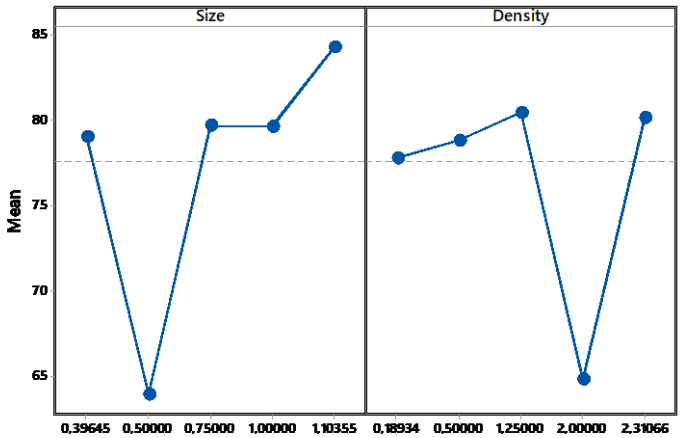

(c)ΔA

Figure 2.15 – Analysis of variance for the main effects for (a) natural frequency, (b) loss factor and (c) amplitude shifts.

Equally important, this can be proven with residual analysis using a normal probability plot (Appendix A) for each response. In order to state the effect of interactions between the factors and that parameters contributed to the response variability were generated Pareto chart effects, as shown Figure 2.16. The Pareto charts represent the main effects and their interactions, the dashed red line symbolizes the relevance of the effects.

It can be seen that the natural frequency depends on factors A (size) and B (density) as shown in Figure 2.16 (a). The structural damping (although small) depends strongly on the BB (density²), AA (size²) and A terms, Figure 2.16 (b). Finally, the amplitude of vibration of the laminate depends on the iteration of factors AB (size × density) and factor A. In all three responses evaluated, factor A, i.e, the pin size, is of crucial importance in terms of modalities.

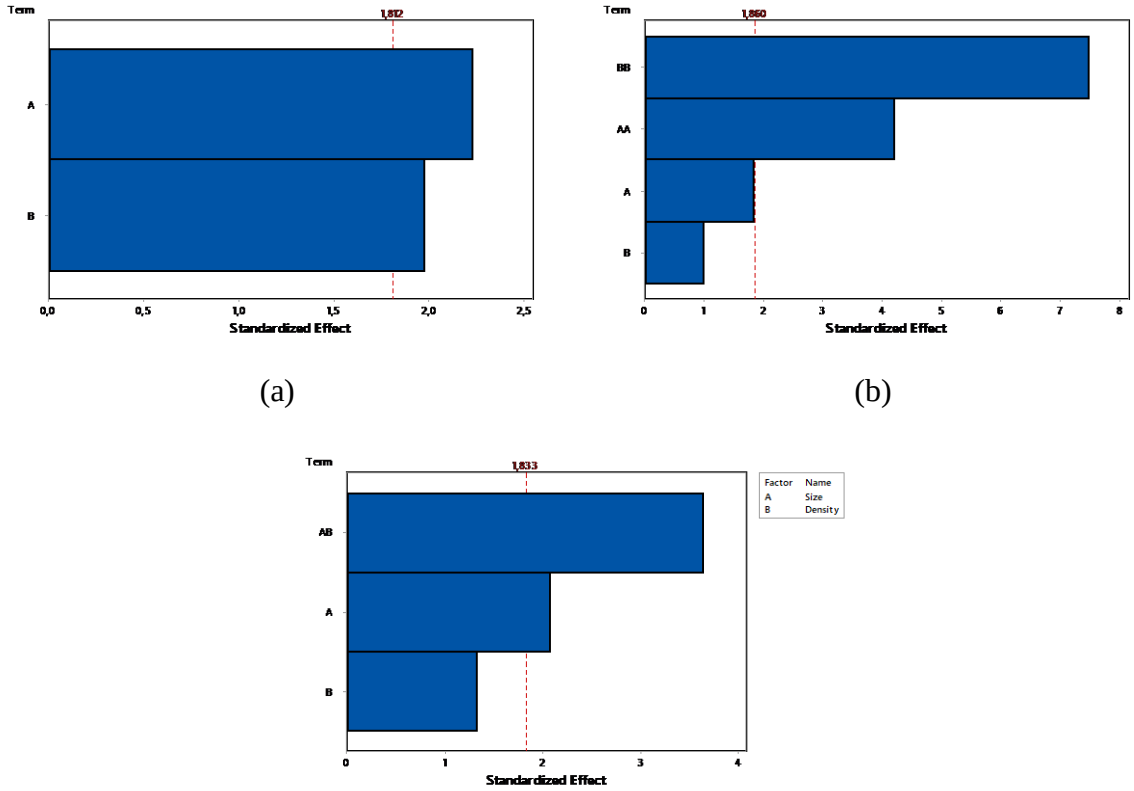

(a) (b)

(c)

Figure 2.16 – Pareto main effects plots for (a) natural frequency, (b) loss factor and (c) amplitude shifts (legend: A = size, B = density)

Considering the relevance of the effects in each factor, as depicted in Pareto charts, main effects charts were elaborate aiming to provide the difference between the levels of

factors in relation the responses, as is depicted in Figure 2.17. The main effects chart (Figure 2.17) shows that the smaller the pin size is, the lower the frequency and amplitude values of vibration are. On the other hand, the higher the density of pins per area, the lower the frequency and amplitude values will be. The frequency and amplitude responses of vibration have a similar relationship with the manufacturing variables. The damping response has an evident curvature, where the maximum damping value is only obtained for a specific size and density value, being outside the limits addressed in the RSM (bounds).

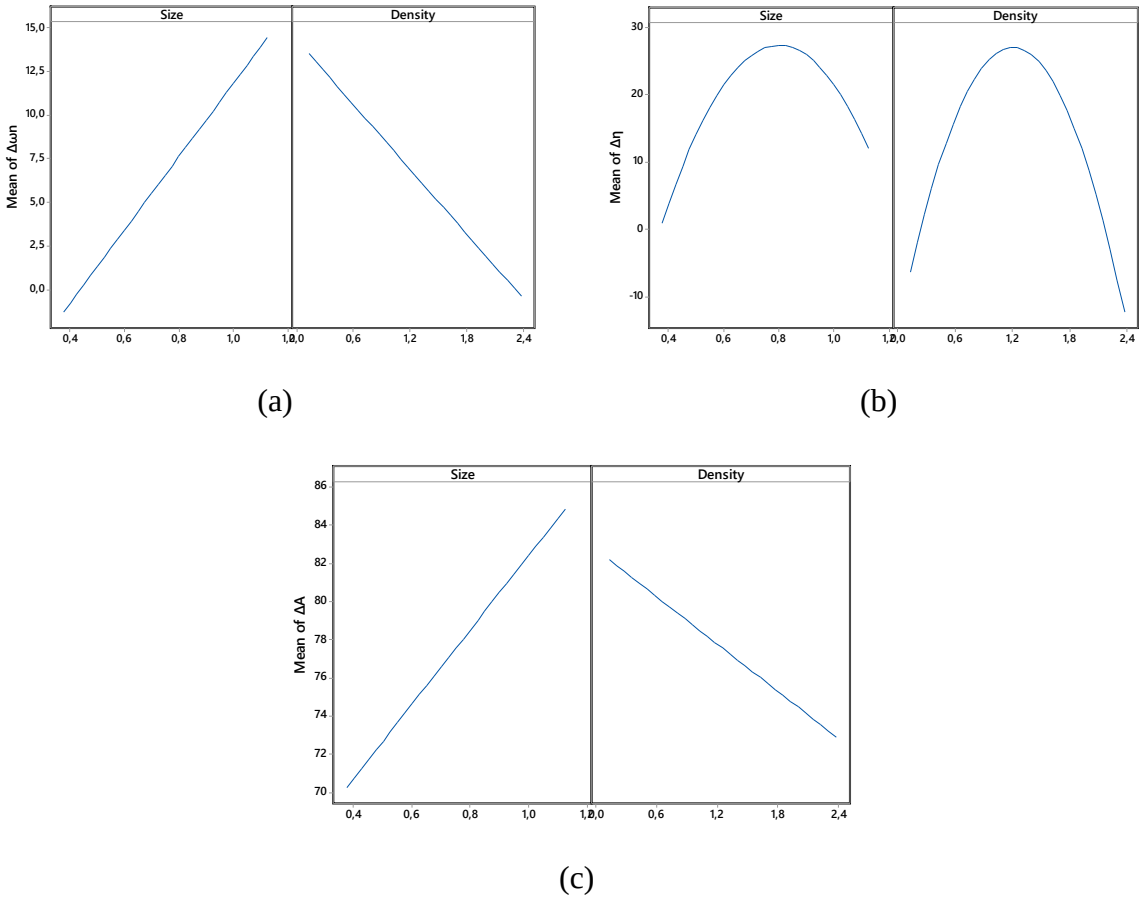

Figure 2.17 – Main effect for fitted means: (a) natural frequency, (b) loss factor and (c) amplitude shifts.

2.4.4 Optimization

The experimental arrangement carried out by means of RSM allowed the obtainment of a model (or meta-model) that is able to represent the modal responses according to the construction parameters in question. The modal responses in terms of frequency variation, loss factor and amplitude are represented in Equation 2.10 to Equation 2.12. The equations

obtained are derived from the second order regression model shown in Equation (4). The model obtains the constant β coefficients in order to better fit the real experimental response.

The three-dimensional results of these equations are represented on the surfaces of Figure 2.18. Note that only significant terms are part of the model in question. Once you have the nonlinear equations that represent the problem, an optimization process can be performed:

$$\Delta\omega_n = -1.40 + 20.94x_p - 6.19x_d \tag{2.10}$$

$$\Delta\eta = -107.800 + 233.60x_p + 69.25x_d - 145.90x_p x_d - 28.76x_d^2 \tag{2.11}$$

$$\Delta A_{\max} = 128.30 - 60.80x_p - 52.20x_d + 64.10x_p x_d \tag{2.12}$$

where x_p = pin size and x_d pin density.

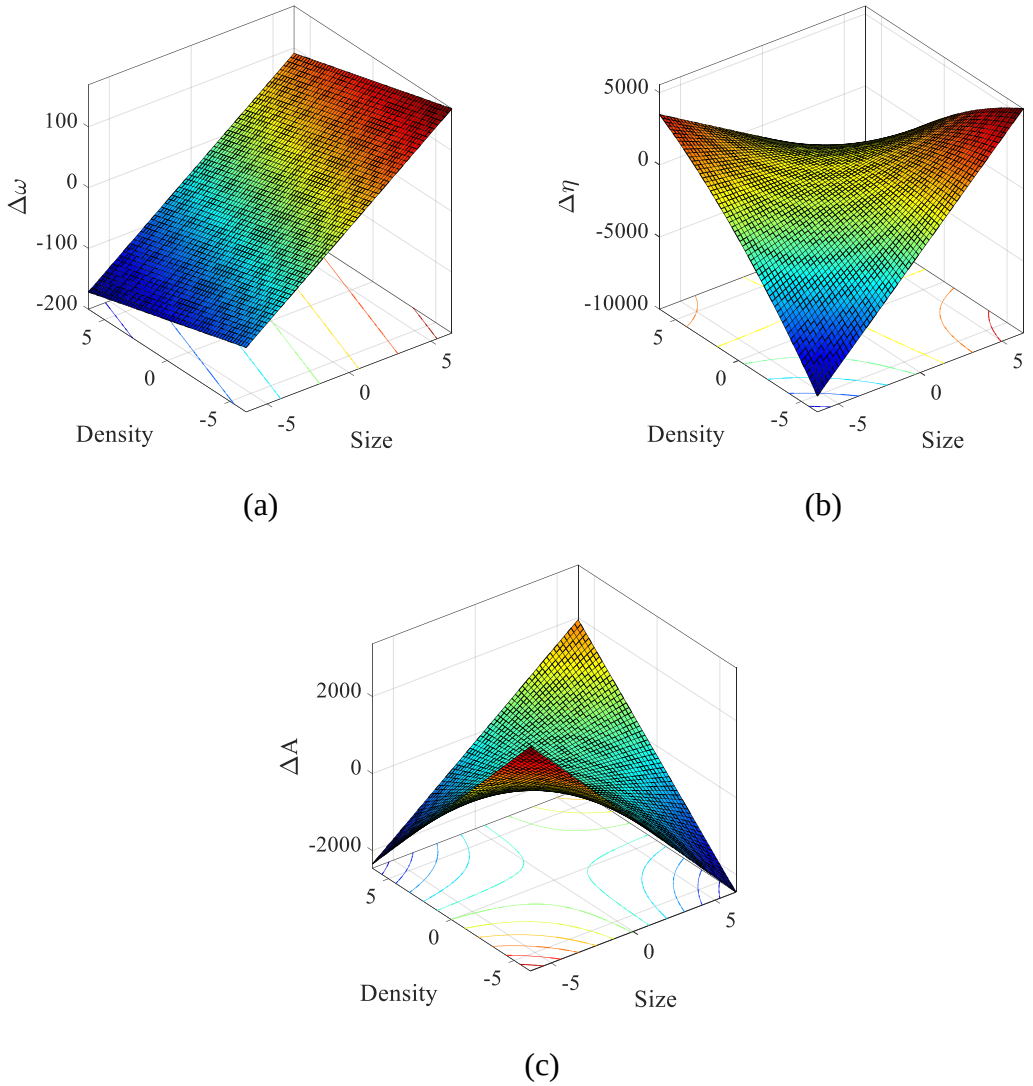

Figure 2.18 – Response surfaces in space for (a) natural frequency, (b) loss factor and (c) amplitude shifts.

The surface plots showed in Figure 2.18, reveal a quadratic response surface, especially for the loss/damping factor response where the maximum point are localized in optimum region. Table 2.7 shows the optimization results (search for maximum or minimum points) considering only one objective at a time (mono) and in a multi-objective character. Note that the most significant result was for optimization regarding the reduction of vibration amplitudes, reaching values in the order of 115% reduction. Furthermore, in a multiobjective nature (where there are no ever-lasting gains), reductions of the order of 81% have been achieved for amplitude where at the same time there has been an increase of 25% in the loss factor and 11% in natural frequency.

Table 2.7 – Mono and multiobjective optimization considering the meta-model obtained by RSM.

Case	Objective	Variable	Size	Density	Response
1	Maximize	$\Delta\omega_n$	1.1036	0.1893	20.5405%
2	Maximize	$\Delta\eta$	0.8036	1.2067	27.4654%
3	Maximize	ΔA_{max}	1.1036	2.3107	114.1195%
4	Maximize	$\Delta\omega_n$ $\Delta\eta$ ΔA_{max}	0.9536	1.2179	11.0357% 24.0643% 81.3236%

The optimal solution is shown in Figure 2.19 with the design space limited by manufacturing and response constraints. It can be seen that only the damping response has an active constraint (contour) and the others are non-trivial solutions.

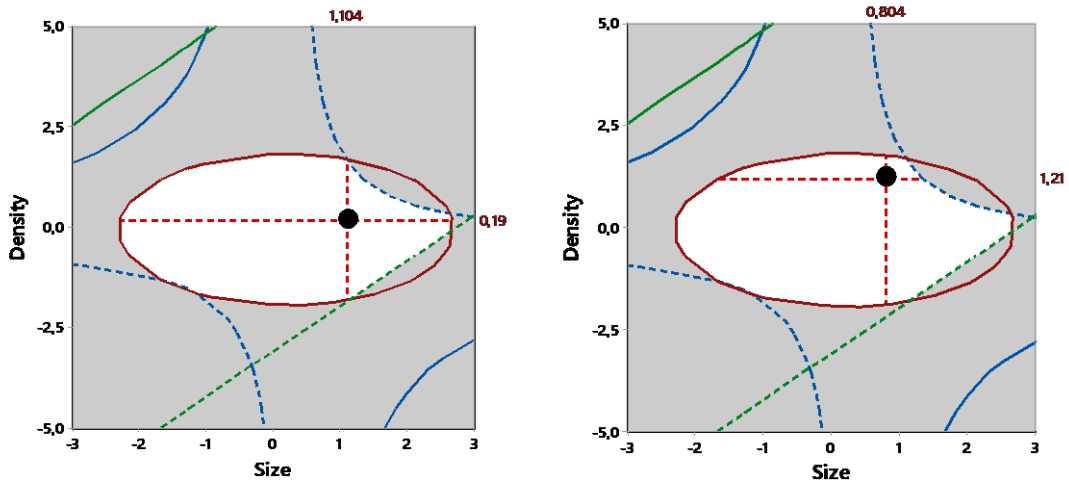

(a) (b)

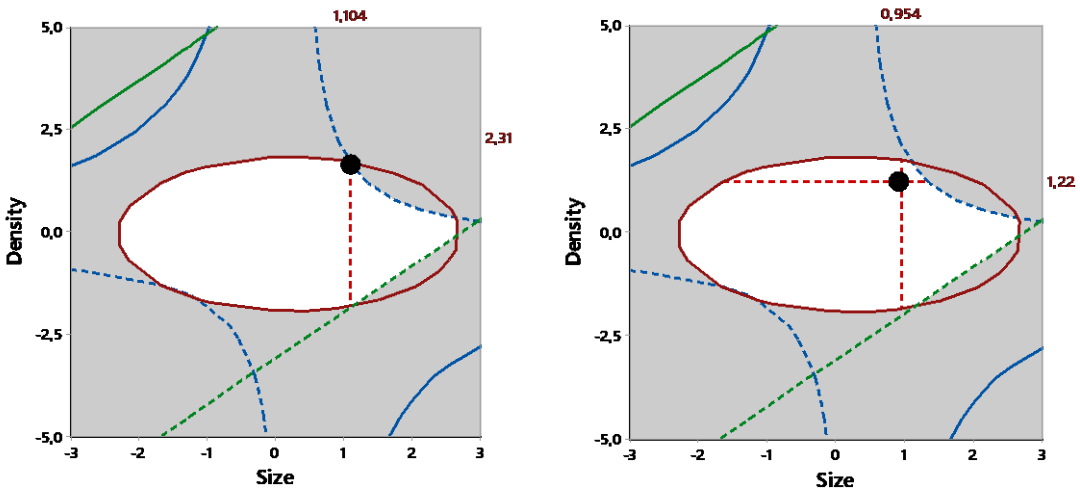

(c) (d)

Figure 2.19 – Optimal responses over the constrained objective space for the case (a), (b), (c) and (d).

2.5 Conclusions of Chapter 2

In this study, an experimental characterization of the modal response of carbon beams with z-pins was performed. The experiment procedure was guided by DOE using an RSM. Several specimens were manufactured and their modal responses such as frequency, amplitude were evaluated. The main conclusions of this study can be listed:

- The insertion of pins promotes a change in modal responses since it changes the stiffness matrix of the material.
- Natural frequency and damping (loss factor) are significantly dependent on the pin size and also on the number of pins per unit area
- The amplitude of vibration depends exclusively on the size of the pin in question. There is a significant interaction between size and number of pins on this response.
- The RSM methodology was able to adjust the response as a quadratic model and to optimize the manufacturing process (mono and multi objective).

CHAPTER 3: ON THE INFLUENCE OF RECTANGULAR Z-PINS PARAMETERS ON MODE II DELAMINATION RESISTANCE OF THROUGH THE THICKNESS REINFORCED COMPOSITES

Z-pinned composites are an important class of materials increasingly used in aerospace applications, civil construction, and automotive industry. Although many numerical and experimental studies exist on this topic, few works employ modern and efficient computational techniques. This chapter presents for the first time in the literature a study using Artificial Neural Network (ANN) to predict mode II interlaminar fracture toughness in composite materials using z-pinned materials. Z-pins with different rectangular shape and pin area densities are manufactured with design variables generated from Design of Experiments. Thus, Response Surface Model and Analysis of Variance are used to support a detailed statistical discussion of the experimental results. The generated data are used to training an Artificial Neural Network, which is applied to predict and assess the influence of the pin size and density configuration in the interlaminar fracture properties of z-pinned composites structures.

3.1 Introduction

Carbon fiber reinforced plastics (CFRP) are largely used in structural components, in aerospace applications, civil construction, automotive industry, and so on, due to their excellent mechanical properties and weight to stiffness ratio of the material (LIAO *et al*., 2021; WEI *et al*., 2019). Apart from these excellent properties which can be achieved in the laminate plane (in-plane), there is also a drawback in out-of-plane properties such as insufficient impact, pull out and delamination properties (LIU *et al*., 2019; WEI *et al*., 2020) . Interlaminar fracture, or delamination, is the most frequent failure mode in thermoset and thermoplastic matrix composites and to improve the interlaminar performance of composite laminates, a variety of 3D reinforced composite materials structures such as braiding, stitching, tufting and z-pinning have been developed (GOMES *et al.*, 2018a; BARBOSA *et al*., 2019, BORTOLUZZI *et al*., 2019).

The z-pinning through the thickness reinforcement technique has been widely researched due to its simple process and low cost, which is made inserting metal or carbon rods (Z-pins) into dry preforms and uncured composites. The z-pin insertion in the thickness direction has been proven to mitigate the delamination crack propagation in mode I and mode II and the improvement for the impact damage resistance reducing the delamination propagation. The enhancement in the interlaminar fracture toughness (G_{IIc}) and impact properties of composites can be controlled by the volume content or density insertion, diameter, shape and material type of the z-pins (FEI *et al*., 2021; M'MEMBE *et al*., 2016; MOURITZ & KOH, 2014; CARTIÉ *et al*., 2006).

The subject has attracted industrial and scientific attention. Knaupp & Scharr (2013) studied the influence of circular and rectangular z-pins on impact and Compression After Impact (CAI) properties in composite laminates. The composites reinforced with both rectangular and circular z-pins showed a considerably greater capacity to mitigate the growth of delamination (damaged area) after impact and showed values of 25% and 15% higher for rectangular and circular z-pins, respectively, compared to without reinforcement.

In this sense, Knaupp and Scharr (2014) investigated the influence of insertion, with different densities (0.5% and 1%), of rectangular and circular z-pins on fracture toughness properties interlaminar in mode I. For composites with a density of 0.5% these composites showed an increase in properties in mode I, compared to unreinforced, of 92% and 140% for the circular and rectangular z-pins, respectively. For the insertion of 1% the increase in properties was 140% and 220% for the circular and rectangular z-pins, respectively.

Equally important, Pegorin *et al.* (2015) studied the behavior of reinforced composite laminates through thickness with 0.28mm diameter z-pins with insertion density 0.5%, 2% and 4%, subjected to out-of-plane shear loading (mode II) and these showed an increase in fracture toughness properties, in relation to those without z pins in the thickness direction, of 236%, 372% and 963%, respectively.

In the same way, Yasaee *et al.* (2016) determined the properties of (G_{IIc}) in 0.28mm diameter z-pin reinforced composites with a density of insertion of 2% and described an increase of 294% in relation to composites not reinforced. In another study, the same authors (YASAEE *et al*., 2017) conclude that thermosetting brittle epoxy composite showed minor increase in the apparent (G_{IIc}). In addition, Ravindram *et al.* (2019b) showed the behavior under mode II loading of composites reinforced through the thickness with circular z-pins of

different diameters, 0.28mm and 0.51mm, with an insertion density of 2%. The results obtained for the (G_{IIc}) showed an increase, compared to those without 3D reinforcement, of 248%, for the 0.28mm z-pin, and 370% and 0.51mm for z-pins.

Complementarily to several experimental studies, soft computing techniques including machine learning algorithms have been applied for predicting or identifying behaviors in composite materials. Zhang and Friedrich (2003) presented a review with a neural network approach for predicting certain properties of polymer composite materials such as fatigue life, response under loading situations, mechanical properties also composite processing optimizations.

Recently, Gomes *et al*. (2018) presented a review on structural health monitoring (SHM) methodology and development of solutions for structural monitoring problems such Genetic Algorithm (GA) and Artificial Neural Networks (ANN). Di Benedetto *et al.* (2021) studied the use of computational methods to describe mechanical and structural properties and developed an ANN to predict the energy absorption of thermoplastic commingled composite materials.

Maurya *et al.* (2022) investigated an ANN to determine delamination length and location defect in carbon fiber reinforced polymer composite analyzing the first three natural frequencies obtained using finite element analysis (FEA) and achieved great results. Balcioglu & Seckin (2021) analyzed the fracture behaviors of polymer composites in Mode I, Mode II, and Mode I/II loading situations using and comparing several machine learning algorithms. The efficiency of these algorithms was proven with experimental validation, although only more specialized algorithms in classification algorithms were used: K Nearest Neighbors, Decision Trees, Random Forest, and Support Vector Machine.

This paper not only presents for the first time in the literature a study using ANN to predict interlaminar fracture toughness in composite materials, but also using z-pinned materials. The influence of z-pinning in the interlaminar fracture toughness, in mode II, of laminated structures is carried out. For this, specimens with different rectangular shape inserted z-pins sizes and pin areal densities are manufactured after Design of Experiment (DOE) matrix determination. Thus, Response Surface Model (RSM) and Analysis of Variance (ANOVA) are used to deeply interpret and discuss the results. So, a determinate part of the generated data is used to train an Artificial Neural Network (ANN), which is applied as technique to predict and assess the influence of the pin size and density configuration in the

interlaminar fracture properties of z-pinned composites structures and the remaining data is used for validation. Also, is important to point that the ANN was used because RSM quadratic response surface did not obtained a model able to represent the fractures toughness responses due to its high the nonlinearity.

The manuscript is organized as follows: Section 2 presents a theoretical background. Section 3 presents the methodology of this work. Section 4 brings the results and discussions, and Section 5 concludes the research.

3.2 Theoretical Background

3.2.1 Z-pinning

Z-pinning is a well-established technology to insert rods in the thickness, or Z, direction of fiber reinforced plastics polymer matrix composites and this rods, or z-pins, can be inserted in areas prone to delamination (ALLEGRI *et al*., 2014). Most z-pins are circular and manufactured of high strength carbon, SiC, titanium and stainless steel with sizes varying from 0.28 mm to 1.00 mm diameter and are usually inserted through-the-thickness of uncured laminates to a volume content of 0.5 – 5% (DANTULURI *et al*., 2007; MOURITZ & CHANG, 2014). This technique has proven to be very effective to increase the interlaminar fracture toughness in mode I and mode II, impact damage and also delamination resistance in bonded composite joints (MOURITZ, 2013).

Aztex Inc. (Waltham,USA) developed the Ultrasonically Assisted Z-Fibre (UAZ) process to insert a large number z-pins UAZ. This is the most common process for the z-pinning of prepreg laminates. In this process the z-pins are inserted into a foam carrier, varying the pins' density and size. The foam preform with the z-pins is placed on top surface of the uncured laminate and the ultrasonic horn is passed over the preform, generating high frequency compressive waves that collapse the foam and slowly push the pins through the thickness of the prepreg preform. The excess of z-pins length with the crushed foam are cut. This is achieved by the pulsating waves that heat the preform, softening the matrix, and slowly push the z-pins through the laminate thickness (KOSTOPOULOS *et al*., 2020; MOURITZ, 2007). Figure 3.1 shows the scheme for z-pin insertion in UAZ technique.

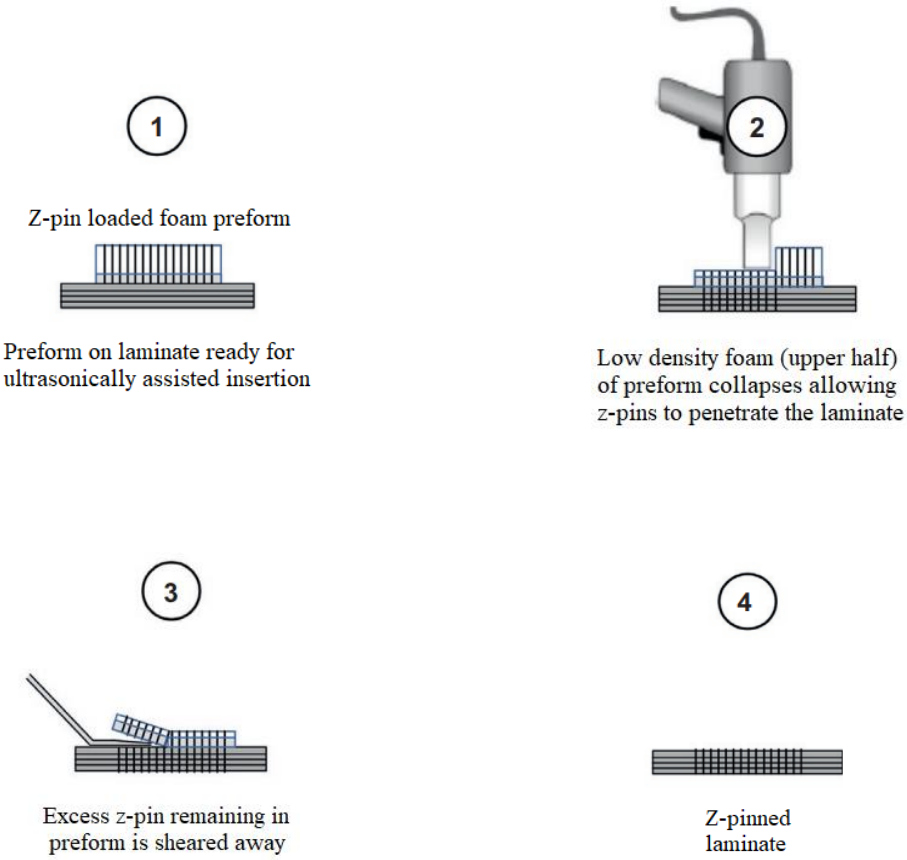

Figure 3.1- Schematic of UAZ z-pinning reinforcement technique (adapted from PARTRIDGE et al., 2015).

In addition to the UAZ process, other methods can be used to insert z-pins through the thickness of prepreg, manually impregnated and dry fabric preforms. A manual and ease of application, low-cost, laboratory-based method was used by Fert (2016) at Imperial College London. This technique consists in the use of a metallic sewing needle with a diameter of 0.8 mm, attached to a small mandrel to perforate the prepreg preform. The chuck with the needle was placed in a bench drill to have a high level of alignment and to facilitate the needle penetration. Due to the polished surface and the sharp point of the needle, penetration of the needle into the preform does not cause so much misalignment in the fibers. After the needle is withdrawn, the z-pins are positioned, without applying force, in the holes made with the metallic needle and the excess is cut.

Another method was developed by EADS IW (VAZQUEZ *et al.*, 2011). The process is automated and performed with the aid of a robot with 7 axes movement. This process consists of inserting a vibrating hollow needle through the thickness of a dry preform. When the needle with a z-pin positioned inside it reaches the desired insertion depth occurs the

withdrawal movement and the z-pin remains inside the preform. After the insertion, the z-pins' excess were cut and the part was manufactured by Resin Transfer Molding (RTM).

Ladani *et al* (2016) carried out the the z-pinning process by placing the z-pin foam carrier in the wet-hand layup and compressed the laminate assembly within a hydraulic press with a pressure of 350 kPa. The excess z-pin length was trimmed after the laminate was cured. In another study, Bortoluzzi *et al* (2021) manually inserted rectangular z-pins, aided by a hollow needle, in the thickness direction of dry fabric preforms and the composite laminates were manufactured using the VARTM process.

Loh *et al.* (2021) used the z-pinning technique to reinforce braided fabric stacks thought the thickness and the preforms were infused with liquid epoxy at room temperature using the vacuum bag resin infusion process.

Efforts to make z-pinning economically attractive were performed in this work where the z-pins were manufactured in house, inserted manually in a dry fabric preform and the composite laminates were manufactured using the VARTM process.

3.2.2 Design of Experiments and Response Surface Methodology

Response surface methodology (RSM) is a statistical approach widely applied for reduce the number of experiments and to optimize the variables through a regression model created by a fitting quadratic surface (MONTGOMERY, 2017). It refers to an experiment planning process that relates the independent variables (input factors) to the dependent variables (output response), creating a mathematical model. In this model, the input factors and their levels are constantly changed, making it possible to establish the factors with the greatest influence on the output response, along with the relevance of the interactions between them (WERDINE *et al*. 2021). Further, the RSM considers that an order-second equation should be able to describe the behavior of a dataset, as can be seen in Equation 3.1 (MONTGOMERY, 2017).

$$y = \beta_0 + \sum_{i=1}^{k} \beta_i x_i + \sum_{i=1}^{k} \beta_{ii} x_i^2 + \sum_{i<j} \sum \beta_{ij} x_i x_j + \varepsilon \qquad (3.1)$$

where y is the response variable of the issue under study, the β is the model constant, k represents the number of design parameters, x_1 and x_2 are the factors, and e the random error term.

A central composite design (CCD) is employed for fitting a second-order modal created by RSM. The CCD consists of a two-level factorial design with factorial (+1 and -1), axial (+α and –α) and center points, which in this case is composed of two input factors, such as pin area density and pin size, and two response factors related to (G_{IIc}) values on generated in the mode II tests for NPC and PC steps (MONTGOMERY, 2017).

Analysis of variance (ANOVA) has been used for the regression analysis of experimental data, defining the interactions between the variables and the responses through comparison between the means. In the ANOVA, the quality of fit is measured by the adjusted coefficient of determination (R^2_{adj}) that determines the predictive capability of the model, where a model with a value above 80% is considered appropriate, revealing that it explains the variability of the fitted data (Montgomery *et al*. 2012).

3.2.3 Mode II Interlaminar Fracture Toughness (ENF – End-notched Flexure)

One of the evaluation methods used to calculate the Interlaminar Fracture Toughness (G_{IIc}) is the Compliance Calibration Method (CCM). The force P, the punch displacement δ and the crack length *a*, are provided for the evaluation of (G_{IIc})according to Equation 3.2 of Irwin-Kies (KANNINEN & POPELAR, 1985).

$$G_{IIc} = \frac{P^2}{2B} \cdot \frac{dC}{da} \tag{3.2}$$

where *B* is the width of the specimen, compliance *C* is the relation δ/P and *a* the crack length. For the ENF test, The CC coefficients, *A* and *m,* are determined using a linear least squares linear regression analysis of the compliance, C, versus the crack length cubed measured (DAVIES *et al*., 2001, ASTM D7905) by the Equation 3.3

$$C = A + ma^3 \tag{3.3}$$

where *A* is the intercept and *m* is the slope obtained in the regression analysis. The mode II fracture toughness is calculated as Equation 3.4

$$G_{IIc} = \frac{3m \cdot P_{Max}^2 \cdot a_0^2}{2B} \tag{3.4}$$

where P_{Max} is the highest force at crack length a_0 = 30 mm.

Thus, the ENF is suitable test for mode II fracture characterization of unidirectional z-pinned specimens.

3.2.4 Artificial Neural Networks

The artificial neural network (ANN) is a computational technique, which resembles to the biological nervous system. Mathematical models are proposed in this technique with the ability to learn from experience based on training via dataset. After training, it is expected that the ANN will be able to recognize output response according to unknown input data (KHATIR *et al*. 2021).

An ANN encompasses at least three major components: input, hidden and output layers, which each one has a certain number of neurons. The action of neuronal connections is represented by their weights, which can be negative or positive depending on whether the connections are inhibitory or excitatory. The influence of a signal obtained from another neuron is calculated by multiplying the value (intensity) of the received signal by the weight of the relevant connection (Xi · Wi). The total of the values of all Xi · Wi connections is completed, and the resulting value is transmitted to the activation function. The activation function describes how the weighted sum of the input is turned into an output from a node or nodes in a network layer (RIBEIRO *et al.,* 2022).

Learning paradigms govern the interaction between data and an ANN. The main classes of learning paradigms are supervised learning and unsupervised learning. In supervised learning, examples are provided to the network, and the network response is compared to the desired answer. The difference between the two replies, referred to as the error signal, is utilized to alter the network's synaptic weights.

This approach is repeated until the network answers appropriately in a statistical sense. In unsupervised learning, the algorithm does not seek to know the intended outputs, hence they do not utilize instances of input and output to be learnt by the network (YEGNANARAYANA, 2005). Also, neural networks can be divided by their information propagation, which can be a feed-forward network or a back-propagation network. In feed-forward networks, information flows in only one direction; that is, it goes from the input layer to the output layer in only one direction. In networks with backpropagation, the information can go back from one layer to the other (ZENZEN *et al*. 2020).

In this study to achieve good performance, the multilayer feedforward network with backpropagation training algorithm with supervised learning was chosen. Using this algorithm, the network is trained, and its generated errors are transmitted to the previous layers until they reach negligible values (HAYKIN, 2009). In order to promote a fast

convergence rate and correct training, the Levenberg-Marquardt algorithm was used on the ANN architecture.

3.3 Methodology

3.3.1 Response Surface Design

The RSM elaborated in this study considers two design factors associated with the manufacturing conditions: pin size (x_p) and number of pins per unit area (x_d). There are three response factors: Precracked (PC), Non-precracked (NPC), and structural mass. The design boundaries for CCD were defined considering the maximum and minimum size for the pin edge and a maximum and minimum allowed density, as can be seen in Table 3.1.

Table 3.1 - Input factors and their levels for α = 1.4142.

Control variables	**Symbol**	**Level**				
		$-\alpha$	-1	0	+1	$+\alpha$
Pin area density	x_d	0.1893	0.5	1.25	2.00	2.3106
Pin size	x_p	0.3964	0.5	0.75	1.00	1.1035

The specimens were manufactured using CFRP composite material with insertion of pinning reinforcement through the thickness, as depicted in Figure 3.2.

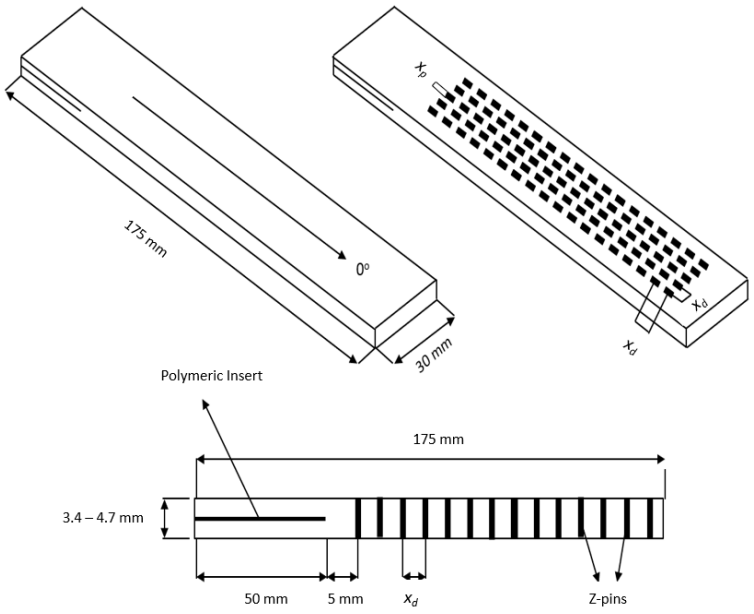

Figure 3.2 - Scheme of the z-pinned beam considering the design parameters xd and xp and its measurements.

3.3.2 Composites Manufacturing

Two different types of composite laminates were manufactured: (a) a thin laminate used to machine and fabricate the carbon fiber rods (rectangular z-pins) and (b) a laminate reinforced through the thickness by z-pins.

The thin laminate contained 4 plies with a [0/±45/0] stack sequency of an Unidirectional (UD) Tape (6K warp carbon yarns and areal weight of 149 g/m² supplied by Hexcel) with the warp tows oriented along the length of the laminate. A two-part epoxy resin system (AMPREG AR21) resin and the A21 SLOW hardener supplied by GURIT was used to manufacture the laminate by the Vacuum Assisted Resin Transfer Molding (VARTM). After the VARTM process, the laminated was cured in an oven at 80 ^{o} C for 4 hours. Then the carbon fiber/epoxy rods (z-pins) were machined in a Computer Numerical Control (CNC) Router machine with the dimensions obtained with the SRD and cited in the Table 3.2. After machining and before the z-pins insertion, the rods were sonicated in a cleaner ultrasonic bath and dried.

Table 3.2 – Details of investigated Mode II specimens.

Specimen	Pin density x_d (%)	Pin width x_p (mm)
#1	0.50	0.50
#2	0.50	1.00
#3	2.00	0.50
#4	2.00	1.00
#5	1.25	0.40
#6	1.25	1.10
#7	0.20	0.75
#8	2.31	0.75
#9	1.25	0.75
#10	1.25	0.75
#11	1.25	0.75
#12	1.25	0.75
#13	1.25	0.75
Reference	Unpinned (0.00; 0.00)	

Prior the z-pin insertion, 2 polystyrene (PS) plates were drilled in a CNC Router (with the areal density obtained in the SRD) to be used as a template and to achieve the right position during the z-pins insertion.

Also, these plates are useful to keep the z-pins aligned during the VARTM process and the PS was chosen because its glass transition temperature (T_g > 80 ^{o}C) is higher than the

resin cure temperature. The Figure 3.3 shows the scheme of the preform between the drilled PS plates.

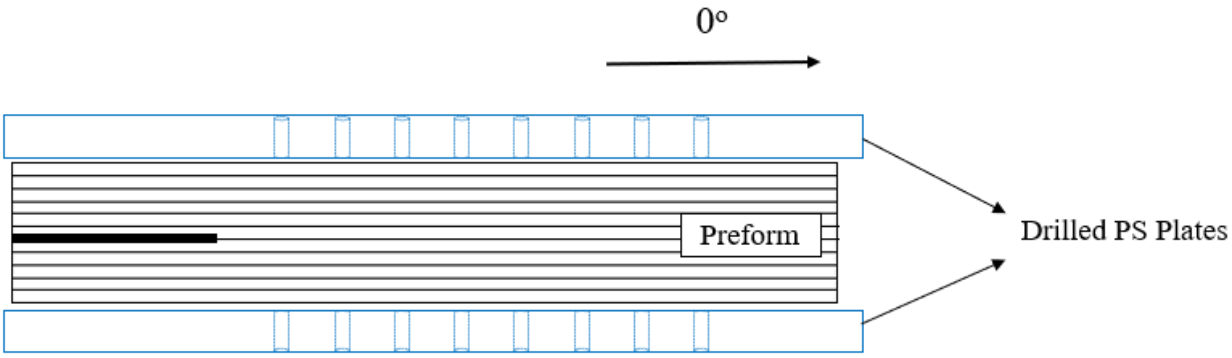

Figure 3.3 – Scheme of a preform between 2 PS drilled plates before the z-pin insertion.

The through the thickness laminate reinforced with z-pin was manufactured with the same materials, cited above, used in the thin laminate. Therefore, a preform with 18 plies stacked in a $[0]_{18}$ sequences was laid up between the two PS drilled plates with a 13 μm Teflon (PTFE) film in the center plane of the preform to act as a crack initiator. Figure 3.4 shows the polymeric film in the mid-plane of the preform.

Figure 3.4 – The PTFE film placed in the mid-plane of the preform.

To manually insert the z-pins in the thickness direction a hollow needle was used. The rods were placed inside the needle, and it was pushed through the thickness of the perform. Thereafter, the needle was pushed back, the z-pin stayed inside the perform and the rod was cut. The z-pins were inserted with the first z-pin row starting 5 mm beyond the edge of the crack starter film and when the z-pinning process was finished, the composite laminate was manufactured. The Figure 3.5 show the steps inserting the needle with the rod and the rod being cut.

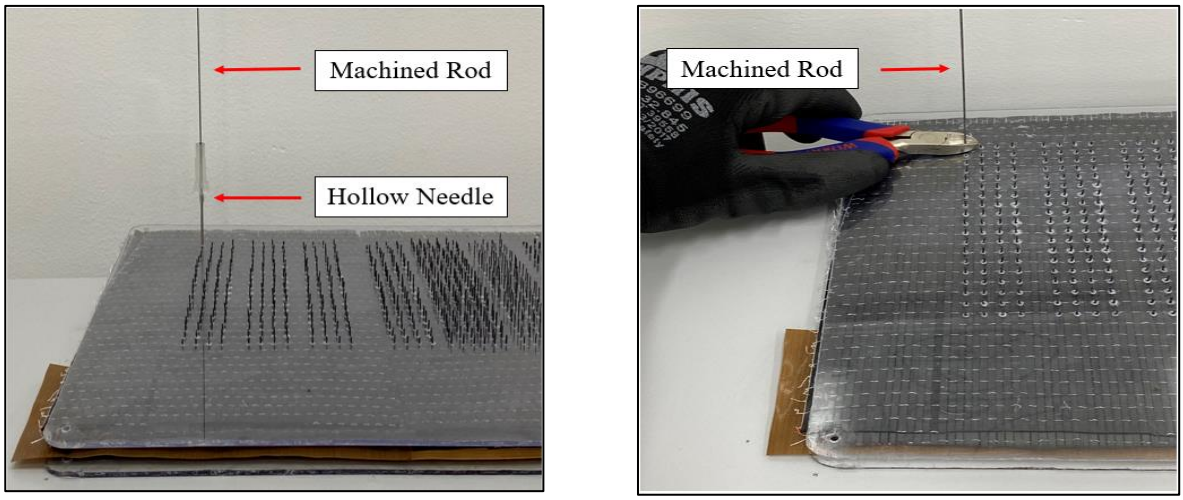

(a) (b)

Figure 3.5 – Z-pinning insertion process where (a) is the needle with the carbo rod inside and (b) the rod inserted in the preform and the excess is cut.

Figure 3.6 shows the preform (a) before, (b) during and (c) after cutting the z-pins' excesses.

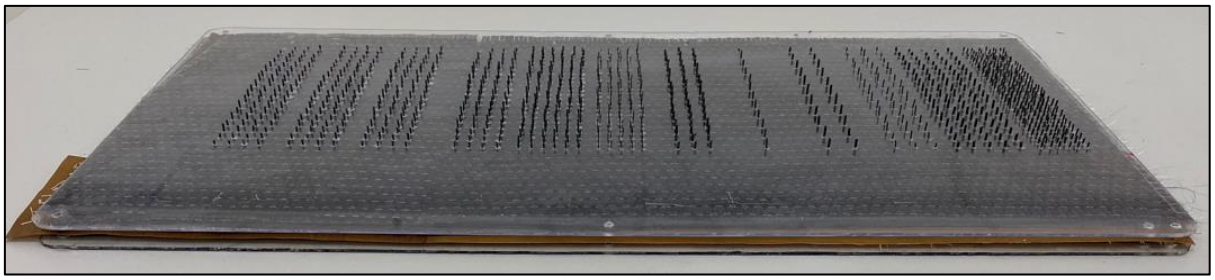

(a)

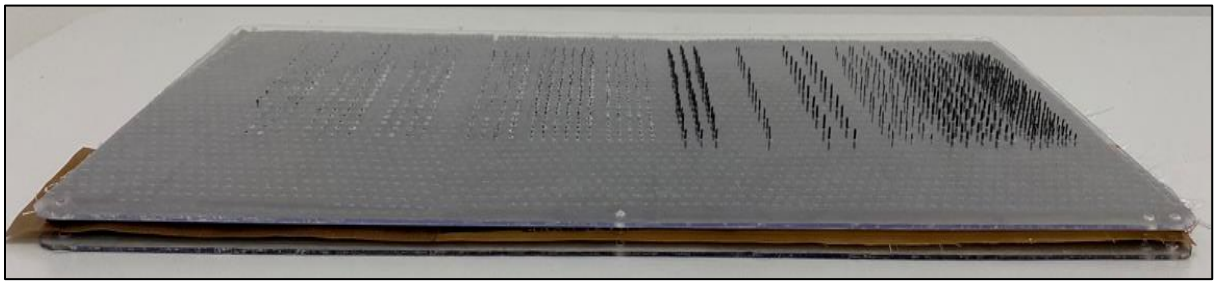

(b)

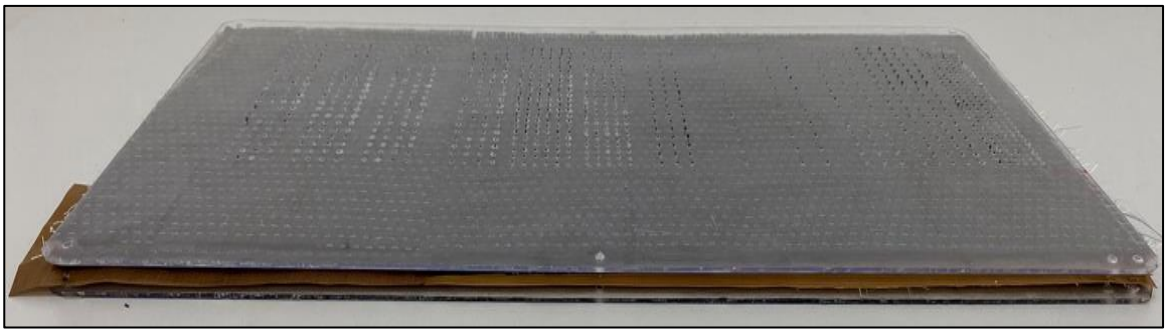

(c)

Figure 3.6 – Z-pins (a) before, (b) during and (c) after cutting the z-pins' excesses.

The VARTM process was carried out at room temperature and after the resin infusion is completed the laminate was cured in an oven at 80 ^{o}C for 5 hours. Even though the excess of z-pin was cut before the infusion, after the vacuum pressure the preform is compressed and there is a new z-pin excess length. To ensure a more even pressure and avoid the z-pins to perforate the vacuum bag, the metallic sticks were added in the surface of the top PS plate to separate each sort of specimen. The Figure 3.7 shows the VARTM process (a) before and (b) after the resin infusion.

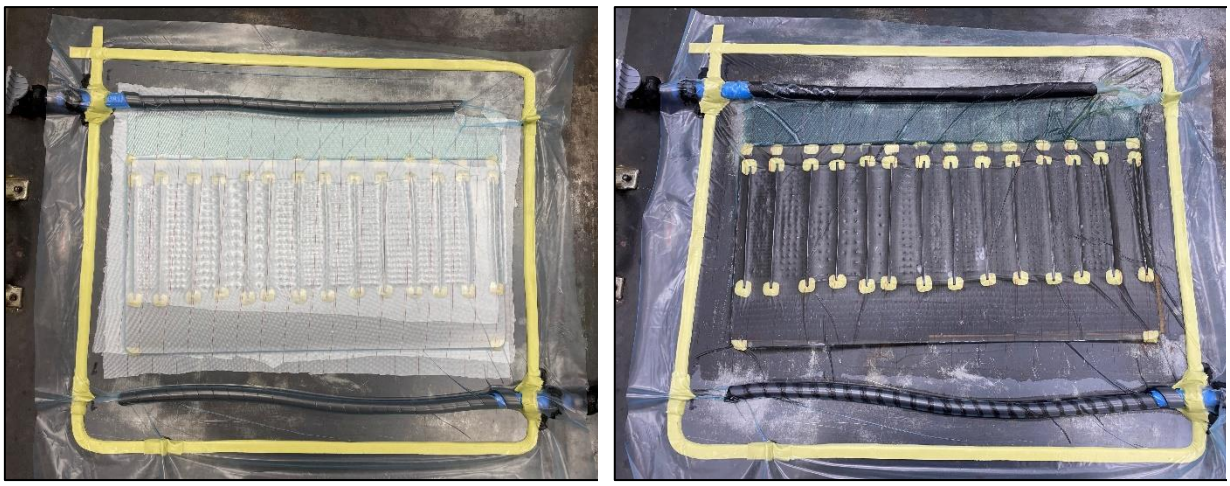

(a) (b)

Figure 3.7 - VARTM process (a) before and (b) after the resin infusion.

After cure, the laminate is demolded, the PS plates are removed and the specimens are machined. The Figure 3.8 shows the laminated after demolding and the machined specimens with the z-pins' excesses removed.

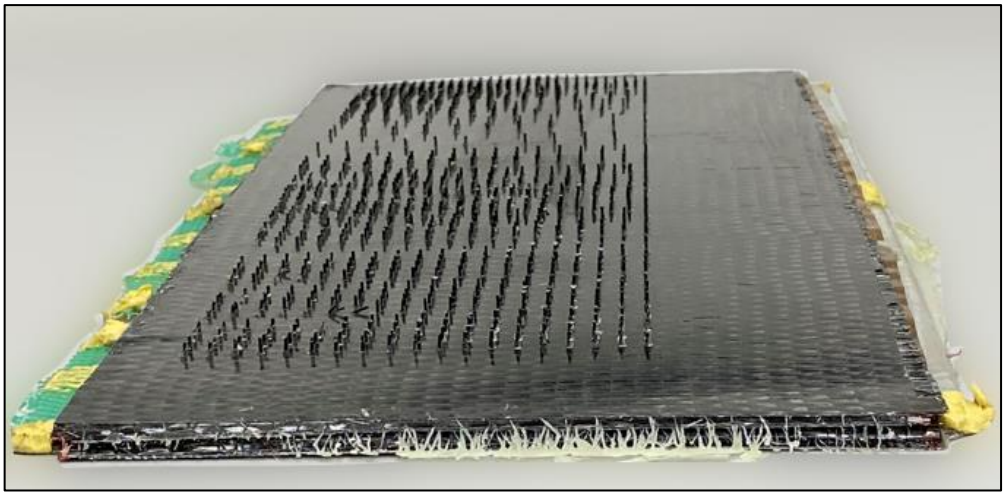

(a)

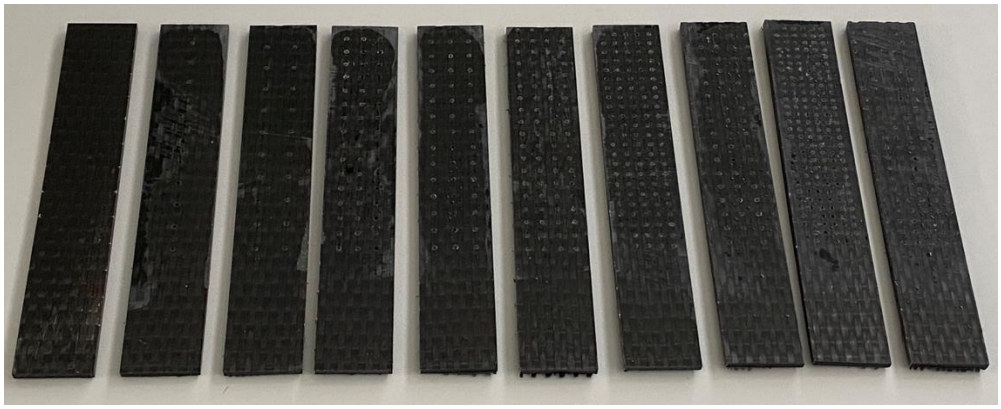

(b)

Figure 3.8 – (a) Laminate after demolding and (b) the machined specimens.

The ENF specimens were 175 mm long with a width of 30 mm. The z-pinned area with a length of 120 mm was starting 5 mm beyond the edge of the crack starter PTFE film (50 mm length). The pinned area extended across the width and length of the samples. Specimens reinforced with rectangular z-pins with a z-pin density of 0.19% to 2.31% and 0.40 mm to 1.10 mm sizes were investigated. Additionally, unpinned samples were also tested to be used as reference. An overview of the specimens investigated was presented in Table 3.2.

The insertion of z-pins in the thickness direction of a composite laminates, creates additional volume and the laminate thickness will increase in the z-pinned areas. Also, due to needle insertion and the presence of the z-pin it will occur fibers breakage, separation and deflection of fibers what will cause waviness and free areas surrounding the z-pins in which will collaborate to the thickness' increase and resin pockets formation.

Figure 3.9 (a) shows the resin-rich zones, or resin pockets, formed around the z-pin after the resin infusion and Figure 3.9 (b) shows the waviness (white stripes) with an eyelet shape caused due to the insertion of the z-pin.

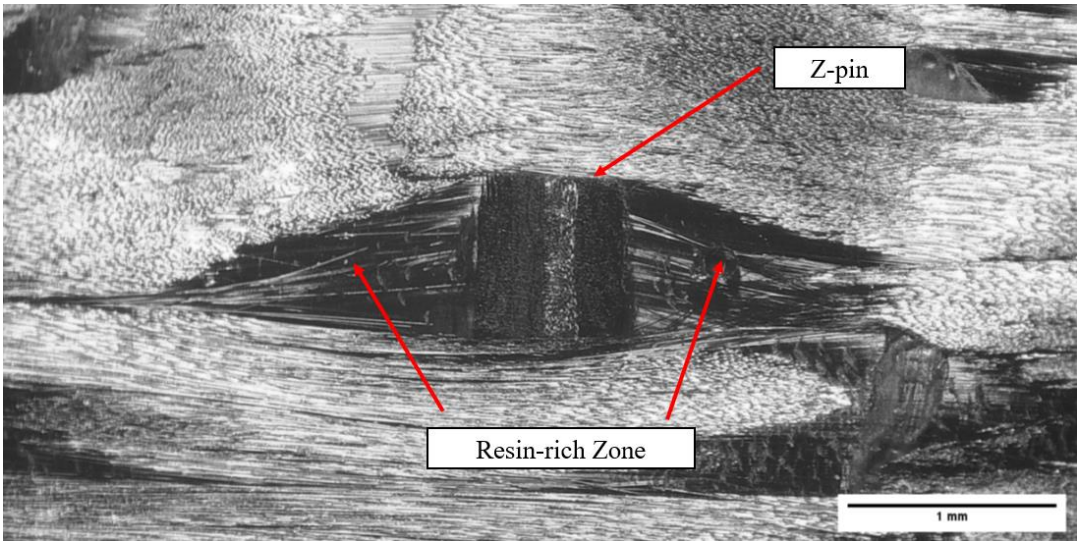

(a)

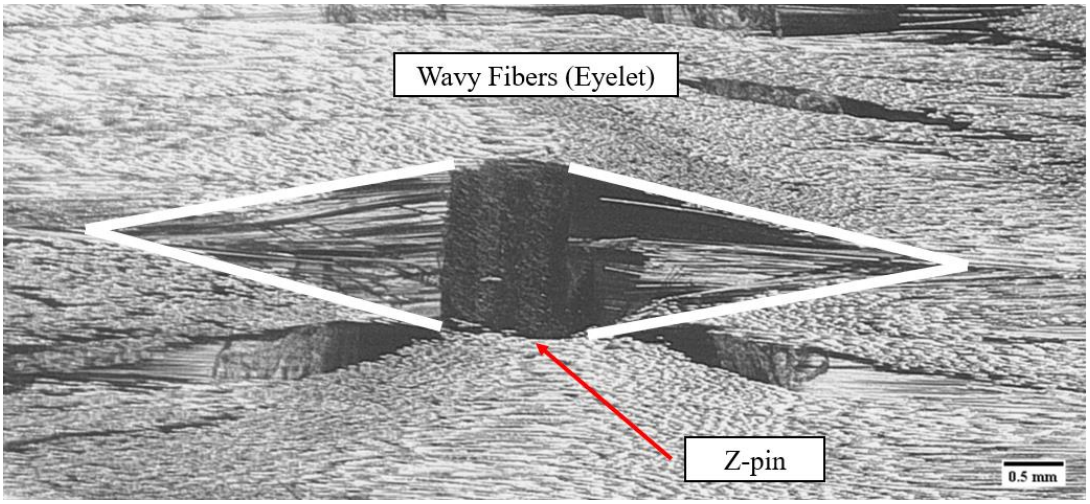

(b)

Figure 3.9 – (a) Z-pin and resin-rich zone and (b) wavy fibers (eyelet) formed after z-pin insertion and resin infusion.

3.4 Experimental Setup

3.4.1 Mode II interlaminar fracture toughness testing

The mode II interlaminar fracture toughness, (G_{IIc}), was determined using the end-notched flexure (ENF) test based on ASTM D7905. The 3-point bending device was installed

in a Instron universal servo-hydraulic test machine with a load cell of 100 kN and a displacement rate of as 0.5 mm/min for both NPC and PC tests. Prior to the test, it was necessary to apply a white ink on the side edges of the specimens to make the compliance calibration (CC) markings from the tip PTFE insert. The CC markings chosen where a = 20 mm, a = 30 mm and a = 40mm. The specimens where also marked every 1 mm right after the crack tip mark (the edge of the polymeric insert) to help determine and measure the crack propagation. The NPC test is made in three steps. The first step is flexure test with the specimen position in a = 20 mm and when a determined Force is achieved, the test is stopped. In the second step the specimen is positioned in another CC mark, a = 40 mm, and, again, when a determined Force is achieved the test must be stopped. For the third step, with the specimen placed on a = 30 mm, when the maximum force is achieved and, the delamination starts, the test is stopped again. The Figure3.10 (a-c) shows the specimen before the NPC test at every CC marking and (d) when the test is stopped (a = 30 mm) and happens the delamination crack growth (marked in blue line inside the red circle). The tests for the PC step will be performed in the same way for the NPC step; however, with different force and displacement values. The CC coefficients and the (G_{IIc}) will also be determined and calculated in a similar manner to the NPC step.

(a)

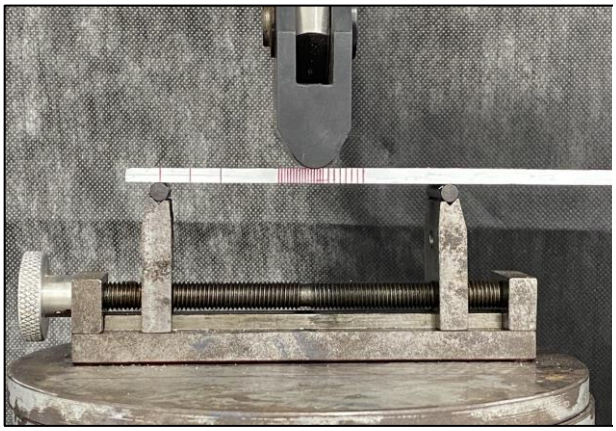

(b)

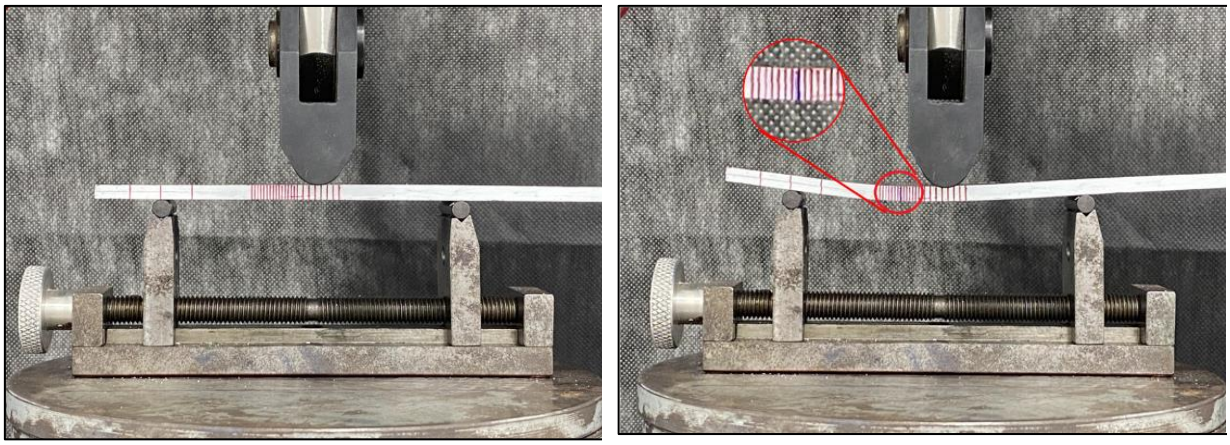

(c) (d)

Figure 3.10 – (a – c) specimen before the NPC test at every CC marking and (d) when the test is stopped (a = 30 mm).

Figure 3.11 (a-c) shows the specimen before the PC test at every new CC marking (in blue) and (d) at the end of the test. After the NPC and PC tests the P_{Max}, at a_0 = 30 mm, and the CC Coeficient *m*, calculate in Equation 3.3, were inputted in Equation 3.4 to calculate the (G_{IIc})values. Figure 3.12 shows a flowchart describing the methodology and steps used to develop the present study.

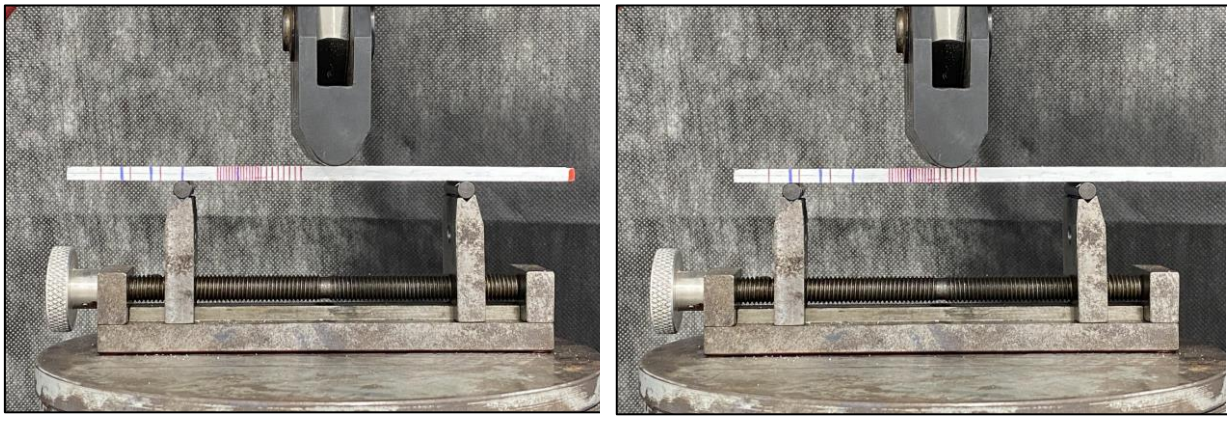

(a) (b)

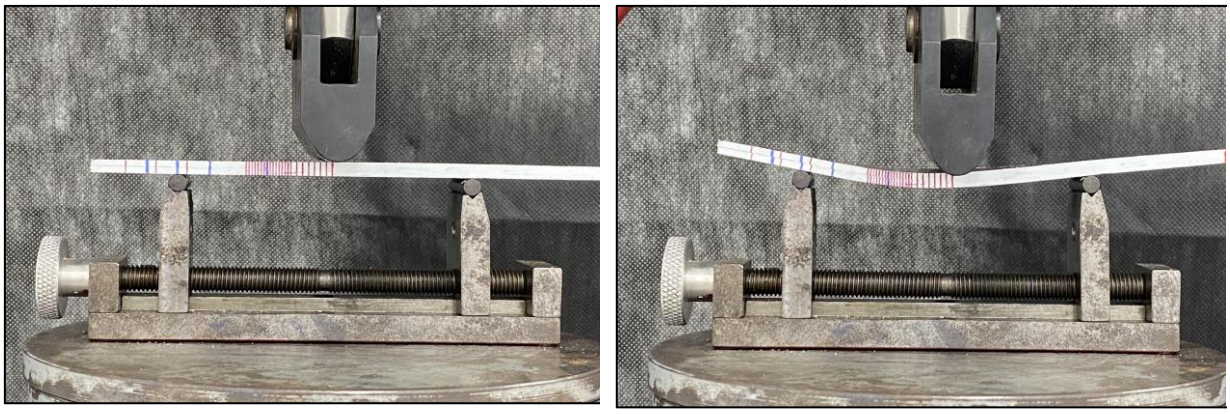

(c) (d)

Figure 3.11 - (a – c) specimen before the PC test at every new CC marking and (d) when the test is finished (a = 30 mm).

(Intentionally left in blank)

The Figure 3.12 shows the general flowchart describing the entire methodology and main steps used to develop the present study.

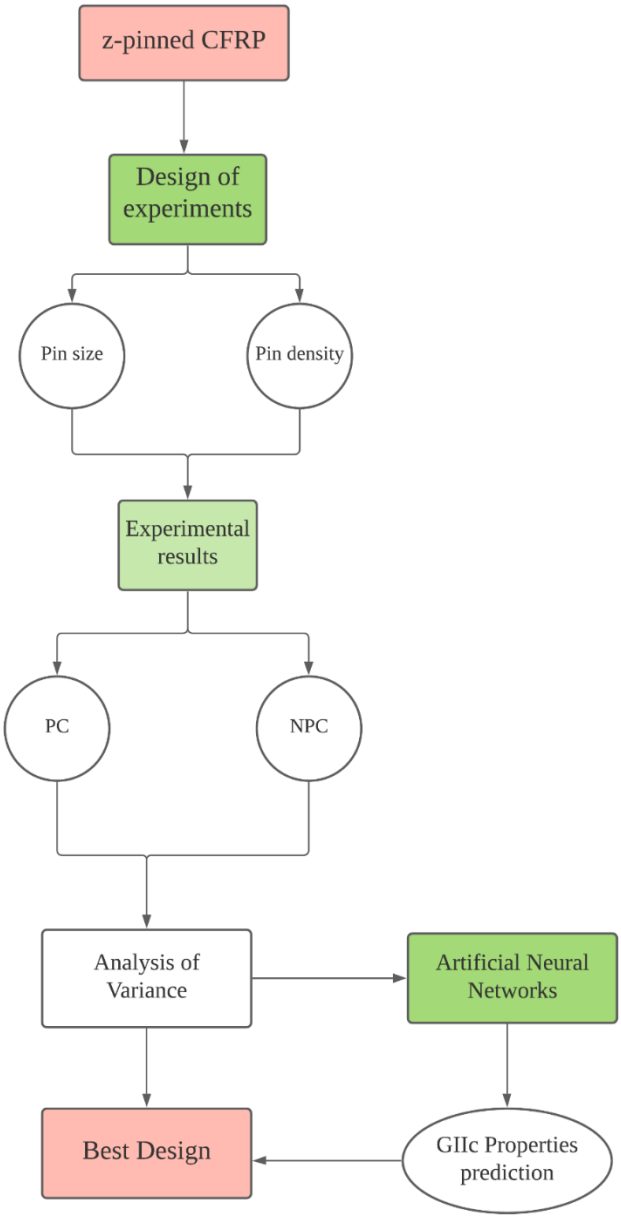

Figure 3.12 - General strategy used for optimum manufacturing conditions of z-pinned CFRP beams.

3.5 Experimental Results

3.5.1 Mode II Interlaminar Fracture Toughness

To calculate the interlaminar fracture toughness in mode II (G_{IIc}), the ENF tests for NPC and PC steps were carried out in a 3-point flexural device and the Force and displacement data were obtained. Table 3.3 presents the values of force and displacement.

Table 3.3 – Force and displacement values for all the specimens' conditions.

	Variables		Experimental Responses					
Experiment	Pin Size (mm)	Pin Density (%)	Force NPC (N)	δ (mm)	Force PC (N)	δ (mm)	ΔNPC (%)	ΔPC (%)
1	0.50	0.50	2049.71	3.22	2482.17	3.69	60.10	39.86
2	1.00	0.50	2006.31	4.23	2344.93	4.30	56.70	32.12
3	0.50	2.00	2097.81	4.17	2437.10	4.57	63.85	37.32
4	1.00	2.00	1932.96	4.43	2457.95	4.90	50.98	38.49
5	0.40	1.25	2061.35	3.95	2468.39	4.39	61.00	39.08
6	1.10	1.25	2046.06	4.34	2488.67	4.59	59.81	40.22
7	0.75	0.19	1853.60	4.35	2123.30	4.64	44.78	19.64
8	0.75	2.31	2017.78	3.86	2414.23	3.93	57.60	36.03
9	0.75	1.25	1602.47	3.99	2013.48	4.17	25.16	13.45
10	0.75	1.25	2100.01	3.38	2441.80	3.98	64.00	37.58
11	0.75	1.25	2163.68	4.23	2227.18	4.19	69.00	25.50
12	0.75	1.25	1803.60	4.26	2158.72	4.47	40.87	21.63
13	0.75	1.25	1819.97	3.65	1912.09	4.29	42.15	7.73
unpinned	0.00	0.00	1280.27	4.07	1774.74	4.17	-	-

The Force values, on NPC and PC steps, for the unpinned (reference) specimen were smaller than all the z-pinned specimens, showing that the z-pins help to mitigate delamination and higher forces are needed to start the crack propagation. Figure 3.13 and Figure 3.14 show the Force *vs.* displacement curves for all the specimens in the NPC and PC steps. The curves are referred to the part of the test when the crack length, or CC mark, is a =30 mm either for the NPC and PC steps. For the NPC step, when the P_{Max} is reached and the crack, or delamination, is extended the test is stopped. Figure 3.

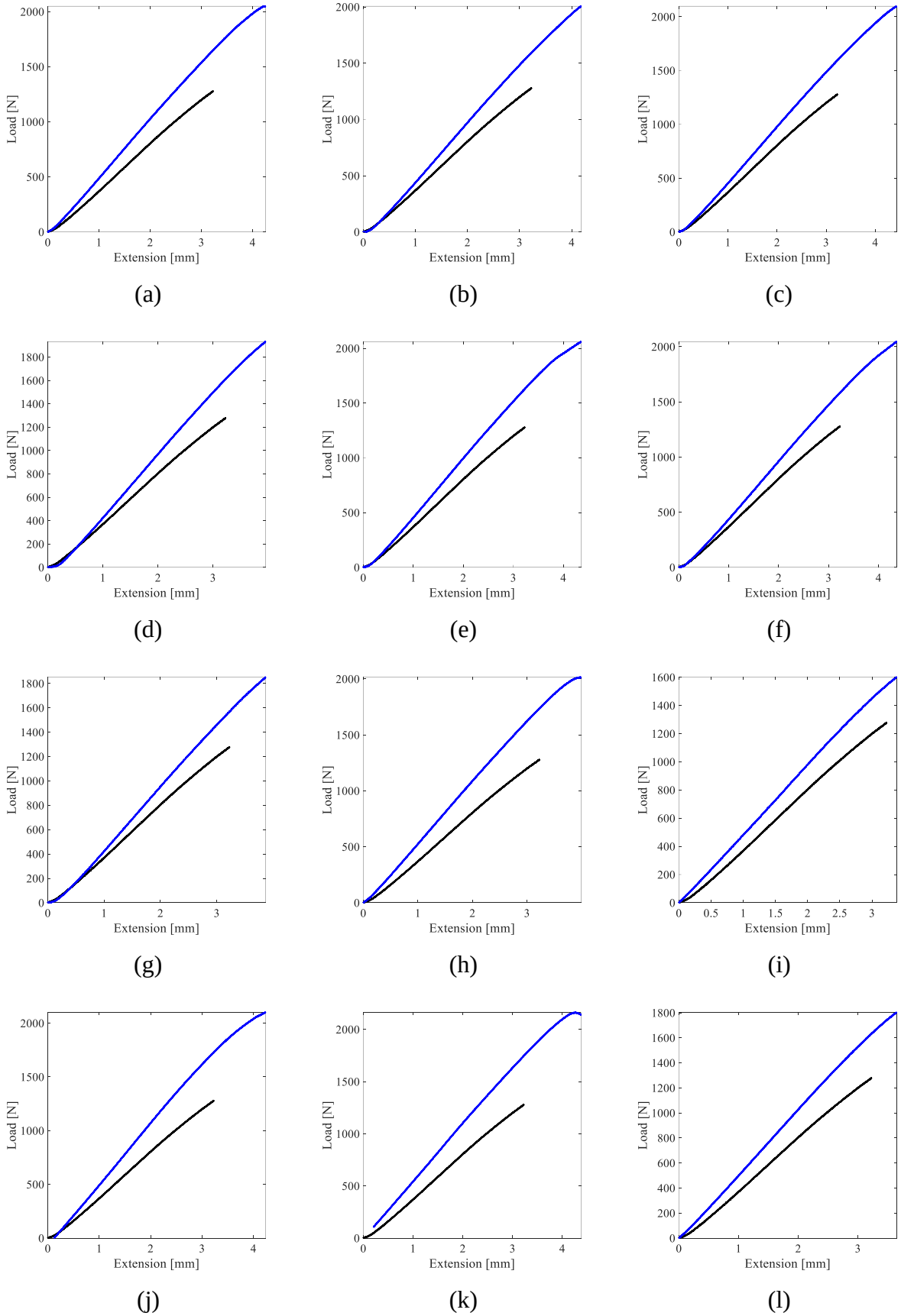

Figure 3.13 - NPC steps force vs. displacement results (legend: ▬ reference, ▬ reinforced specimens)

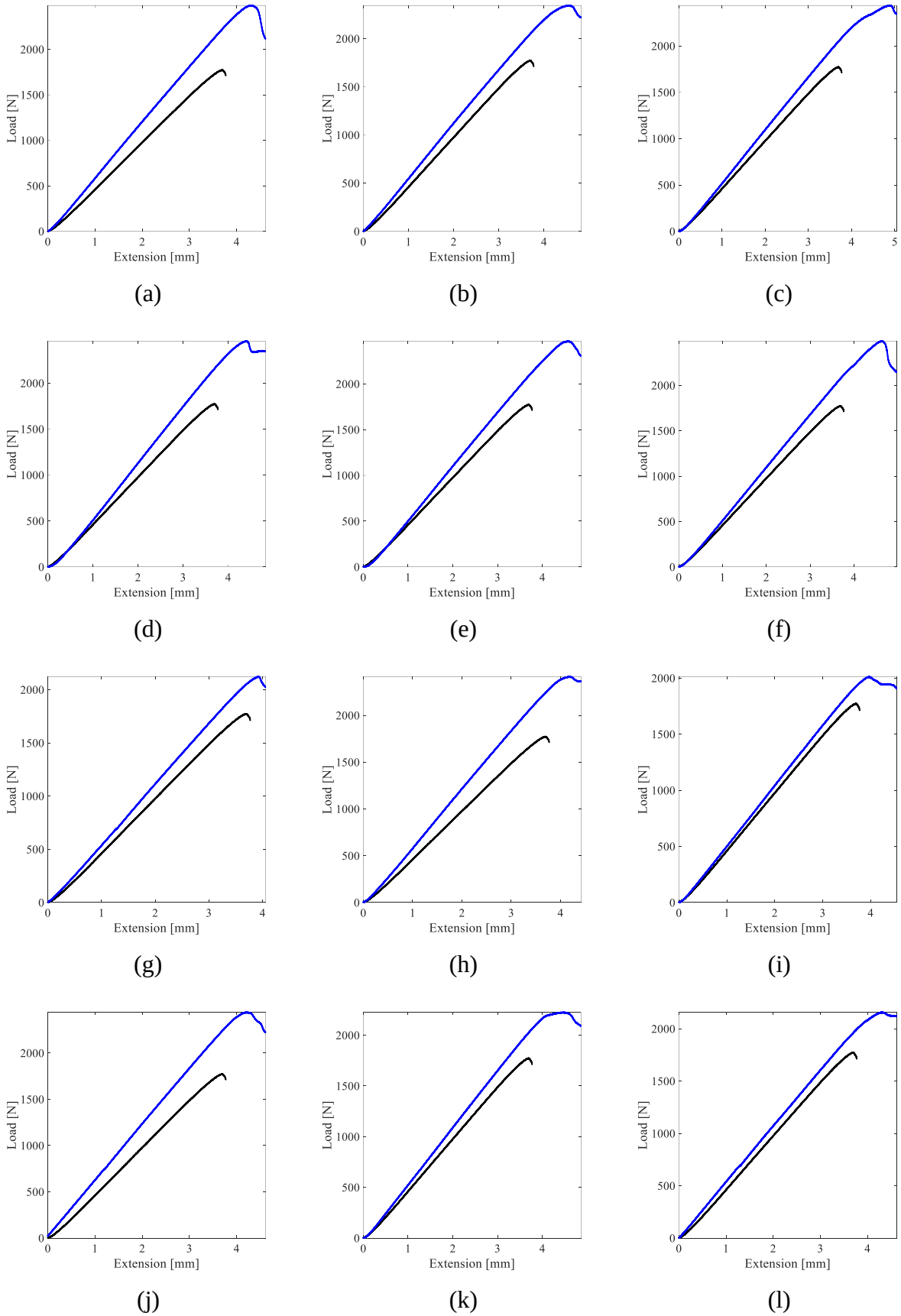

Figure 3.14 – PC steps force vs. displacement results (legend: ▬ reference, ▬ reinforced specimens)

The results and the effects for unpinned and z-pinned specimens with different conditions for (G_{IIc})in NPC tests are shown in Figure 3.15 and Table 3.4.

Table 3.4 - ENF different manufacturing design conditions of CFRP with SMA considering a RS design.

	Variables		Experimental Responses			
Experiment	Pin Size (mm)	Pin Density (%)	G_{IIc} - NPC (J/m^2)	G_{IIc} - PC (J/m^2)	ΔNPC (%)	ΔPC (%)
1	0.50	0.50	3403.07	3077.51	97.17	34.86
2	1.00	0.50	3260.48	3612.64	88.91	58.31
3	0.50	2.00	3564.64	3875.49	106.53	69.83
4	1.00	2.00	3093.67	4050.83	79.24	77.51
5	0.40	1.25	3441.81	3454.71	99.41	51.39
6	1.10	1.25	3108.38	4069.10	80.09	78.31
7	0.75	0.19	2674.94	2911.33	54.98	27.58
8	0.75	2.31	3076.78	2880.86	78.26	26.24
9	0.75	1.25	2519.11	2937.21	45.95	28.71
10	0.75	1.25	3277.26	2361.11	89.88	3.47
11	0.75	1.25	3391.74	2745.53	96.51	20.31
12	0.75	1.25	2927.68	3355.24	69.62	47.03
13	0.75	1.25	3460.22	3496.33	100.05	53.21
unpinned	0.00	0.00	1725.96	2281.95	-	-

For the NPC step, the (G_{IIc}) calculated for the unpinned (reference) was roughly 1726 J/m^2. All the specimens reinforced through the thickness with rectangular z-pins had an increase, at least of 45.95%, in the (G_{IIc}) values in comparison to the reference specimen, showing that the z-pin insertion improve the delamination properties in mode II. The results of thicker z-pins 1.00 mm and 1.10 mm showed increases above 80% in the (G_{IIc}) values when compared to the reference specimens. Thin z-pins (0.40 and 0.50) with different density insertion also presented improvements above 97% in the delamination properties compared to the unpinned. Also, the combination of 0.50 mm pin and 2% density insertion presented the best result (106.5%) for the NPC step compared to the specimen not reinforced. Thus, even with a low-density insertion of 0.2%, the specimen 7 achieved an improvement of more than 50% in the fracture toughness compared to the reference.

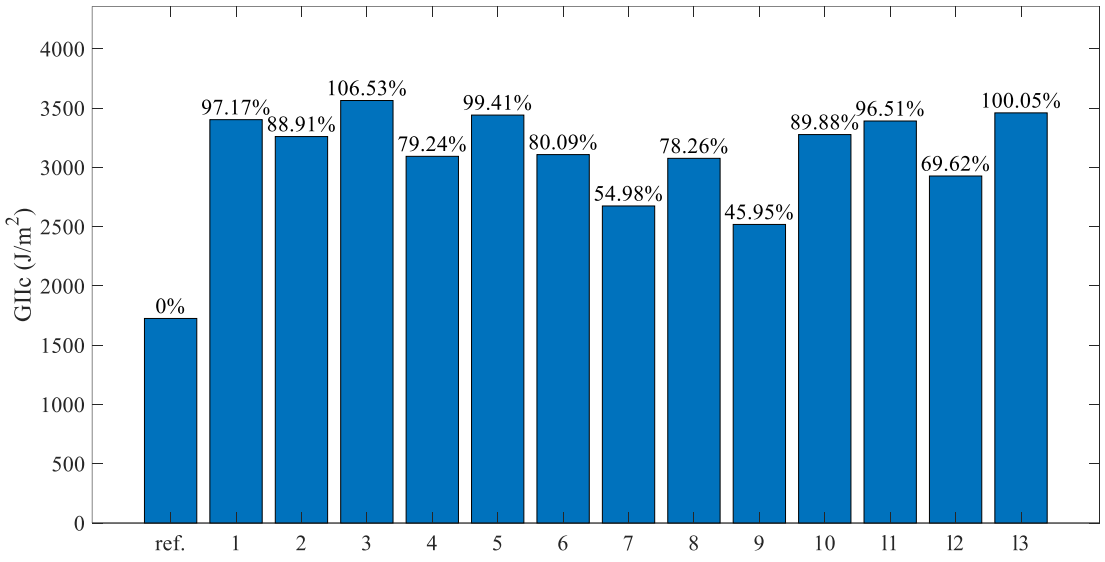

Figure 3.15 – Results for mode II delamination mode for unpinned and z-pinned specimens for the NPC step.

Regarding the PC step, it was shown that the through the thickness reinforcement with z-pin also improved the delamination properties and the energy released rate to propagate the crack was higher than the unpinned specimen. The (G_{IIc}) values for the reinforced specimens were above at least 25% of the reference specimen. For the PC tests, the highest values of (G_{IIc}) were achieved for the 0.50 mm and 1.00 mm pins with 2% density insertion, 3875.49 J/m^2 and 4050.83 J/m^2, respectively and for the specimen reinforced with 1.10 mm pin and 1.25% density insertion (4069.10 J/m^2). Also values of (G_{IIc}) with 50% improvement compared to the unpinned specimen were achieved for specimens with 0.40 mm and 1,25% density insertion and with 1.00 mm and 0.50% density insertion. Although not so expressive, between 26% to 35%, the other specimens also presented delamination properties higher than the unpinned specimen. This shows that the method used to reinforce the composites can be used and compared to other studies, mostly with circular z-pins, are effective at increasing the mode II delamination resistance of laminated composites. The results and the effects for unpinned and z-pinned specimens with different conditions for (G_{IIc}) in PC tests are shown in Figure 3.16

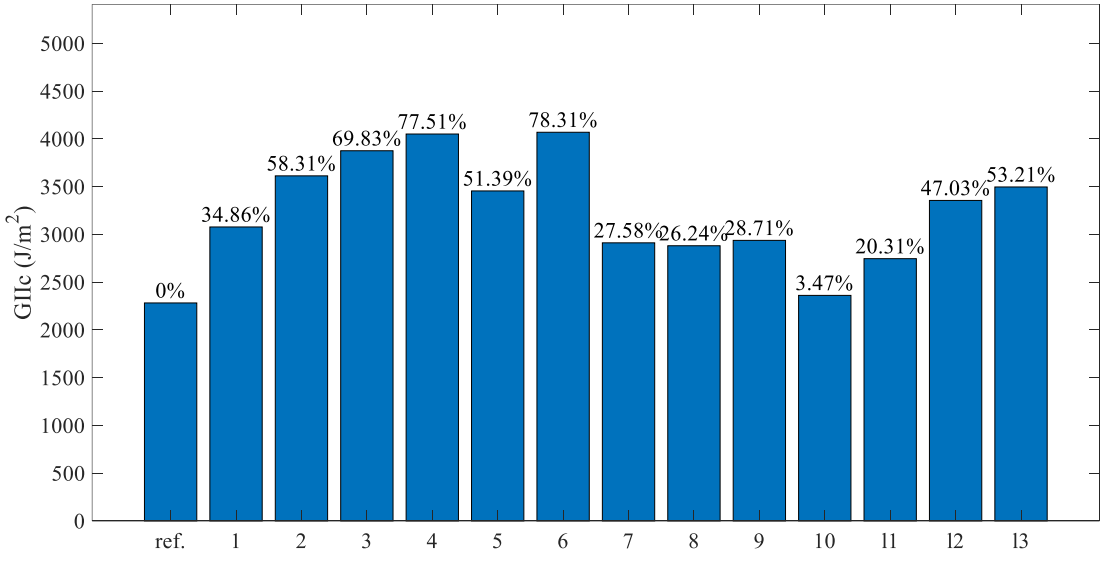

Figure 3.16 - Results for mode II delamination mode for unpinned and z-pinned specimens for the PC step.

The mode II fracture toughness (G_{IIc}) increases with the delamination length due to the initiation and development of the mode II bridging zone by the z-pins (Mouritz, 2020), involving shear deformation, interfacial bonding and snubbing against the epoxy composite interface, and shear rupture (Ravindran, 2019b; Ladani, 2016). However, the improvement in

(G_{IIc}) is not as drastic as in mode I fracture toughness (G_{Ic}) (KNOPP *et al*., 2022; MOURITZ, 2020). Also, the energy release rate is defined as the amount of energy that is released when a crack is extended, thus forming a crack surface. If a critical value (G_{IIc}) is exceeded, crack growth starts in the specimen and the z-pin insertion helps to increase the necessary increases the energy threshold to start shear delamination from the polymer film edge (NPC step) and from the new crack end (PC step). Although most of the studies in mode II fracture toughness that presented improvements in (G_{IIc}) and the effectiveness at increasing delamination resistance in composite laminates (RAVINDRAN *et al*., 2019c; CUI *et al*., 2019; HUANG & WAAS, 2014; ZHENG & YANG, 2010; PARTRIDGE & CARTIÉ, 2005) are related to circular pultruded z-pins, the results obtained in this study shows that machined rectangular z-pins increased the delamination properties compared to unpinned specimen and these improvements may be related to the geometry, size and areal density insertion of the z-pins.

3.5.2 Response Surface Model and Analysis of Variance

The RSM results are in Figure 3.17. It is possible to notice that for the NPC case (Figure 3.17 a), the increase in density of pins always generates an increase in the fracture toughness when no damage is present, with the exception of the middle regions of pin size and density, where a slight decrease can be observed in the midst of growth. Still, it is possible to notice that the growth of the value of NPC is more accentuated in the beginning of the increase of the density (starting from 0.5%). The contribution of the size of the pin to increase of the fracture toughness in this case is more accentuated while the density is less than 1%, still showing a slight convexity in this region. From there, increasing the size of the PIN has little influence. It is important to note that the highest NPC values are when the density is close to 2%, where the pin size has little impact, but more when the pin is too thin or too thick. $\Delta NPC\ (\%)$ graph is qualitatively identical, but confirms what was found in the experimental data, fracture toughness is always increased with pinning.

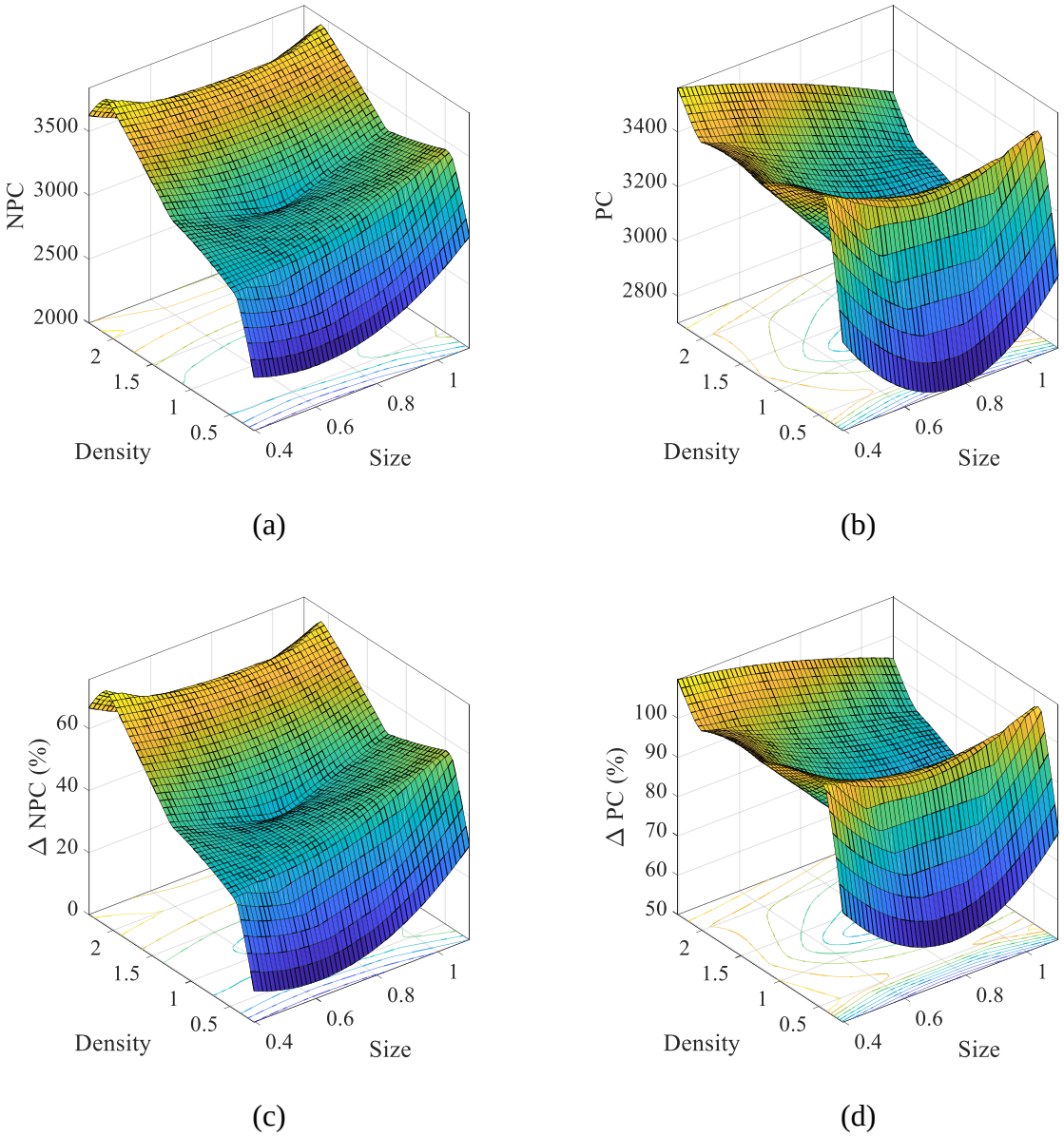

Figure 3.17 – Response surfaces in the space for (a) NPC, (b) PC, (c) ΔNPC e (d) ΔPC.

When damage arises, the pinned structure exhibits behavioral differences from what was said for the healthy structure (See Figure 3.17). The biggest detail is that the graphic convexity in the medium density and medium post size points is accentuated, but now strongly highlighting the decrease in fracture resistance with increasing pin size. The PC is decreasing in all these situations, except for when the pin density is low. The most expressive increase in fracture resistance is even greater when the density of the posts starts to increase, a region where very thin or very thick posts have the same PC value. However, if the stitch density is higher, the smaller post has greater fracture resistance. Generally speaking, the

highest PC value is for any pin value at low density and thin pins at high density. The ΔPC *(%)* plot is qualitatively identical, but it also shows that pinning always improves the fracture resistance of the structure, even when damage is already present.

The results from ANOVA are depicted in Figure 3.18 and Figure 3.19 using the main effect plots that provide the difference between the levels of the design factors according to the response factors. It is possible to affirm that the manufacturing conditions for the pins have a positive influence in the NPC and PC steps. In the NPC step, the behavior of the design factors was dissimilar when compared with the PC step, as depicted in Figure 3.18. The lowest value in NPC was found with pin size of 0.75 mm while that the high with pin size of 1.00 mm. The small pin density provided the lower value for NPC, approx. 0.19 and 2700, respectively. The pin density of 2% generated the highest NPC, as depicted in Figure 3.18. It is clear that the small size for the pins provides a high PC value while larger pin sizes reduce the PC. In relation to density for the pin in PC step, in general, denser specimens increase the PC and the less dense decrease the PC, as can be seen in Figure 3.19.

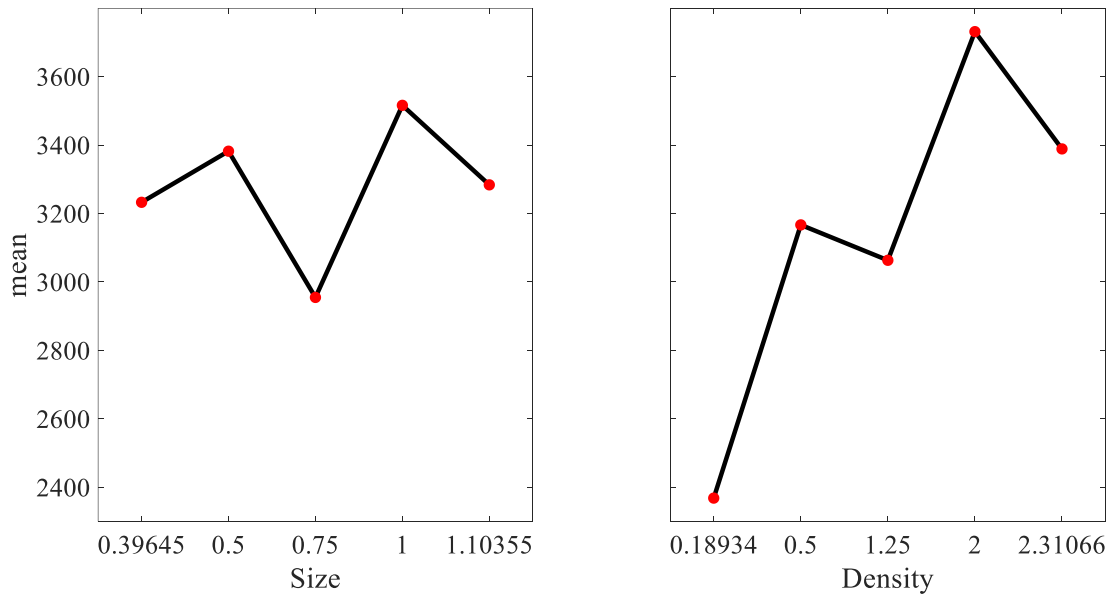

Figure 3.18 - Main effect plots considering the response variables obtained in the ENF test for the NPC step.

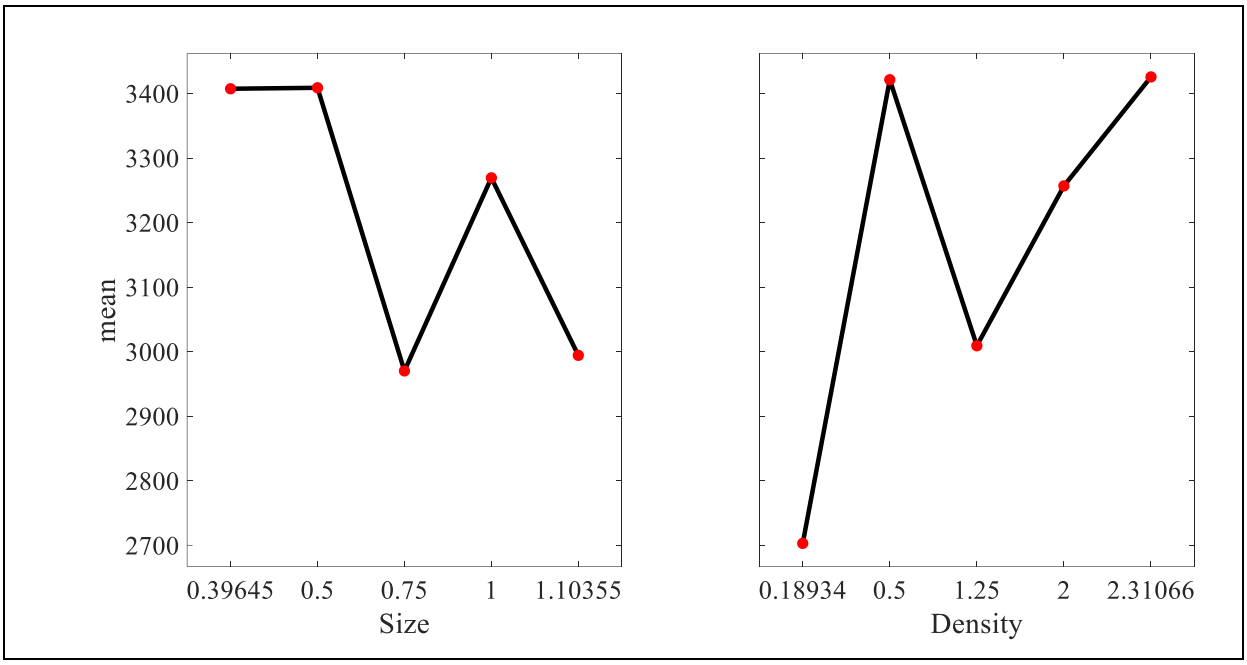

Figure 3.19 - Main effect plots considering the response variables obtained in the ENF test for the PC step.

3.5.3 Mode II Interlaminar Fracture Toughness Prediction using ANN

The generated experimental data can be used for an ANN to learn about the pinning behavior in relation to the interlaminar fracture toughness of z-pinned composites. The first step is to determine the architecture for the ANN considering input layers, hidden layers and output layers, as depicted in Figure 3.20. Three sets of 13 experiments were generated for experimental evaluation: unpinned structure and pinned. The 39 data were shuffled, normalized and two thirds will be used for training the algorithm.

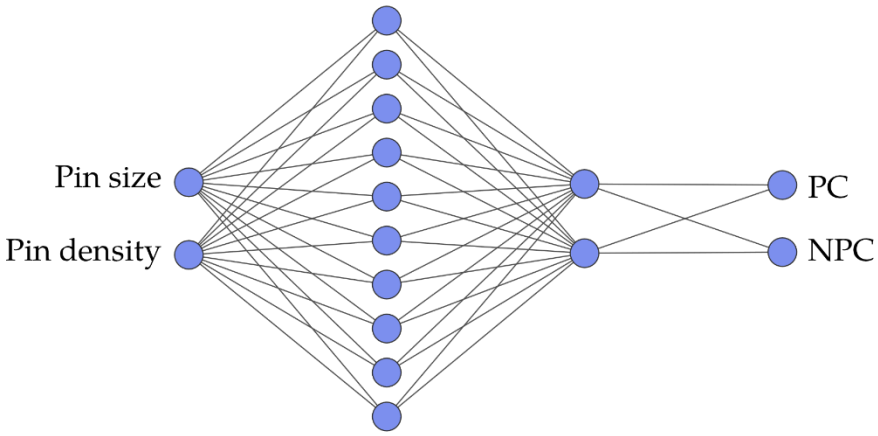

Figure 3.20 - The architecture for the ANN considers two input layers, ten hidden layers, and two output layers.

After defining the number of layers for the network considering the manufacturing conditions, it is important to define the optimal configuration for the algorithm. For this, a multilayer feedforward network with backpropagation training algorithm with supervised learning was chosen. This type of algorithm allows that the network is trained, and its generated errors are transmitted to the previous layers until they reach negligible values (HAYKIN, 2009). For the learning of the neural network was used the Levenberg-Marquardt algorithm responsible by promote a fast convergence rate and correct training. The main parameters used in the ANN are shown in Table 3.5.

Table 3.5 – Optimal ANN configuration taking modal behavior into account.

Parameters	**ANN model for Z-pinned beams**
Learning algorithm	Levenberg-marquardt
Activation function (hidden layers)	Hyperbolic tangent
Activation function (output layers)	Linear
Number of hidden layers	10
Mean squared error	0.10
Training data	26
Test Data	13
Number of iterations	2000
Learning rate	0.30

(Intentionally left in blank)

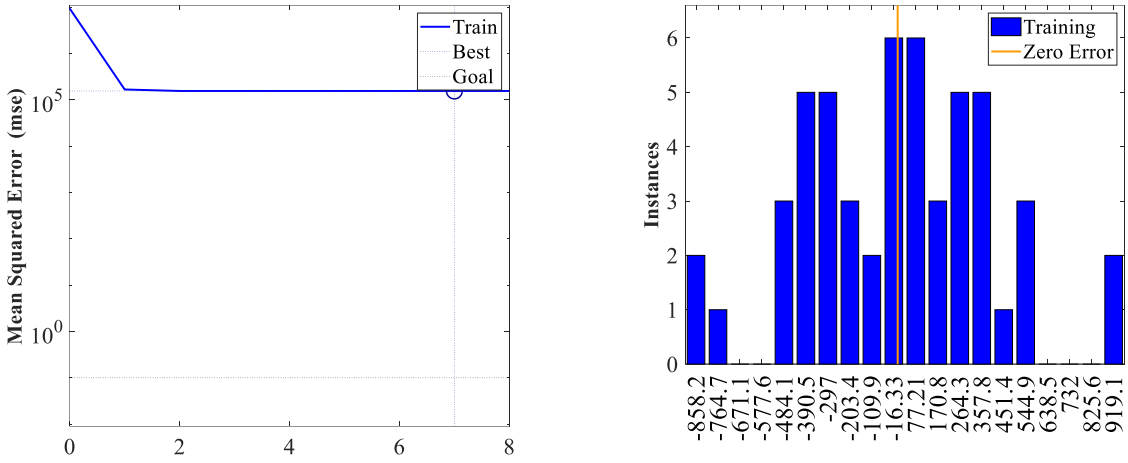

(a) (b)

Figure 3.21 - Results of ANN global training taking into account: (a) the best training performance and (b) the histogram of error values.

Figure 3.22 shows the actual values and the values that were predicted by ANN after training. It is possible to observe an excellent ability to predict by the ANN, being greater in the case of the healthy pinned structure, where the non-linearity of the problem is smaller.

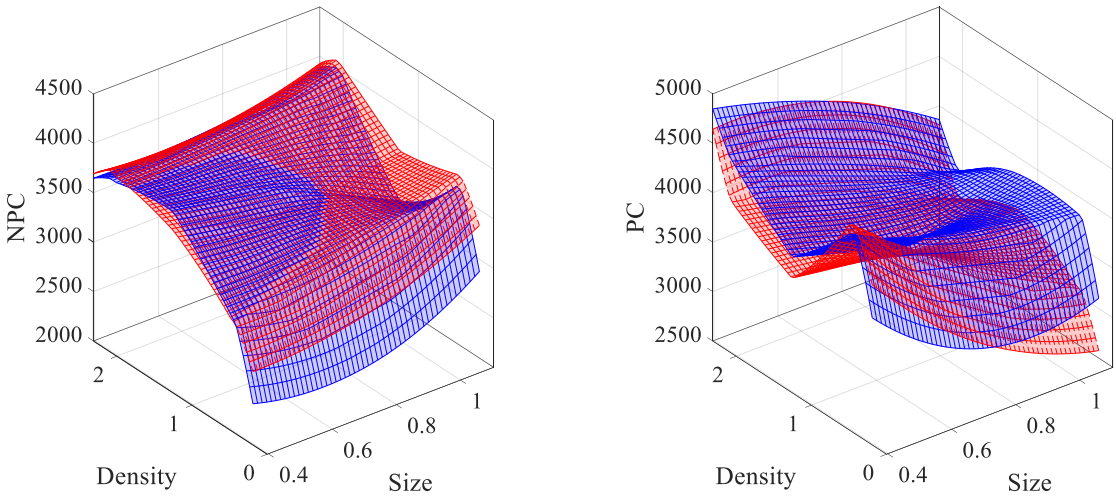

(a) (b)

Figure 3.22 - ANN graphical results of (a) G_{IIc} for NPC and (b) G_{IIc} for PC (legend: — Real, — ANN predicted).

3.6 Conclusions of Chapter 3

This study has demonstrated that the presence of machined rectangular manually inserted Z-pins improved the Mode II fracture toughness properties in comparison to unpinned specimen. Pinned boards were manufactured and tested to meet the Design of Experiments. The results were discussed and supported by the Response Surface Model and the Analysis of Variance.

The experimental results showed that for the Non-precracked step the highest (G_{IIc}) value achieved, 3564.64 J/m^2, was for a 0.50 mm with a 2% pin density insertion, being 106% higher than the unpinned specimen. Also, the thicker pins 1.00 and 1.10 mm presented good response and High (G_{IIc}) values, 88.9% and 80.1%. Thus, the 0,4 mm pin improved the crack propagation in 99.4%, however it did not have the same improvement in the PC step. For the PC step, the thicker pins 1.00 mm and 1.10 mm acted again as a positive influence to mitigate the delamination and achieved elevated values of (G_{IIc}), 77.5% and 78.3% higher than the unpinned specimen, respectively. Also, the 0.50 mm pin with a 2% pin density present a good behavior in comparison to the unpinned with a 69.8% improvement in the (G_{IIc}) value. The results were confirmed by the response surface model and analysis of variance, which also pointed that for the NPC case, the increase in density of pins always generates an increase in the fracture toughness and the contribution of the size of the pin to increase of the fracture toughness in this case is more accentuated while the density is less than 1%. From there, increasing the size of the pin has little influence in NPC. For PC case, was showed that the pin size increasing decreases the fracture resistance, except for low pin density. Furthermore, the ANN trained with part of these experimental data showed excellent predictive capacity for the NPC case, where the model linearity is lower than in the PC case.

Further studies are necessary to fully characterize and understand the effects of in house manufactured rectangular z-pins on the resulting interlaminar fracture toughness properties. More studies on the Mode-II fracture mechanical properties in this kind of approach and the influence of the pin size, density insertion and composite laminate manufacture process used and chosen in this work may help to explain the resulting mechanisms responsible for the achieved results.

CHAPTER 4: AN EXPERIMENTAL CHARACTERISATION ON RECTANGULAR Z-PINNED PARAMETERS IN THE DYNAMIC MODAL RESPONSES OF REINFORCED COMPOSITES

A great deal of research has been carried out and demonstrates that through-thickness reinforcement in the form of z-pins can greatly improve the mechanical properties of carbon fiber composite laminates. In this chapter, the modal responses of composite laminates reinforced through the thickness with rectangular z-pins sizes and areal density insertion design variables generated from Design of Experiments (DOE) are studied with free and forced vibration tests being carried out. Although many studies reported the use of experimental, statistical, numerical and computational tools applied to composite structures, to date, very few have been focused on the application of analysis of variance (ANOVA), to analyze the experimental data, and Artificial Neural Network (ANN) as a technique to predict the modal responses of z-pinned composites.

4.1 Introduction

Advanced composite laminates have been widely used in many structural applications, especially in aerospace, automotive, marine, and civil engineering applications due to their strength-to-weight ratio and specific stiffness, corrosive resistance and fatigue performance compared to metallic materials (CUI *et al*. 2019; CHANDRASHEKHAR *et al*., 2010; YAN *et al*., 2004). These materials known as bidirectional (2D) composites, are typically processed by stacking individual layers of unidirectional or bidirectional fabrics previously impregnated with polymer matrices and the lack of reinforcement in the thickness direction of laminated composites makes interlaminar delamination, caused from high interlaminar loads, impact or environmental degradation of the composite, a major concern (PINGKARAWAT & MOURITZ, 2014; YASAEE *et al*., 2014; PARTRIDGE & CARTIÉ, 2005; PARDINI, 2000).

As the Interlaminar fracture, or delamination, is the most common failure in thermoplastic and thermosetting composite laminates (GOMES *et al.*, 2018; BARBOSA *et al*., 2019a), several through the thickness techniques, e.g., 3D braiding and 3D weaving, stitching, tufting, z- tolerance of laminated composites (BORTOLUZZI *et al*., 2019;

MOHAMED *et al*., 2018; FUNARI *et al*., 2016; BILISIK, 2010). In this scenario, Z-pinning comes as an effective through-thickness reinforcement (TTR) technology improving the delamination resistance and hence arrests or delays crack growth extension (KUMAR & BABU, 2018; ZHANG *et al*., 2016).

Regarding the z-pins design, past research showed that different shapes, surface density insertion, diameter and surface characteristics can influence the reinforcing effects (CARTIÉ *et al*., 2006). In this context, Zhang *et al* (2017) manufactured twisted fiber reinforced Z-pins through pultrusion process and conducted a pullout test to measure the bonding force of Z-pins. The enlarged contact area between 80 twist/m Z-pins and the laminate imparts achieved an improvement and a 19.4% of debonding load higher than the not pinning have been developed aiming to improve the delamination resistance and damage twisted (0 twist/m) regular pultruded z-pin.

Equally important, Hoffmann and Scharr (2018a) evaluated the influence of rectangular and circular z-pins geometry of the pins on the resulting bridging force during pull-out on unidirectional (UD) and quasi-isotropic (QI) epoxy laminates. In both laminate types, rectangular z-pins showed a superior bridging response. the rectangular z-pins showed a higher pullout work during crack growth and thereby a greater potential for increasing the interlaminar fracture toughness of fiber reinforced laminates with an identical pin volume content, an increase in the debonding force of 59% and 149% could be determined in the UD and QI laminates, respectively.

As a matter of fact, Knaup *et al*. (2013) showed that rectangular z-pins reinforced composites significantly slowed down the delamination growth compared to circular z-pins and unpinned composites in impact tests and also described that rectangular z-pin need half areal density insertion of circular z-pin to achieve same performance. In the Compression after impact (CAI) at low impact energy, rectangular and circular z-pin with 1.0% areal density had an improvement of 25% and 15, respectively, compared to the unreinforced composites.

In another study, Grigoriou *et al* (2019) demonstrated that metallic (copper and titanium) and carbon fiber z-pins (0,51mm diameter), inserted with different areal densities (from 0.5% to 2.0%) can be used in the manufacture of multifunctional sandwich composite materials to improve the mechanical properties such as flatwise crush resistance and fracture

toughness in mode I and the through-thickness electrical conductivity, also showed that z-pins application is capable to detect damage continuously with the electrical resistivity changes. Recently, Ravindran *et al* (2019c) investigated the improvements to the mode II interlaminar fracture toughness of composites varying volume fractions (0.5% and 2.0%) of 0.28 mm diameter carbon fiber z-pins and. In the study it was achieved 248% and 55.4% higher values for the fracture toughness of 2.0% and 0.5% areal density insertion, respectively, compared to unpinned composites.

As a result, 3D reinforcement techniques tend to modify the natural frequencies, damping and amplitude, thus the dynamic response is also changed. Fan *et al* (2019) Studied the damping coefficient and variations in vibrating amplitude in different composites manufactured with 3D and 2D woven. The damping coefficient of the 3D composite was higher than the 2D laminated composite as well as the decreasing rate sequence of vibrating amplitude, implying that the Z-binder yarns (thickness reinforcement) in the 3D reinforced structures can transfer the vibration energy to the middle or bottom layer, speeding up the dissipation of energy.

For this reason, Abdellah *et al* (2019) investigated the vibration behavior of woven-glass fiber-reinforced epoxy laminate a hybrid laminate of epoxy reinforced by glass fibers and steel-mat mesh compared with those of wrought 1100 aluminum and tinned steel. The results showed that composite laminated structures have high damping ratios than their metallic counterpart, what implies the usage of these materials for applications in the aerospace and automobile industries, where low vibration damping ratios are required.

Another study regarding modal analysis in composites, De Borbón *et al* (2014) performed free vibration tests of sandwich and single composites beams with different types of multi-walled carbon nanotubes (MWCNTs) as fillers in epoxy matrix to study the damping response in comparison with neat epoxy resin samples. It was found that 5 wt% of SM5 carbon nanotubes (CNTs) in the epoxy matrix led to an improvement on damping ratio of 35% for sandwich beams and 73% for simple beams compared to beams with neat epoxy.

In addition, Bortoluzzi *et al* (2021) studied influence in the modal properties of unidirectional CFRP reinforced through the thickness with rectangular z-pins and the results have shown that the z-pin has a statistically significant influence on modal responses, allowing a reduction of up to 110% in vibration levels.

Statistical and computational tools such as Artificial Neural Network (ANN) have been an object of interest to the development and enhance the behavior of thermoplastic and thermosetting composite materials (DI BENEDETTO *et al*., 2021; BARBOSA *et al*., 2019b; PARIKH & GOHIL, 2019), design optimization of composite parts (LEPŠÍK & KULHAVÝ, 2017), and to improve the mechanical properties correlation of composite laminates (IBRAHIM *et al*., 2019; ALMEIDA *et al*., 2015).

Therefore, the novelty of this work is to present the influence of rectangular z-pinning parameters in the modal response of composite materials. For this, specimens with rectangular z-pins with sizes and pin area densities are manufactured after a Design of Experiment (DOE) matrix determination and Response Surface Model (RSM) and Analysis of Variance (ANOVA) are used interpret and discuss the results. Thus, the experimental results are used as training and test data for an Artificial Neural Network (ANN), which is technique applied to predict and assess the influence of the pin size and density configuration in the modal responses such as natural frequency, damping or loss factor and maximum vibration amplitude in forced vibration and in the mass of the specimens. To the authors' knowledge, there are no (or very scarce) studies investigating the effects of 3D reinforcing techniques, especially z-pinning, on modal responses in composite laminates.

The manuscript is organized as follows: Section 2 presents a theoretical background. Section 3 presents the methodology of this work. Section 4 brings the results and discussions, and Section 5 concludes the research.

4.2 Theoretical Background

4.2.1 Z-pinning

Z-pinning is a well-established technique used to increase the interlaminar fracture toughness of fiber reinforced polymer (FRP) composites (PEGORIN *et al*., 2015). The z-pinning process involves the insertion of carbon or metal rods through the thickness of uncured composite material during manufacture. Z-pins are most commonly less than 1 mm in diameter and inserted in standard areal densities of reinforcement range from 0.5% to 4% (KOH *et al*., 2013; MOURITZ, 2007; PARTRIDGE & CARTIÉ, 2005).

Various methods are used to manufacture z-pinned laminates, with the most common method being the UAZ (Ultrasonically Assisted Z-Fibre) process that involves the insertion of

rigid rods (Z-pins) into an uncured prepreg stack using an ultrasonic hammer (MOURITZ, 2020). In this process, the pins are inserted in a double layer carrier foam containing the z-pins arranged in an orthogonal square pattern allowing place the pins in accurate location area of the uncured laminate to be reinforced and a large amount of pin insertion. The Z-pins are pushed through the thickness of the laminate layup using a specially designed ultrasonic machine. Once inserted to the desired pin length, the next steps consist in shear the excess pin length and removal of the collapsed foam (KOSTOPOULOS *et al*., 2020; MOURITZ, 2007, CARTIÉ *et al*., 2006).

In addition to the UAZ process, other methods can be used to insert z-pins through the thickness of prepreg, manually impregnated and dry fabric preforms. EADS Innovation Works developed a z-pinning technique to reinforce dry performs. A device with a hollow needle was installed in a 7 axes movement robot. The z-pin is placed inside the vibrating hollow needle that is pushed through the thickness of the dry perform then the needle is withdrawn, and the Z-pin stays inside the preform. The z-pins' excesses are sheared and then the preform can be injected using a resin transfer molding (RTM) system (VAZQUEZ *et al*., 2011).

Fert (2016) used at Imperial College London a manual, low-cost, laboratory-based method Z-pinning technique using a 0.8 mm diameter metallic sewing needle placed in a bench drill to perforate a prepreg preform. The needle penetration movement have a high-level alignment. The needle sharp-point and the polished surface does not break and cause so much misalignment in the fibers. After the needle is pulled, the z-pins are positioned without applying force in the holes made with the metallic needle and the excess is cut.

Ravindran *et al* (2019c) manufactured through the thickness reinforced composites using a wet compression molding process. This process involved wet-hand layup with the z-pin foam carrier placed in the top surface of the layup and an applied high pressure of 350 kPa in a hydraulic press. The consolidation was at room temperature for 24 hours.

In other study, Loh *et al* (2021) carried the z-pinning process to reinforce braided fabric stacks in thickness direction. After the z-pins insertion, the preforms were infused with liquid resin at room temperature using the vacuum bag resin infusion process.

This work attempted to make z-pinning economically attractive, for this the z-pins were fabricated in-house, manually fed into a dry fabric preform, and fabricate the composite plates using the VARTM process.

4.2.2 Design of Experiments

Design of Experiments (DOE) is a statistical method widely applied to engineering problem solving. It refers to an experiment planning process that relates the input factors (independent variables) to the output response (dependent variables), creating a mathematical model. In this model, the input factors and their levels are constantly changed, making it possible to establish the factors with the greatest influence on the output response, along with the relevance of the interactions between them (MONTGOMERY, 2017; WERDINE *et al*., 2021). The DOE incorporates the Response Surface Methodology (RSM), which yields an empirical model based on a fitted surface. Further, this model obtained considers that an order-second equation should be able to describe the behavior of a dataset, as can be seen in Equation 4.1 (MONTGOMERY, 2017).

$$y = \beta_0 + \sum_{i=1}^{k} \beta_i x_i + \sum_{i=1}^{k} \beta_{ii} x_i^2 + \sum_{i<j} \sum \beta_{ij} x_i x_j + \varepsilon \tag{4.1}$$

where y is the response variable of the issue under study, the β is the model constant, k represents the number of design parameters, x_1 and x_2 are the factors, and e the random error term.

A common RSM consists of a complete quadratic model, which is represented by a central composite design (CCD), which in this case is composed of two input factors, such as pin area density and pin size, and four response factors related to first natural frequency, damping ratio, amplitude of vibration, and structural mass. Figure 4.1 (a) depicts the CCD, while that the Figure 4.1 (b) represents a fitted response surface plotted in a 3-D space.

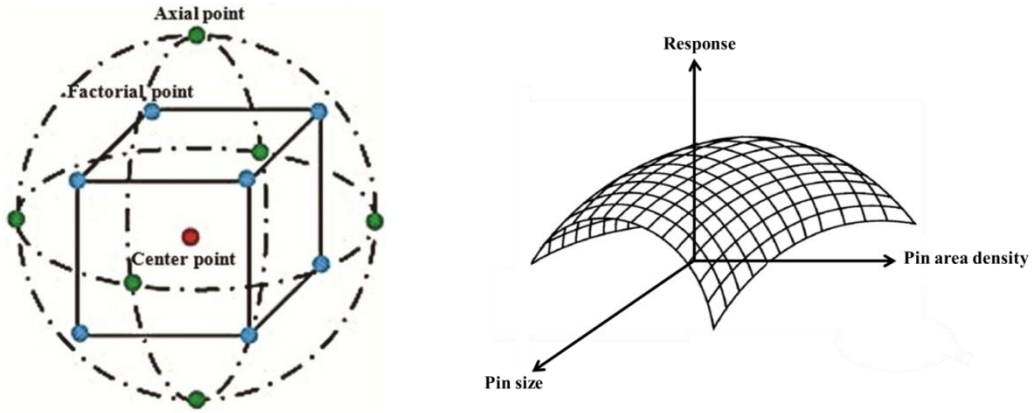

(a) (b)

Figure 4.1 – A typical response surface: (a) Central composite design (RAHIMI et al, 2020) and (b) three-dimensional surface considering the input factors: pin area density and pin size (Adapted from MONTGOMERY, 2017).

The RSM results are examined by an analysis of variance (ANOVA), which studies the quality of fitted data through comparison between the means, establishing a regression model for the system. In the ANOVA, the quality of fit is measured by the adjusted coefficient of determination (R^2_{adj}) that determines the predictive capability of the model, where a model with a value above 80% is considered appropriate, revealing that it explains the variability of the fitted data (MONTGOMERY *et al.* 2012).

The factors analyzed in the present study are considered continuous due to being numeric variables with an infinite number of values between any two factors, while the categorical variables are considered only distinct groups of categories that do not have a logical order (MONTGOMERY & RUNGER, 2010).

4.2.3 Vibration in Composite Structures

The dynamic behavior of structures exposed to different design conditions can be quantified and analyzed using modal analyses. The dynamic characteristics of a system are natural frequency, damping ratio, and mode shape. The natural frequency is represented by the frequency at which a system will vibrate without the application of external forces, after an initial disturbance (RAO & GRIFFIN, 2018). The number of degrees of freedom of a system determines the number of natural frequencies. The deformation suffered by a component when vibrating at its natural frequency is depicted through mode shapes. Due to damping on the system, a decline is observed in the oscillating system, which is represented by the damping ratio (ξ), which is considered as a nondimensional coefficient. The damping causes a loss of energy in the system, which is measured by the loss factor or loss coefficient (η). Loss factor describes the energy lost (ΔE) per radian divided by the potential energy at maximum displacement (U_{max}). The loss factor is represented by Equation 4.2 (INMAN, 2014).

$$\eta = \frac{\Delta E}{2\pi U_{max}} \tag{4.2}$$

In modal tests, the response of the structure can be measured with a laser vibrometer, which obtains data on velocity over time. Using the fast Fourier transform (FFT), the time

domain data is transformed to the frequency domain and then the frequency response function (FRF) is computed.

The FRF is responsible for establishing a relationship between the applied load and the output response caused by the application of this load. The use of the FFT generates FRF real and imaginary components. Furthermore, phase and magnitude components can also be reached and provide important information in relation to the dynamic parameters.

A common method for analyzing the FRF is known as Peak-Amplitude, in which all the responses can be assigned to one mode, disregarding the effects of other modes (EWINS, 2009). This method works properly for structures where the modes are well-separated in FRF. The natural frequencies are calculated through peaks on the FRF magnitude plot, which are confirmed to be resonance frequencies (ω_r) by observing a 180º variation on the phase plot at the same value of frequency as the peak. The local maximums are used to define two points ('a' and 'b'), known as half-power points, generated by dividing the response value by $\sqrt{2}$. Finally, the loss factor (η_r) for this particular mode can be calculated by Equation 4.3.

$$\eta_r = \frac{\omega_a^2 - \omega_b^2}{2\omega_r^2} \tag{4.3}$$

The Least-squares time domain method is also a procedure for analyzing the FRF. This method is based on the model of free decay vibration response for a multi-degree of freedom system, for which a curve-fitting algorithm is used in order to derive the modal parameters (FU & HE, 2004), as can be seen in Equation 4.4.

$$x(t) = \sum_{i=1}^{N} e^{-n_i t} \cdot [a_i \cdot \sin(\omega_{di} t) + b_i \cdot \cos(\omega_{di} t)] \tag{4.4}$$

where the coefficients a_i and b_i represent the vibration amplitude, ω_{di} describe the damped natural frequency and n_i is the damping ratio.

Therefore, the modal parameters are identified through adjusting the response obtained experimentally to Equation 4.4. In this study, the vibration is taken through the velocity response, and then the FRF depicted is known as mobility. That way, the natural frequencies were extracted considering the peak-to-peak method, and the structural damping value (loss factor) was extracted by the curve fitting method of the SDOF model.

4.2.4 Artificial Neural Networks

The theory of artificial neural networks (ANN) was first presented in 1940 by McCulloch and Pitts, and since then has been refined and has begun to gain prominence due to the advancement of technology (KOVÀCS, 2002). ANN resembles the human brain, being built by simple circuits connected by units known as artificial neurons. The connections created between the neurons are responsible for transmitting signals, generating the synapses that have the function of spreading information and are widely used in learning algorithms (CHONG & ZAK, 2004; YAN *et al*. 2020). The ANN technique has the ability to learn from experience obtained through data set training. After the training, it is expected that the ANN will be able to recognize output response according to unknown input data and will become a powerful tool for several applications (KHATIR *et al*. 2021).

The ANN is built with three major components: input layers, hidden layers, and output layers, each of which contains a certain number of neurons. (DINIZ *et al*. 2019; YAN *et al*. 2020). The action of neuronal connections is represented by their weights, which can be negative or positive depending on whether the connections are inhibitory or excitatory. The influence of a signal obtained from another neuron is calculated by multiplying the value (intensity) of the received signal by the weight of the relevant connection ($X_i \times W_i$). The total of the values of all $X_i \times W_i$ connections is completed, and the resulting value is transmitted to the activation function (RIBEIRO JUNIOR *et al.* 2020). The activation function describes how the weighted sum of the input is turned into an output from a node or nodes in a network layer (RIBEIRO JUNIOR *et al*., 2022).

Learning paradigms govern the interaction between data and an ANN. The main classes of learning paradigms are supervised learning and unsupervised learning (HAYKIN, 1994). In supervised learning, examples are provided to the network, and the network response is compared to the desired answer. The difference between the two replies, referred to as the error signal, is utilized to alter the network's synaptic weights. This approach is repeated until the network answers appropriately in a statistical sense. In unsupervised learning, the algorithm does not seek to know the intended outputs, hence they do not utilize instances of input and output to be learnt by the network. The ANN's self-organization (RIBEIRO JUNIOR *et al*. 2020).

Also, neural networks can be divided by their information propagation, which can be a feed-forward network or a back-propagation network. In feed-forward networks, information

flows in only one direction; that is, it goes from the input layer to the output layer in only one direction (SVOZIL *et al*., 1997). In networks with backpropagation, the information can go back from one layer to the other (BUSCEMA, 1998).

For an adequate ANN configuration, you should design a model that is not too stiff to not correctly describe the data, but also not too flexible to model the data's noise.

4.3 Methodology

4.3.1 Response Surface Design

In order to optimize the manufacturing conditions of z-pinned beams, a RSM is proposed, considering the results obtained by modal experimental testing. For example, the optimum manufacturing conditions are associated with reduced amplitude of vibration and reduced mass. That way, the RSM considered two design factors: the pin size (x_p) and the number of pins per unit area, known as pin area density (x_d), and four response factors in relation to modal results (first natural frequency, amplitude of vibration, damping ratio, and mass). Based on preliminary tests, it was possible to define the experimental boundaries for the modal test, where it was considered factorial points (-1 and +1), axial points (-α and +α), and central points, as can be seen in Table 4.1.

Table 4.1 - Input factors and their levels for α = 1.4142.

Control variables	**Symbol**	**Level**				
		-α	-1	0	+1	+α
Pin area density	x_d	0.1893	0.5	1.25	2.00	2.3106
Pin size	x_p	0.3964	0.5	0.75	1.00	1.1035

The experimental boundaries were established according to a maximum and minimum size for the pin edge and a maximum and minimum allowed density. The CFRP beam had the insertion of pinning reinforcement through the thickness, as depicted in Figure 4.2. For this reason, the design of experiments was performed considering the pin size and pin area density as the more relevance factors for an optimum manufacturing of reinforced structures with pins.

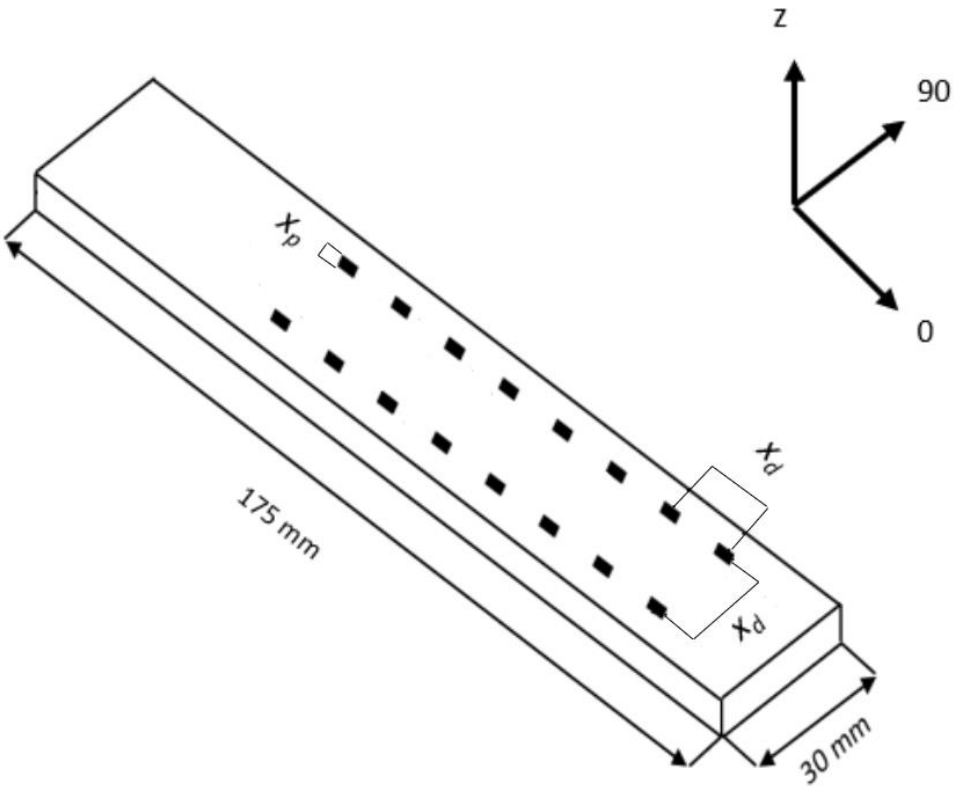

Figure 4.2 – Scheme of the z-pinned specimen considering the parameters xd and xp and its dimensions.

4.3.2 Composites Manufacturing

For the experiments reported here, the materials used to manufacture the rectangular z-pins and the composite through the thickness reinforced laminates were an Unidirectional (UD) Tape (6K warp carbon yarns and areal weight of 149 g/m² supplied by Hexcel) and the two-part epoxy resin system (AMPREG AR21 resin and the A21 SLOW hardener supplied by GURIT). The preforms used to fabricate the machined rectangular z-pins rods were laid up with 4 plies in a [0/+45/-45/0] stack sequence, placed in a flat metal mold and then the composite laminate was manufactured by the VARTM process. This stack sequence was chosen to ease the handle, avoid the laminate to crack or debonding in the 0º direction and to allow the z-pin rods machining process. The VARTM process was carried out at room temperature and after the resin infusion is completed the laminate was cured in an oven at 80ºC for 4 hours. The z-pin rods were then machined with the width obtained in the SRM and cited in the Table 4.1.

To create a reinforcing square pattern and to guide the z-pins insertion perpendicular into the preform, prior the z-pin insertion, 2 polystyrene (PS) plates were drilled in a CNC Router (with the areal density obtained in the SRD) and the holes are also used to keep the z-pins aligned during the VARTM process. The PS was chosen because its glass transition temperature (T_g > 80 ºC) is higher than the resin cure temperature. The Figure 4.3 shows the scheme of the preform between the drilled PS plates and the z-pin insertion with a hollow needle.

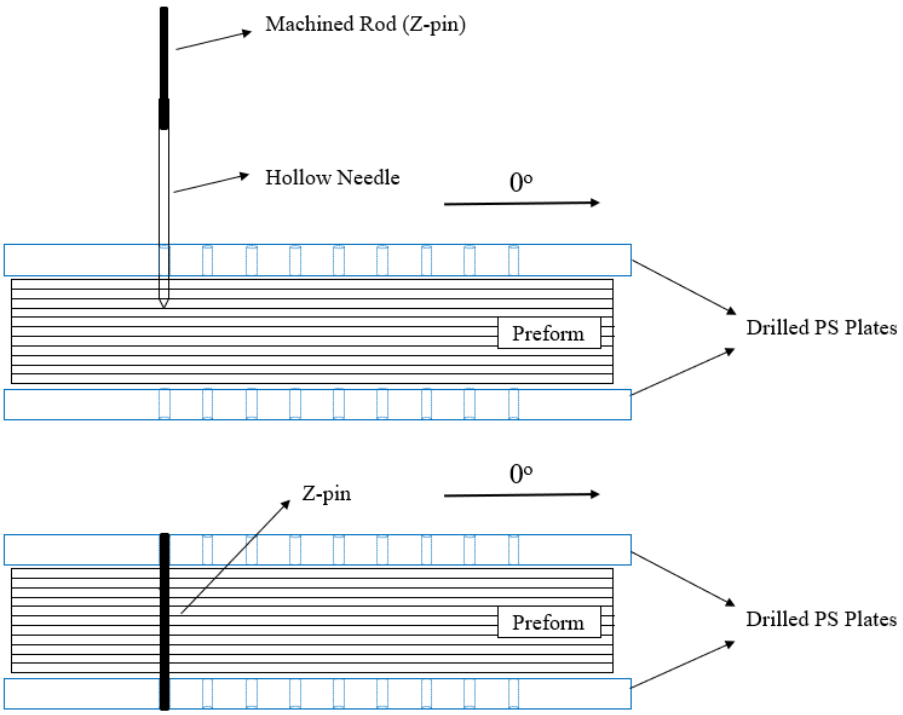

Figure 4.3 – Scheme of the preform between the drilled PS plates and the z-pin insertion with a hollow needle.

The Figure 4.4 shows the UD carbon fiber preform with a $[0]_{18}$ stack sequence between the 2 PS plates being inserted with z-pins through the thickness prior to the VARTM process.

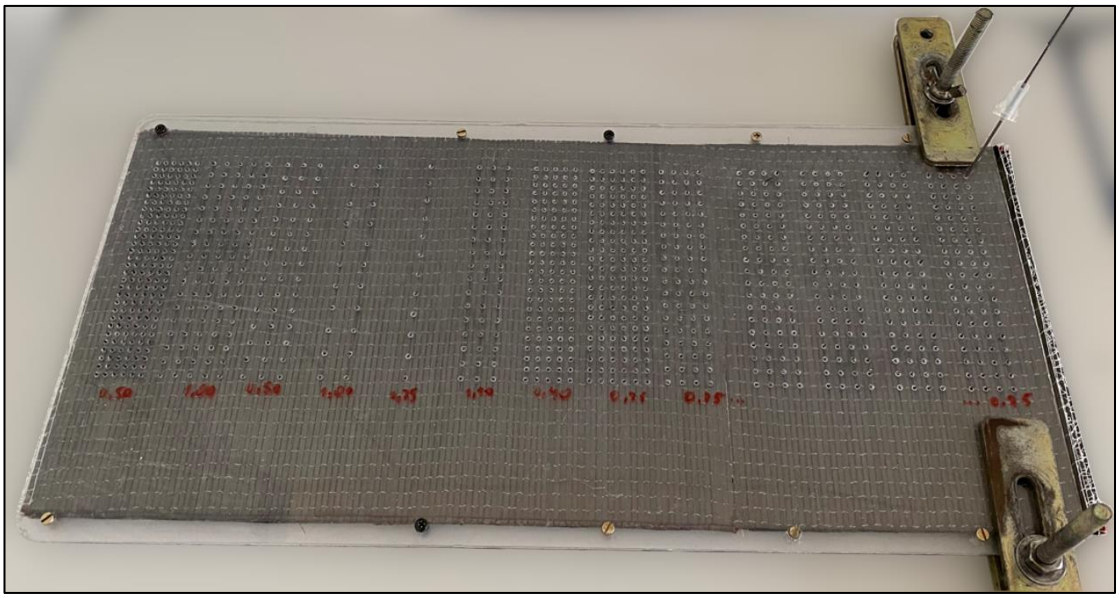

Figure 4.4 – Preform between 2 PS drilled plates before the VARTM process.

The z-pins are inserted in the thickness direction aided by a hollow needle. The needle, with the carbon rod inside, is pushed through the thickness and when it is withdrawn, due to the friction with the fabric, the rod is kept inside the preform. The excess of the rod is cut and the next insertion is done. The Figure 4.5 (a) shows the hollow needle with a carbon rod inside and (b) the carbon rod placed inside the preform and the excess being cut.

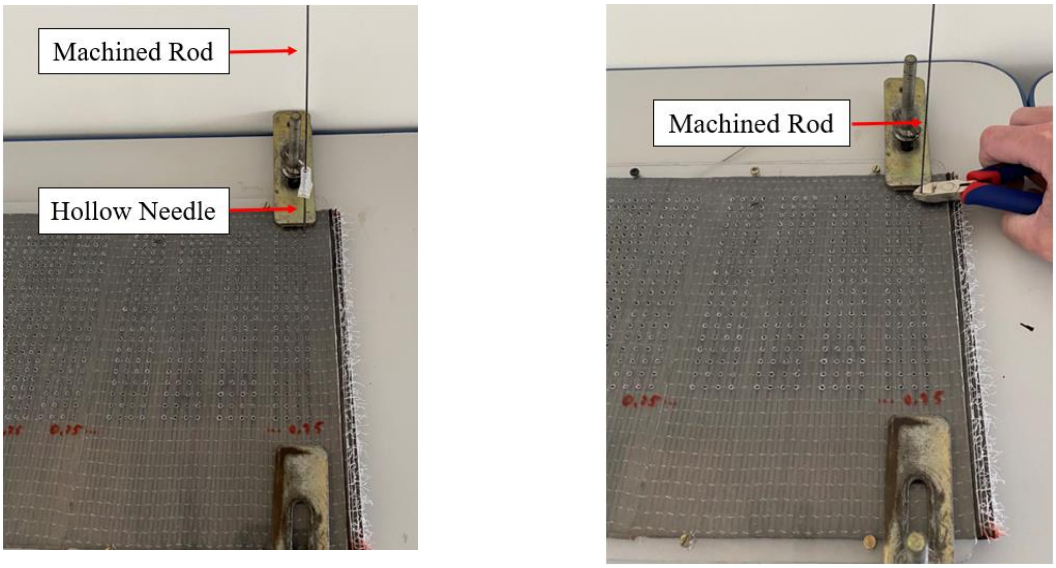

(a) (b)

Figure 4.5 – (a) hollow needle with a carbon rod inside and (b) the carbon rod placed inside the preform and the excess being cut.

After the insertion process, the preform is impregnate by VARTM with the same parameters and materials used to manufacture the laminate used to produce the rectangular z-pins, but the laminate cure time was 5 hours. The Figure 4.6 shows the vacuum bag assembled and the step before (a) and (b) after the resin infusion by VARTM.

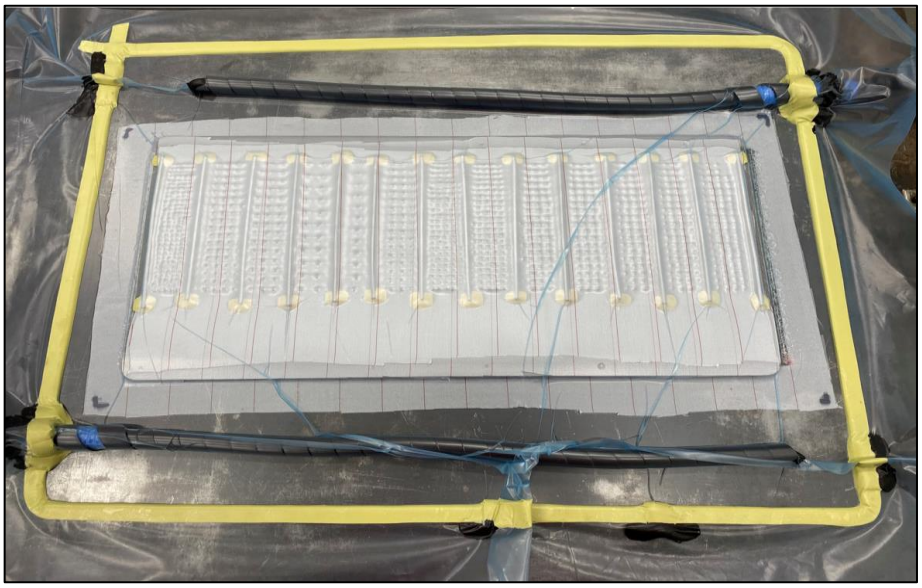

(a)

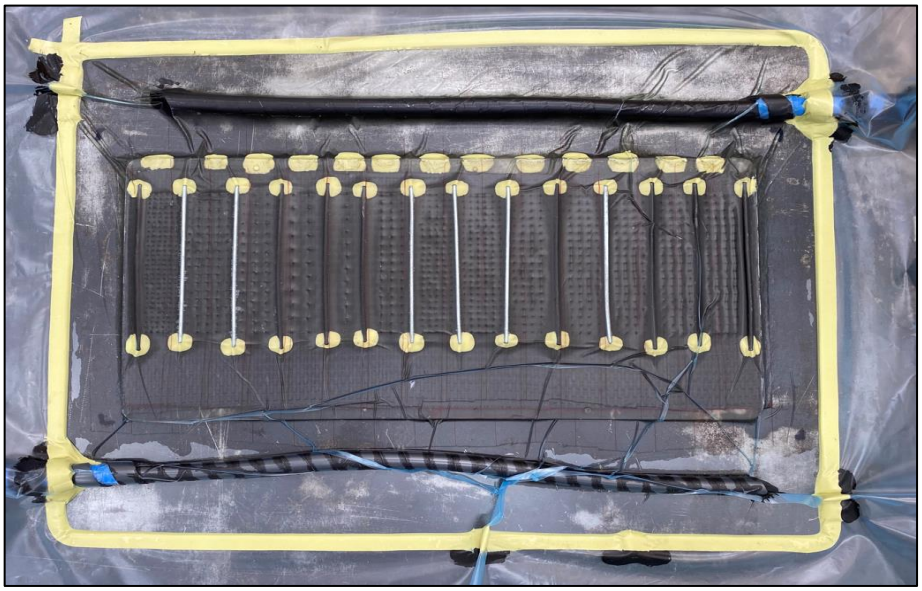

(b)

Figure 4. 6 - Vacuum bag assembled and the step before (a) and (b) after the resin infusion by VARTM.

When the laminate is cured, it is demolded and the PS plates are removed to carry out the specimens' machining process according to the pin width and areal density cited in Table

4.2. The Figure 4.7 shows (a) the composite laminate after demolding and the with the PS plate removed and (b) the machined specimens.

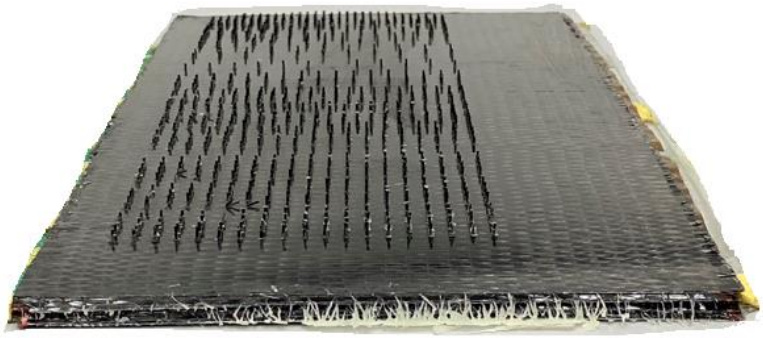

(a)

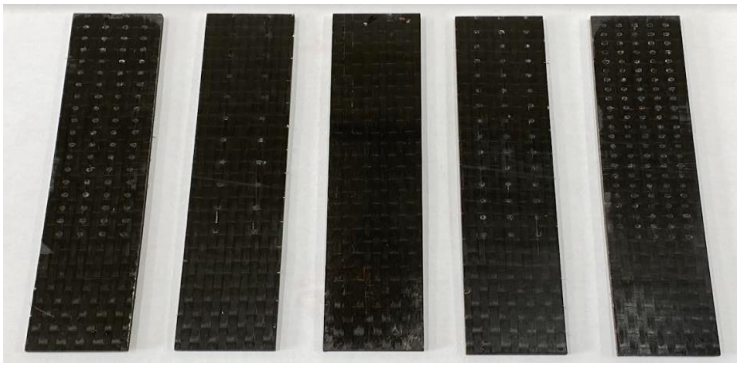

(b)

Figure 4.7 – (a) Composite laminate after demolding and (b) examples of machined specimens.

Table 4.2 - Response surface model considering two manufacturing (design) factors.

Specimen	Areal density x_d (%)	Pin width x_p (mm)
#0 (Reference)	no reinforcement (0.00; 0.00)	
#1	0.50	0.50
#2	0.50	1.00
#3	2.00	0.50
#4	2.00	1.00
#5	1.25	0.40
#6	1.25	1.10
#7	0.20	0.75
#8	2.31	0.75
#9	1.25	0.75
#10	1.25	0.75
#11	1.25	0.75
#12	1.25	0.75
#13	1.25	0.75

The needle insertion and the z-pins placed in the thickness direction of the composite will introduce defects. These defects are such as fiber breakage, wavy fibers (separation and deflection of the tows) and free areas surrounding the z-pins which will collaborate to the thickness' increase and will form resin pockets after the resin infusion. The Figure 4.8 (a) shows the z-pin and the resin-rich region, or resin pockets, and Figure 4.8 (b) shows the waviness (eyelet shape) caused by the insertion of needle and the z-pin positioned through the thickness and Figure 4.8 (c) shows a resin channel, usually formed when the space among the pins is small.

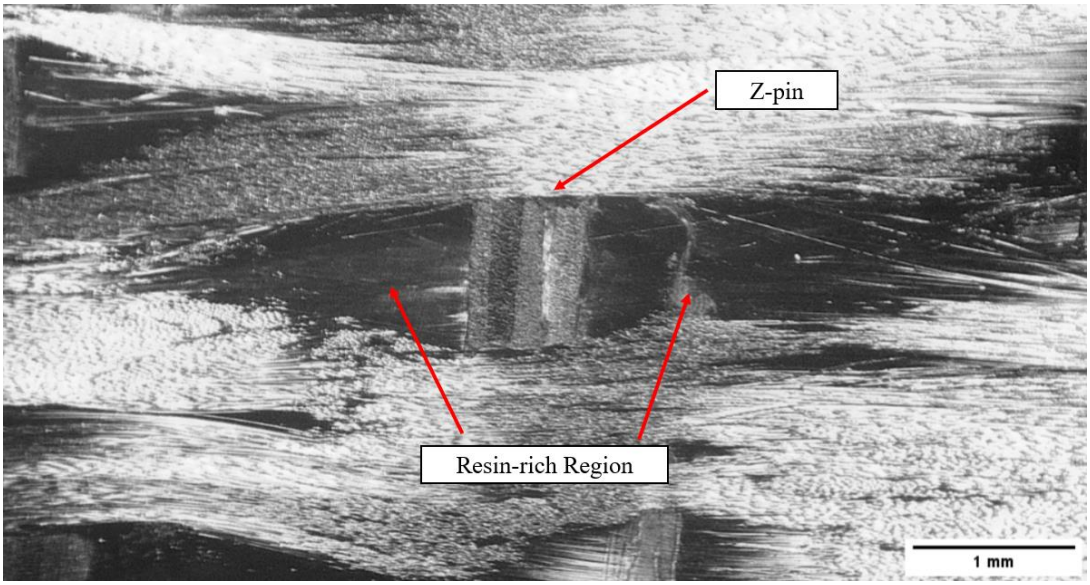

(a)

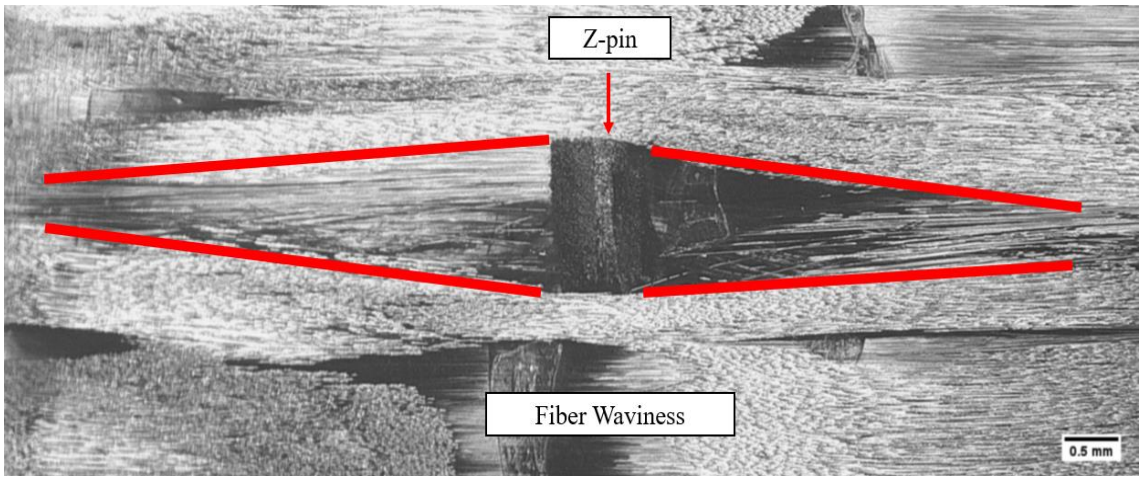

(b)

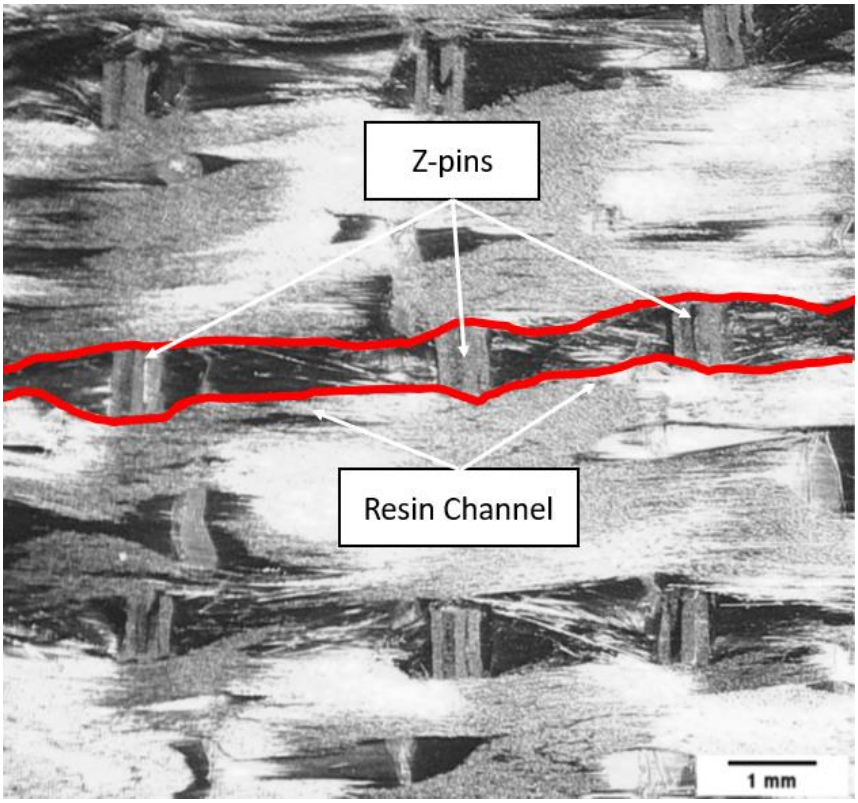

(c)

Figure 4.8 – Example of (a) z-pin and the resin-rich zone, (b) the fiber waviness and a resin channel in composites reinforced through the thickness.

(Intentionally left in blank)

4.3.3 Experimental Setup

Firstly, a modal experimental test was realized considering an analysis of free vibrations without the presence of external forces, and, posteriorly, another modal experimental test considering forced vibrations was performed with the application of external force by a shaker. Figure 4.9 presents the experimental setup used in this study, which is integrated with a sensor, shaker, impact hammer, data acquisition, and signal analysis. The instruments used include LabVIEW programming, a Data Acquisition (DAQ) board, a laser sensor, an impact hammer, and a shaker.

In this experiment the DAQ board utilized was a Brüel & Kjaer Photon Plus type. Ometron's model VQ-500-D laser vibrometer was used to detect vibration displacement at a specified position. An impact hammer made by Brüel & Kjaer was used for the free vibration investigation. The voltage signal from the power amplifier, model 2712 by Brüel & Kjaer, drove the shaker, model 4808 by Brüel & Kjaer. All the signals created by the machine were analyzed by LabVIEW programming. To avoid signal loss due to the low reflective characteristic of the carbon/epoxy skin, all specimens were covered with reflective adhesive tape. These tests were important for the acquisition and characterization of the modal behavior of the z-pinned structures.

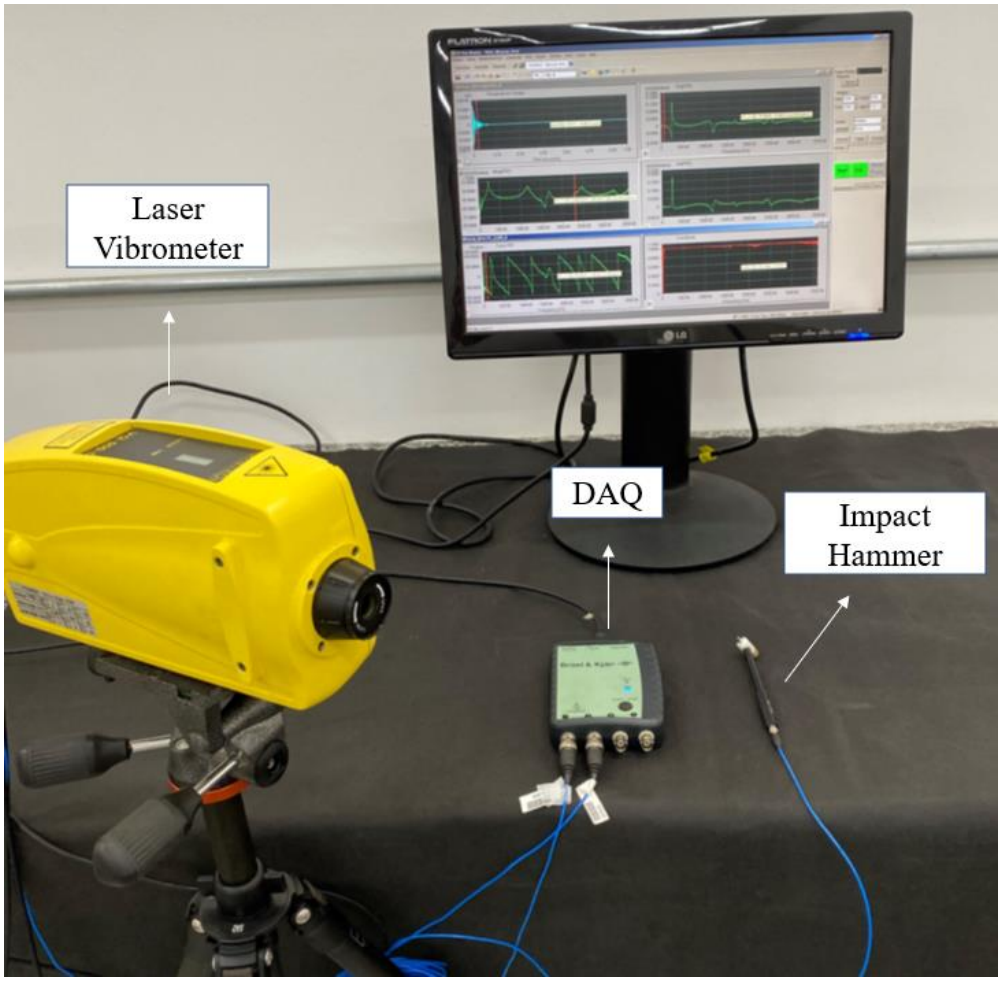

(a)

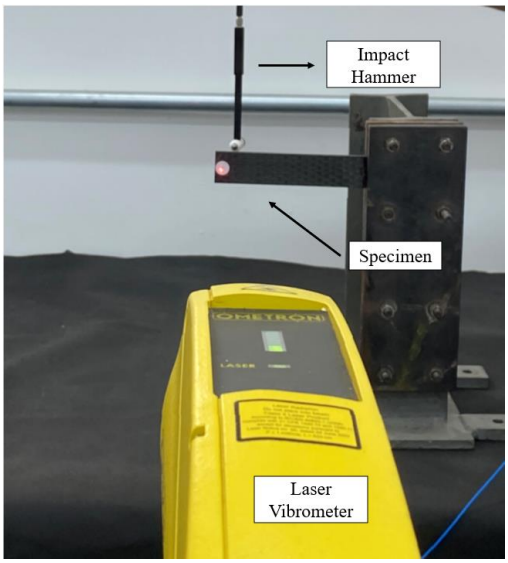

(b)

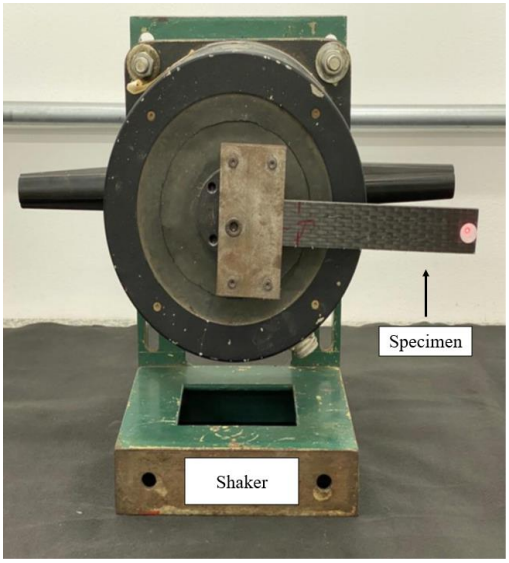

(c)

Figure 4.1 - General experimental setup with a laser vibrometer, DAQ and the impact hammer (a), details for free vibration (b) and forced vibration (c) experiments devices.

The strategy used in this study is fully detailed in the flowchart presented in Figure 4.10.

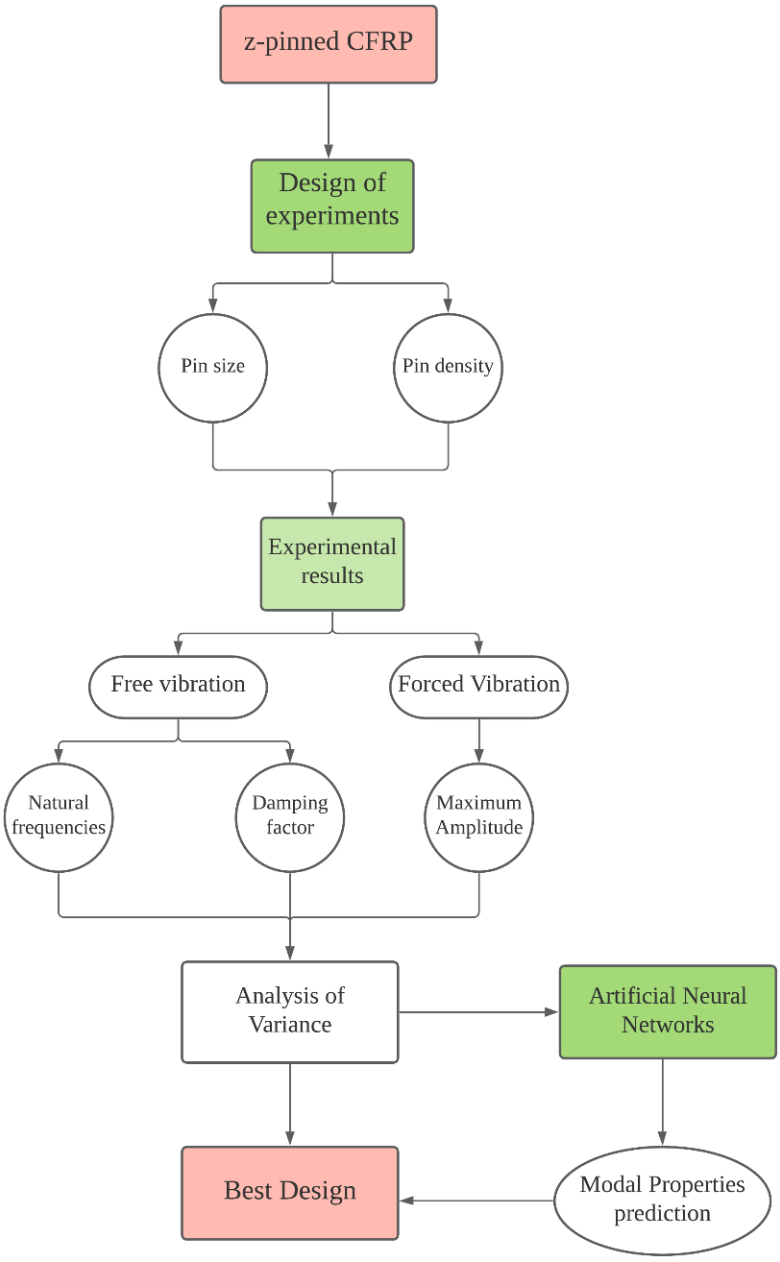

Figure 4.20 – Flowchart of the strategy used for optimum manufacturing conditions of z-pinned CFRP beams.

4.4 Experimental Results and Discussion

In this section, is discussed the results obtained by the proposed method. The first analysis was a free vibration and forced vibration analysis, which allowed the z-pin responses to be compared to a reference. The statistical results are then evaluated using the RSM and ANOVA methods. Finally, the results of ANN are presented.

4.4.1 Free and Forced Vibration Analysis

4.4.1.1 Free Vibration

The first experimental test was for the free vibrations using the setup described in the Figure 4.9 (a) and (b) and from this test was achieved the values for the first natural frequency and the loss factor, or damping.

Free vibration is the response of a system to an initial input, allowing it to vibrate freely. Through it, it is possible to analyze the natural frequencies and their amplitudes, as well as the damping/loss factor of the system. Figure 4.11 shows the main response of free vibration time histories of z-pinned composites with all different design factors tested at the same initial vibration amplitude and it can be seen the decaying of the peak velocity and also the beat phenomenon in the specimens 5 (e), 10 (j) and 12 (l).

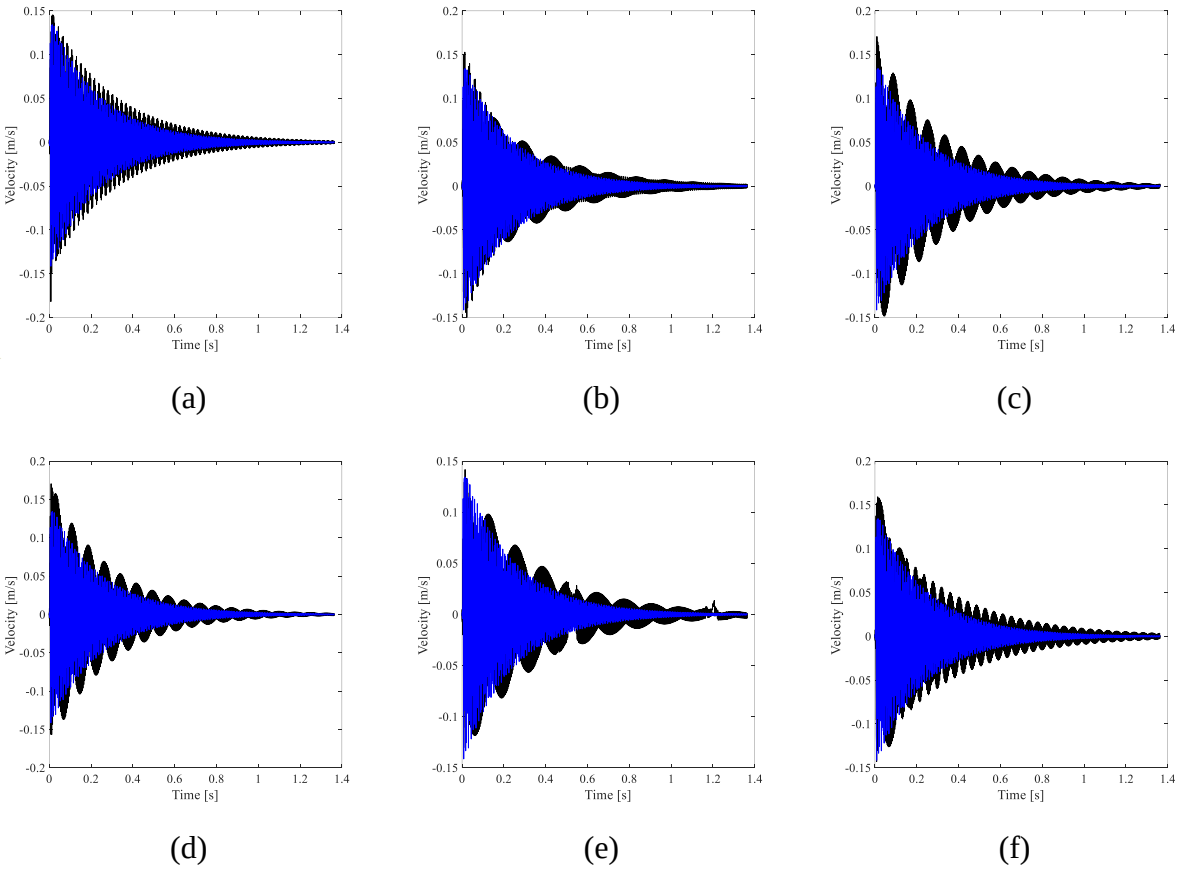

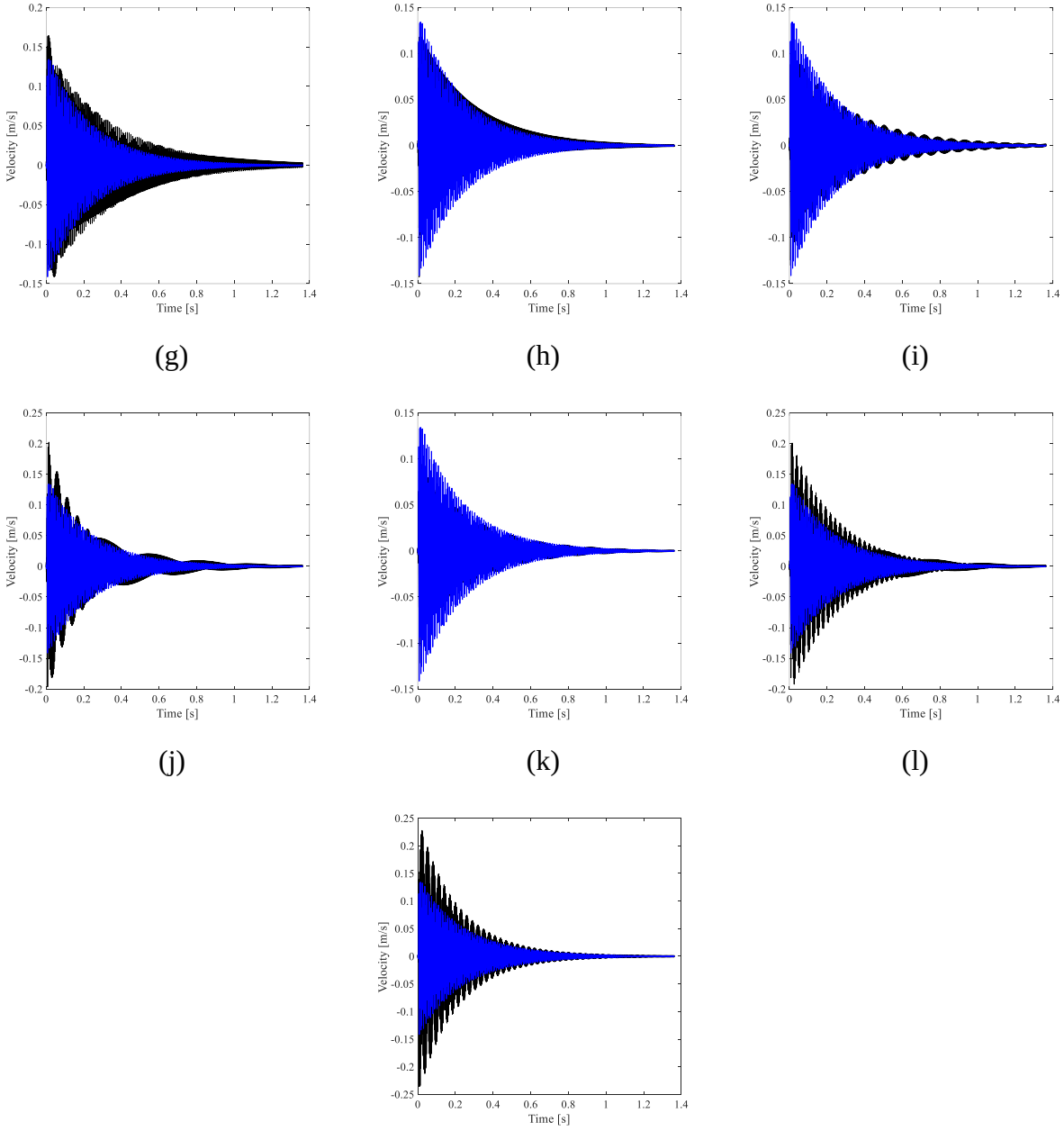

Figure 4.31 - Velocity time response considering the different design factors (legend: ▬ reference, ▬ reinforced specimens).

In addition, Figure 4.12 shows the frequency spectrum (mobility) for the pinned beams examined, emphasizing the first mode of vibration. In most of the cases, there was an increase in the natural frequency of the z-pinned composites compared to the unpinned led by the enhancement of the bending stiffness caused by the z-pins insertion. Although, in the specimens 2 and 7, with a low areal density insertion, and specimens 3 and 6 (higher areal density), had a decrease (from 1.32% to 4.93%) in the values for natural frequency and it may

be related to the size of the pins and the defects caused during the insertion and manufacturing such as resin rich zones surround the pins, the wavy fibers (eyelet shape) and the resin channels showed in Figure 4.8 (a-c).

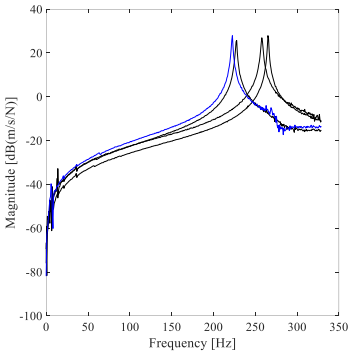

(a) ω_{n1} = 227.78 Hz

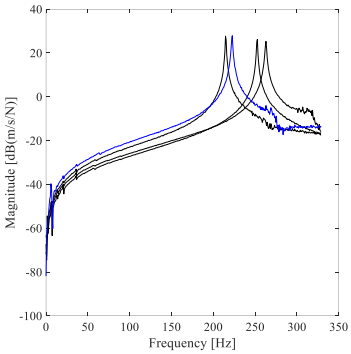

(b) ω_{n2} = 214.60 Hz

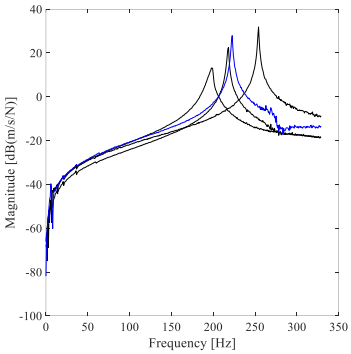

(c) ω_{n3} = 218.26 Hz

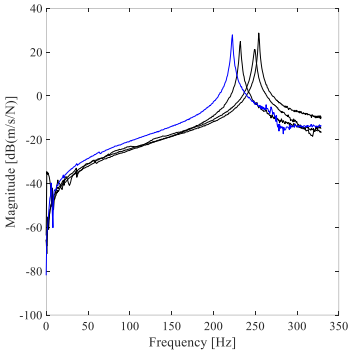

(d) ω_{n4} = 232.18 Hz

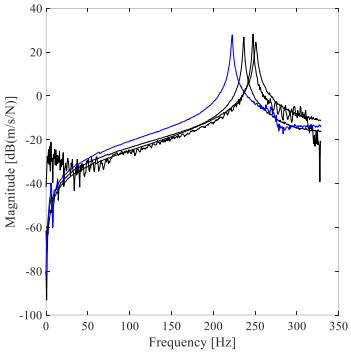

(e) ω_{n5} = 236.57 Hz

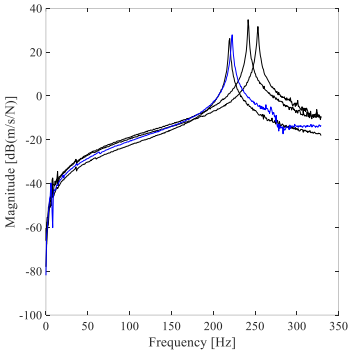

(f) ω_{n6} = 219,73 Hz

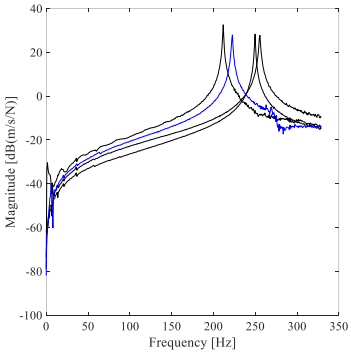

(g) ω_{n7} = 211.67 Hz

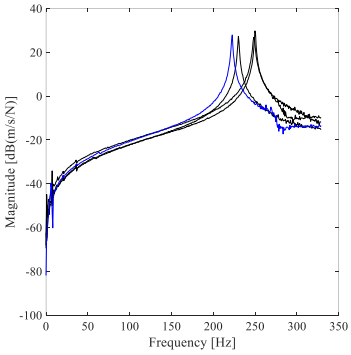

(h) ω_{n8} = 229.98 Hz

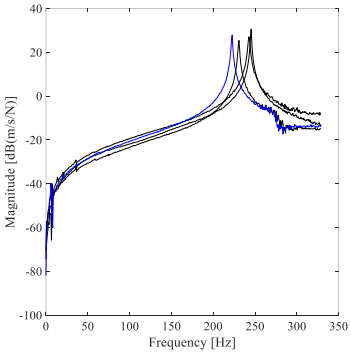

(i) ω_{n9} = 230.71 Hz

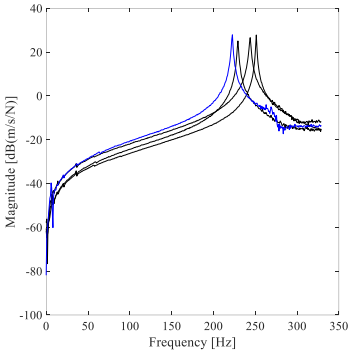

(j) ω_{n10} = 229.25 Hz

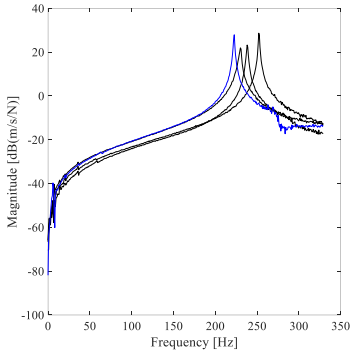

(k) ω_{n11} = 238.04 Hz

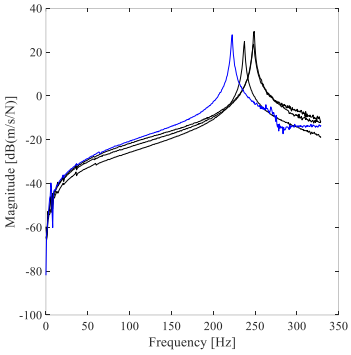

(l) ω_{n12} = 237.31 Hz

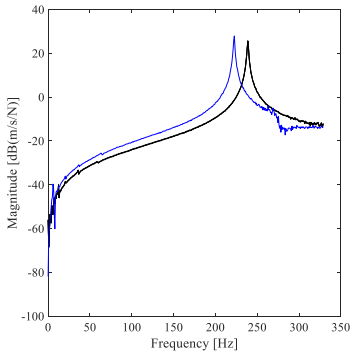

(m) ω_{n13} = 238.77 Hz

Figure 4.4 - Frequency response function for considering the different design factors (legend: ━ reference, ━ reinforced specimens).

(Intentionally left in blank)

4.4.1.2. Forced Vibration

For the forced vibration test the setup described in the Figure 4.9 (a) and (c) and from this test was achieved the values for amplitude. Forced vibration is the response of a system due to a time-varying input. Through it, it is possible to analyze the system's maximum amplitude of resonance. Each specimen was excited with its natural frequency (values in Figure 4.12) and the response over time is showed in Figure 4.13 and the Table 4.3 summarizes the values for modal responses and for the specimens' mass.

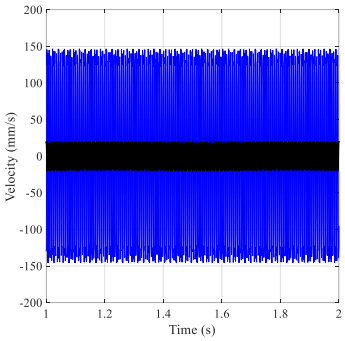

(a) A_1 = 19.46 mm/s

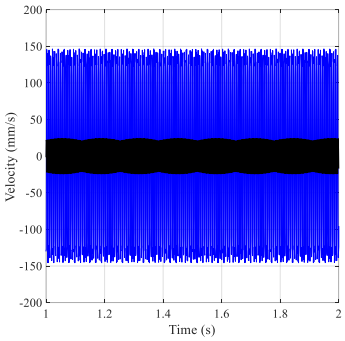

(b) A_2 = 23.12 mm/s

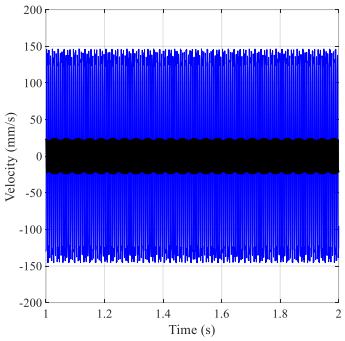

(c) A_3 = 23.17 mm/s

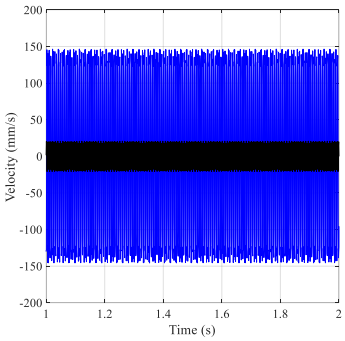

(d) A_4 = 19.65 mm/s

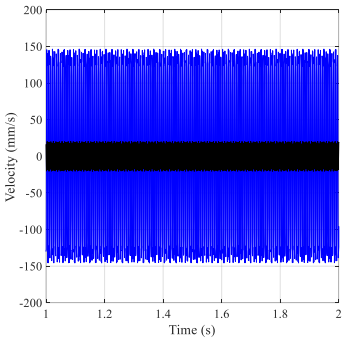

(e) A_5 = 19.19 mm/s

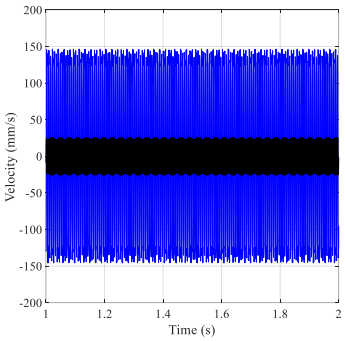

(f) A_6 = 24.64 mm/s

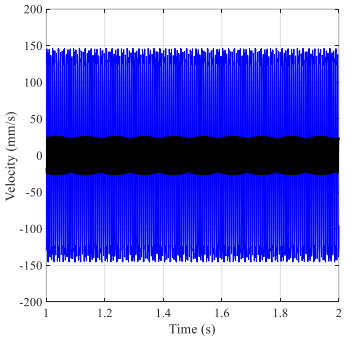

(g) A_7 = 25.17 mm/s

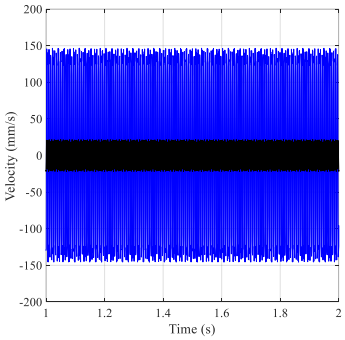

(h) A_8 = 20.56 mm/s

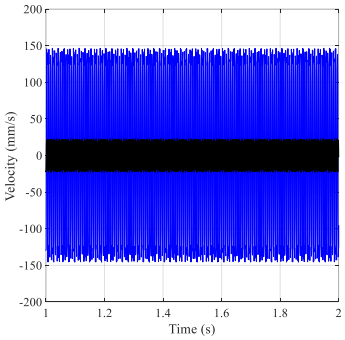

(i) A_9 = 21.59 mm/s

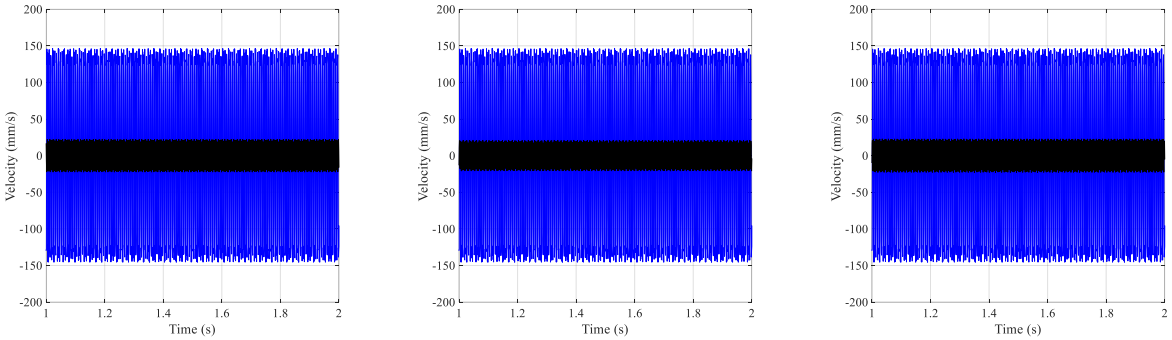

(j) A_{10} = 21.17 mm/s (k) A_{11} = 19.63 mm/s (l) A_{12} = 21.52 mm/s

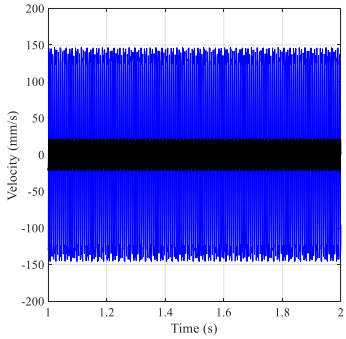

(m) A_{13} = 20.94 mm/s

Figure 4.53 - Forced vibration in time domain considering for the different design factors and the amplitude values for each specimen (legend: ▬ reference, ▬ reinforced specimens).

The plots in Figure 4.13 indicate the forced vibration for each pinned specimen is compared to the unpinned, with a maximum amplitude of resonance of 64.46 mm/s. The results achieved from the test presented a significant decrease, from approx. 60% to 70%, in the values of amplitude in the z-pinned specimens in comparison to the reference.

4.4.2 Analysis of Variance

The primary goal of this research is to dynamically characterize laminated composite structures with z-pinning. The results were conducted from the experimental planning RSM, where the parameterization was based on two choice variables and four responses, namely natural frequency, loss factor, vibration amplitude, and mass. Form Figure 4.14 to Figure 4.17 represents the results obtained by means of an analysis of variance (ANOVA) of the responses as a function of the manufacturing factors.

For the analysis of the statistical results, the modal responses were normalized by analyzing the percentage variation, as shown in Equation 4.5 to Equation 4.8. Table 4.3 summarizes the overall results of this study, with the experimental arrangement and responses.

$$\Delta\omega = \left(1 - \frac{\omega}{\omega_{Ref}}\right) \times 100 \tag{4.5}$$

$$\Delta\eta = \left(1 - \frac{\eta}{\eta_{Ref}}\right) \times 100 \tag{4.6}$$

$$\Delta A = \left(1 - \frac{A}{A_{Ref}}\right) \times 100 \tag{4.7}$$

$$\Delta m = \left(1 - \frac{m}{m_{Ref}}\right) \times 100 \tag{4.8}$$

Table 4.3- Vibrations responses for all the different manufacturing design of CFRP with z-pin insertion considering a RS design.

Specimen	Variables		Experimental Responses							
	Pin Size	Pin density	ω_n (Hz)	η (%)	A (mm/s)	m (g)	$\Delta\omega_n$ (%)	Δη (%)	ΔA (%)	Δm (%)
1	0.50	0.50	227.78	0.60	19.46	29.19	2.30	7.20	69.81	0.14%
2	1.00	0.50	214.60	0.45	23.12	27.94	-3.62	-20.90	64.14	-4.15%
3	0.50	2.00	218.26	0.66	23.17	30.42	-1.97	17.69	64.05	4.36%
4	1.00	2.00	232.18	0.52	19.65	31.05	4.28	-7.30	69.52	6.52%
5	0.40	1.25	236.57	0.41	19.19	30.16	6.25	-26.48	70.23	3.46%
6	1.10	1.25	219.73	0.54	24.64	29.58	-1.32	-4.32	61.78	1.48%
7	0.75	0.19	211.67	0.40	25.17	27.56	-4.93	-28.31	60.95	-5.45%
8	0.75	2.31	229.98	0.55	20.56	31.51	3.29	-1.85	68.10	8.10%
9	0.75	1.25	230.71	0.57	21.59	30.76	3.62	1.04	66.51	5.52%
10	0.75	1.25	229.25	0.56	21.17	30.21	2.96	-1.01	67.16	3.64%
11	0.75	1.25	238.04	0.69	19.63	30.97	6.91	21.93	69.56	6.24%
12	0.75	1.25	237.31	0.50	21.52	30.71	6.58	-10.82	66.62	5.35%
13	0.75	1.25	238.77	0.56	20.94	31.62	7.24	-0.44	67.51	8.47%
reference	0.00	0.00	222.66	0.56	64.46	29.15	-	-	-	-

Figure 4.14 shows the main effects plot results for the first natural frequency, where for larger sizes, we have smaller values of the natural frequency, while for density, it occurs in the opposite way. For larger values, we have a greater value of natural frequency. Figure 4.15 shows the behavior of the main effects of the loss factor. In this case, there is not a well-defined pattern for the size variable, which makes a deeper analysis difficult. However, for density, we have that for higher densities, the loss factor is higher.

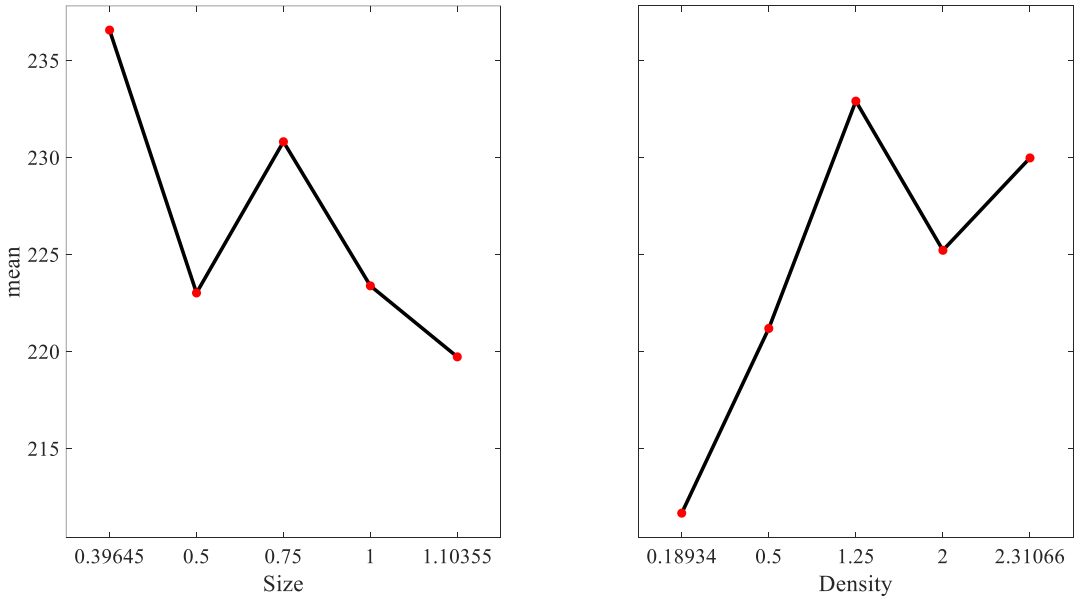

Figure 4.64 - Main effect plot for the first natural frequency.

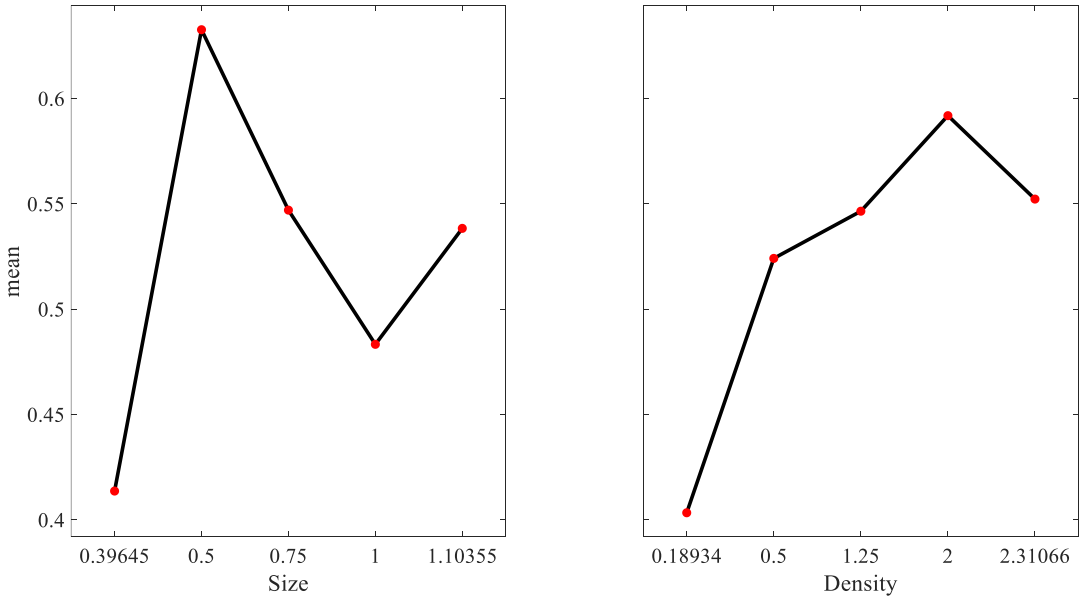

Figure 4.75 - Interaction plot for the loss factor.

Figure 4.16 shows the behavior of the main effects of the vibration amplitude. In this situation, it is clear that for larger sizes we have high vibration amplitude and for higher densities we have lower vibration amplitude. Figure 4.17 depicts the behavior of the main effects of the mass, which concludes the examination of the main effects. It was not noticed a substantial change in mass for the size variable, but it tends to a linear behavior for density values due to the quantity of pins inserted greater are values for mass.

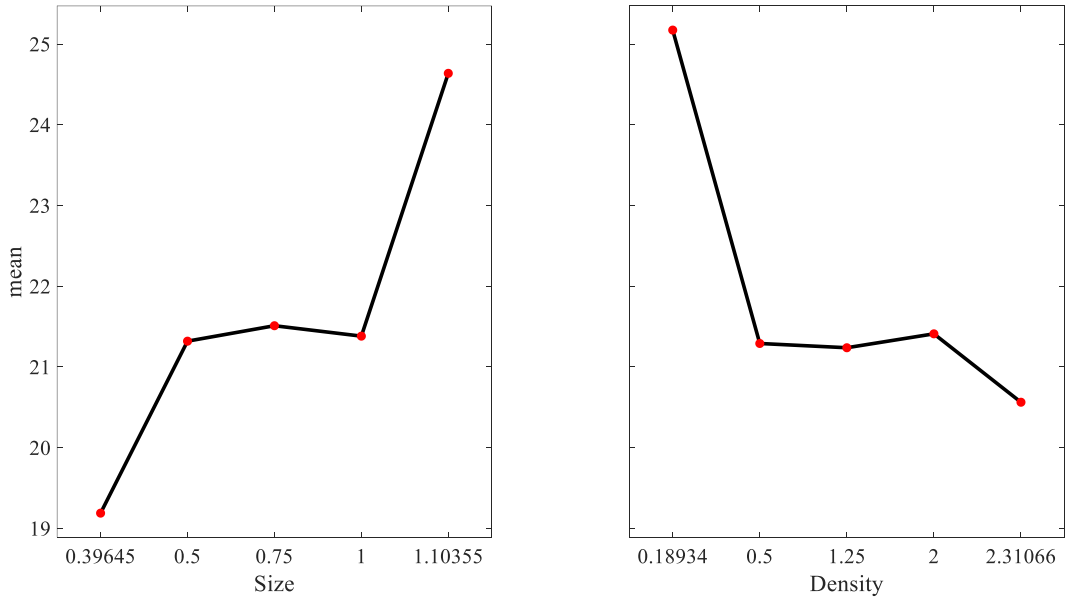

Figure 4.8 - Interaction plot for the vibration amplitude.

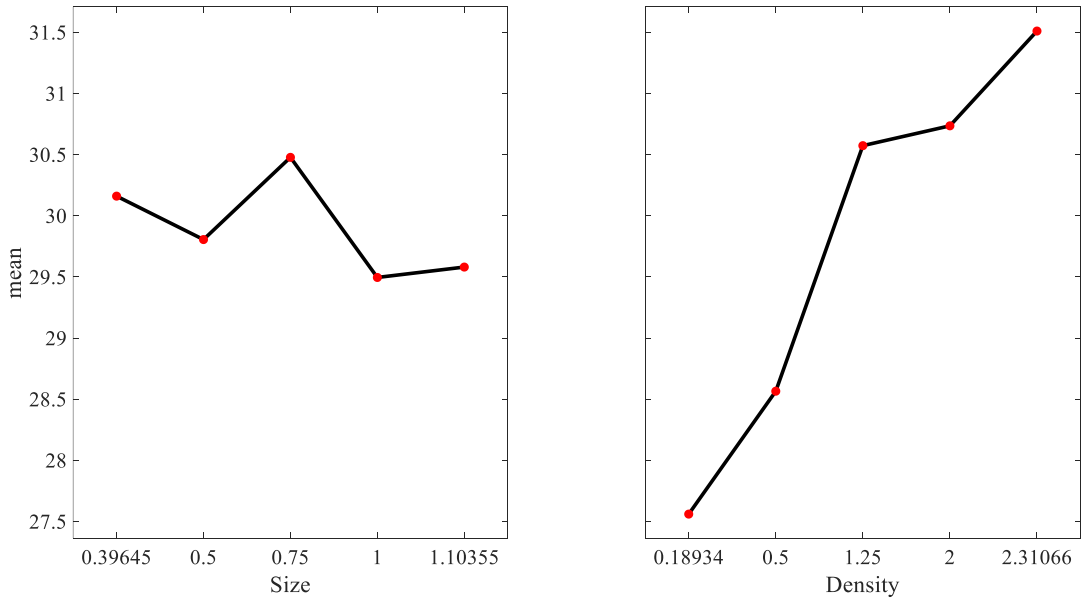

Figure 4.9 - Interaction plot for the mass.

Combining the analyses, Figure 4.18 presents the response surface combining the two variables, from which it is possible to analyze the combined effect of both on natural frequency, loss factor, vibration amplitude, and mass. The response surfaces in the space for natural frequency, loss factor and amplitude presented a nonlinear behavior, and the mass presented a close to plane (linear).

In the Figure 4.18 (a) with thicker pins (≥1 mm) with greater density insertion higher are the values for natural frequency, tending to have a linear behavior. Although for thin pins (≤1) from the medium density insertion in most cases, either increasing or decreasing the density, the natural frequency values will be lower. Figure 4.18 (b) from small to medium pin sizes the lowest values are when the density gets close to medium density insertion (1.25%). From that point either if it has a higher or a lower pin areal density insertion the loss factor increases. However, with the same medium areal density insertion and greater pin sizes, there is a opposite behavior leading to lower loss factor values when the density either increase or decrease. In Figure 4.18 (c) with the smallest pin and an increase in areal density insertion beyond the 0.5% the amplitude values tend to be higher, but it also happens with density insertion smaller than 0.5% and all pin sizes. Also, with medium insertion values and with an increase in the pin size greater are the values for the amplitude. For Figure 4.18 (d) in the middle part of the curve it is possible to notice that with higher density and thicker pins there is an increase in the mass and with lower density insertion and thin pins the mass decrease.

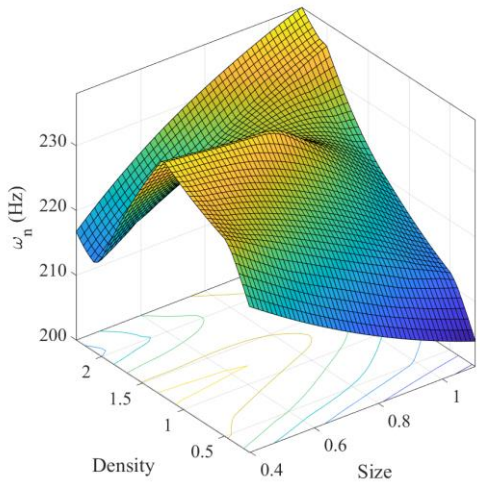

(a)

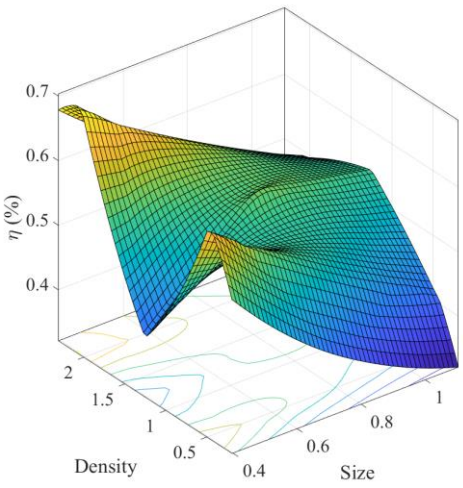

(b)

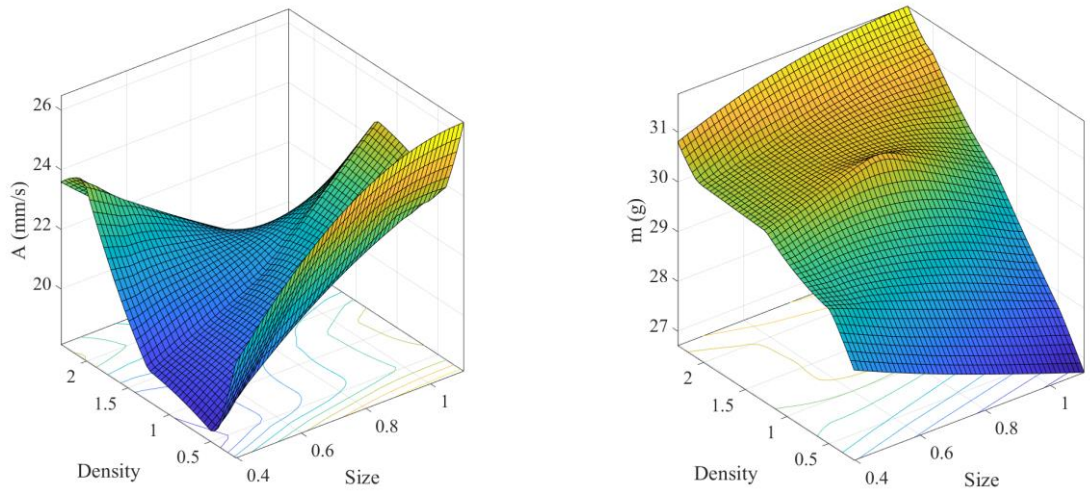

(c) (d)

Figure 4.10 – Response surfaces in the space for (a) NPC, (b) PC, (c) ΔNPC e (d) ΔPC.

with the smallest pin and an increase in areal density insertion beyond the 0.5% the amplitude values tend to be higher, but it also happens with density insertion smaller than 0.5% and all pin sizes. Also, with medium insertion values and with an increase in the pin size greater are the values for the amplitude.

4.4.3 Modal Properties Prediction using ANN

In this study, an ANN was developed to perform the responses in relation to the modal behavior of z-pinned CFRP beams, where the input layers are composed by design parameters such as pin size and pin density, and the output layers by modal response related to natural frequency, damping ratio, amplitude, and mass. That way, the ANN created has one input layer with two neurons, two hidden layers with twenty and four neurons, respectively, and one output layer with four neurons as presented in the Figure 4.19.

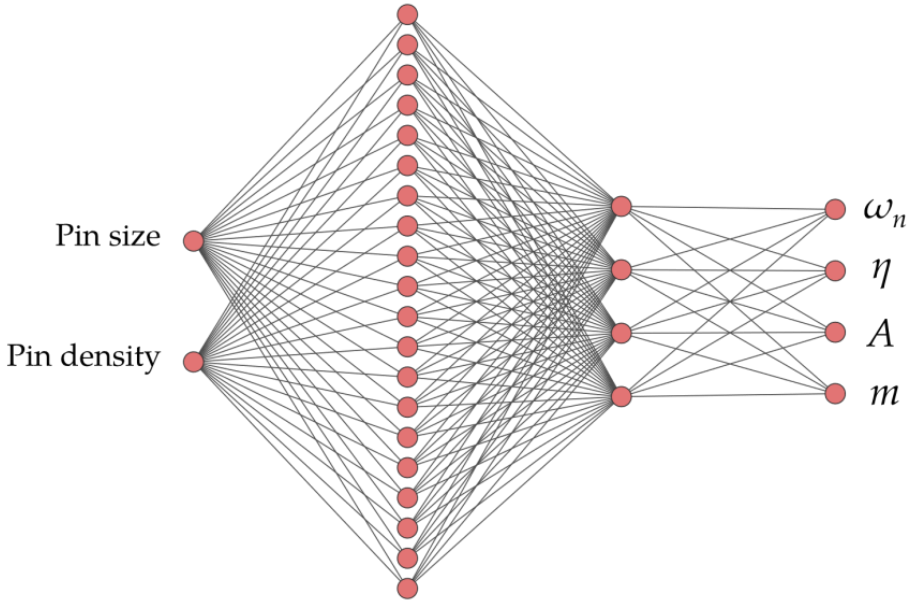

Figure 4.19 –The architecture used for the ANN.

To achieve good performance, the multilayer feedforward network with backpropagation training algorithm with supervised learning was chosen. Using this algorithm, the network is trained, and its generated errors are transmitted to the previous layers until they reach negligible values (Haykin, 2009). In order to promote a fast convergence rate and correct training, the Levenberg-Marquardt algorithm was used on the ANN architecture. The other parameters used in the ANN developed here are depicted in Table 4.4.

Table 4.4 – Optimal ANN configuration taking modal behavior into account.

Parameters	**ANN model for Z-pinned beams**
Learning algorithm	Levenberg-Marquardt
Activation function (hidden layers)	Hyperbolic tangent
Activation function (output layers)	Linear
Mean squared error	0.10
Training data	26
Test data	13
Max number of iterations	2000
Learning rate	0.30

A linear regression analysis was performed in this study in order to verify the correlation between the data set used by ANN for training and validation. The fit is measured by the coefficient of determination (R^2), which has the values $0 \leq R^2 \leq 1$, nearer on one, the

coefficient demonstrates that the variables clarify the regression model (Montgomery *et al*. 2012). As shown in Figure 4.20 (c), the coefficient of determination was close to one, indicating that the data obtained by ANN are reliable and accurately represent the modal behavior of z-pinned beams.

The global training results are shown in Figure 4.20 (a) with the best training performance, measured by the MSE, obtained on the fifth iteration. This demonstrates that the ANN has a fast convergence, which helps to reduce training time.

In Figure 4.20 (b), a histogram of error values is presented. The error histogram depicts the difference between the goal value and the value obtained after training by the neural network. The better the neural network is trained, the more concentrated the histogram is towards zero error.

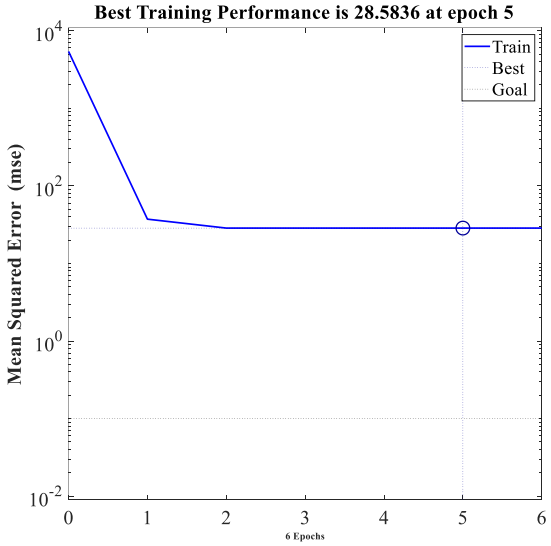

(a)

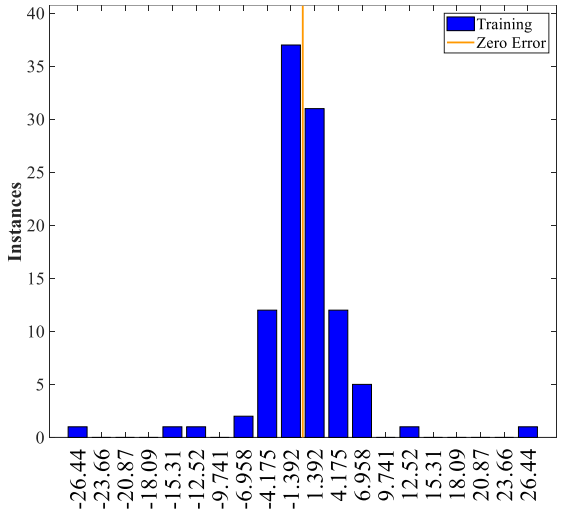

(b)

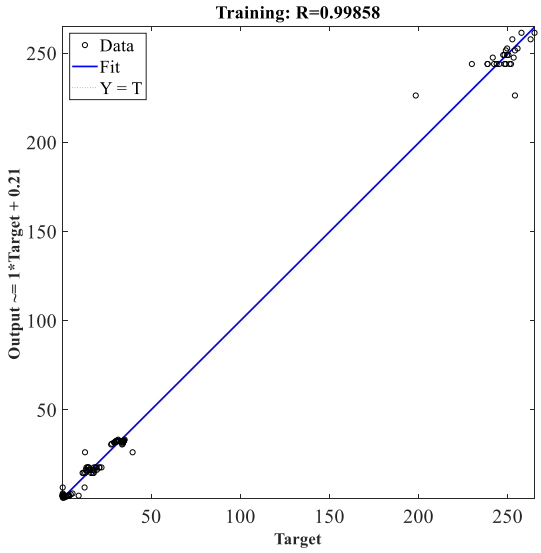

(c)

Figure 4.11 – Results of ANN global training considering: (a) the best training performance, (b) the histogram of error values, and (c) the linear regression analysis with coefficient of determination.

Finally, Figure 4.21 shows ANN results compared to test data in graphical form. Test data is the data that was not used in the training of the network. Because they are unknown, this test is a better way to assess whether the network is well trained or not. Analyzing the results, the network performance was good. It is noticed that the network response has the same pattern as the real response, especially in cases of damping, amplitude, and mass. However, for the extreme values of density and size, the network presented the largest errors.

Therefore, the results of the neural network were extremely satisfactory. Due to the difficulty of performing several tests, the network was able to reproduce the expected patterns of responses, despite the small amount of data. However, with a greater amount of data, the network performance would probably increase.

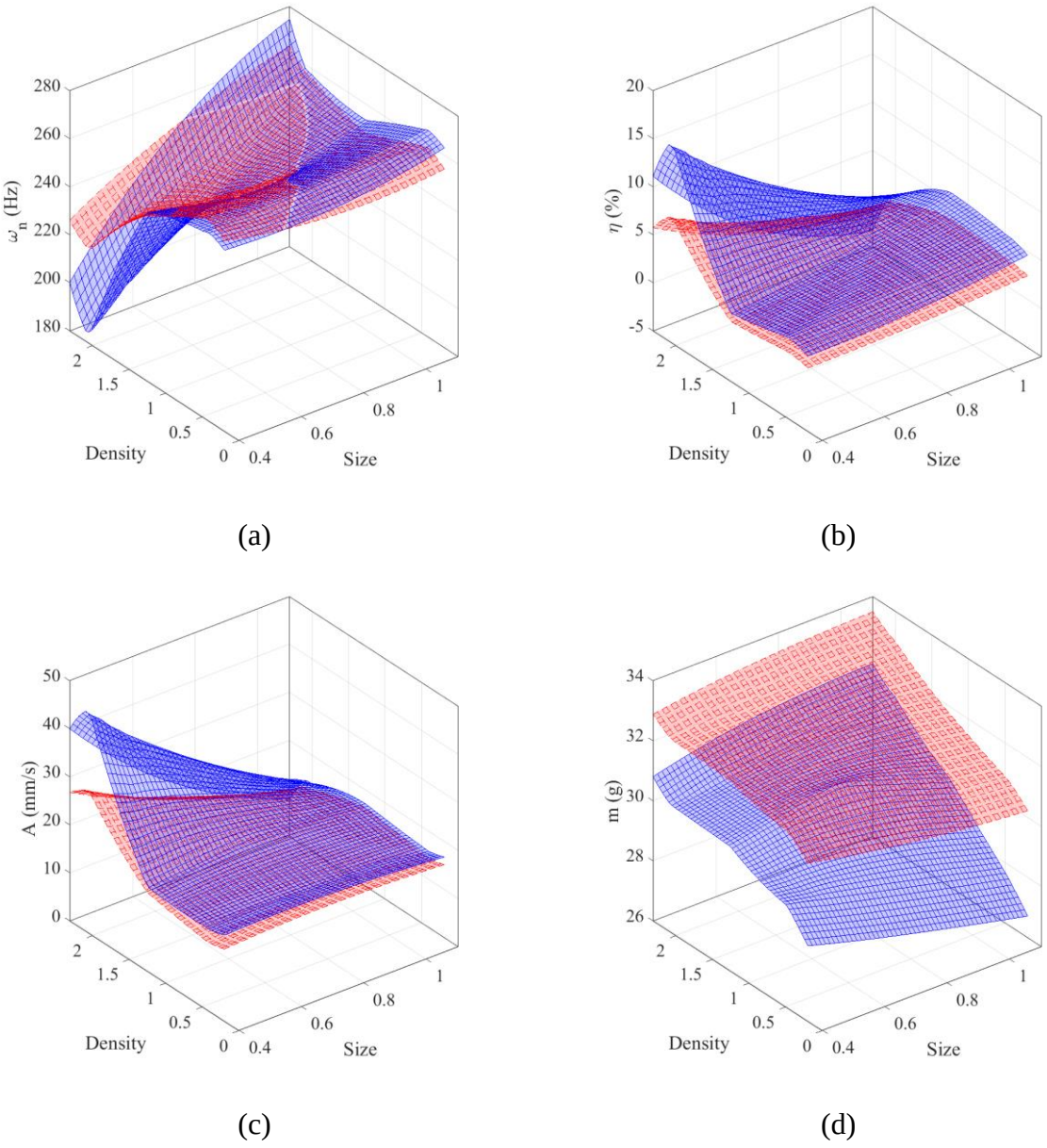

Figure 4.12 – ANN graphical results of (a) Natural Frequency (ωn), (b) damping (η), (c) Amplitude (A) and (d) mass (m). (Legend: — Real, — ANN predicted)

4.5 Conclusions of Chapter 4

An experimental characterization of the rectangular z-pins design variables influence on the modal response of reinforced composite laminates has been presented. For the free vibration tests, in general, the z-pinned composites had an improvement of the natural frequency from approx. 3% to 7%, and 4 specimens had reductions from 1% to 5% in comparison with not reinforced. However, for the amplitude of forced vibration of reinforced composites it was achieved high reductions, from approx. 60% to 70% compared to the unpinned specimen (reference).

In addition, the experimental data compared the statistical results pointed that the z-pins design variables had important role in increasing and decreasing the modal properties natural frequency and forced vibration amplitude of z-pinned composites compared to the reinforced. Furthermore, the ANN trained with part of the experimental dataset showed excellent predictive capacity with experimental tests carried out in this investigation for predicting modal response.

Further analysis and tests are necessary to a better understanding of the effects and behavior on the modal response of composites reinforced through the thickness with rectangular z-pins. More studies regarding free and forced vibration with this kind of method, the z-pins design factors, composite manufacture process used and chosen in this work may help to explain the resulting mechanisms responsible for the achieved results.

CHAPTER 5: GENERAL CONCLUSION

The experimental study of Dynamic Modal Analysis and Mode II Interlaminar Fracture Toughness of composite laminates reinforced through the thickness with rectangular z-pins and manufactured by VARTM is presented in this research. The effects of variables of influence such as the size of rectangular machined z-pins (from 0.40 mm to 1.10 mm) and density insertion (from 0.20% to 2.31%) on the free and forced vibration and in ENF tests were investigated and analyzed resulting in the following conclusions:

Modal response analysis for the reinforced composites manufactured with EVA mold:

- In this part of the research, it was possible to determine and characterize the modal responses of natural frequency, damping, or factor loss, and maximum amplitude of vibrations. The experimental and fabrication part of the composites was based on the information obtained by the DOE through a surface response method (SRM). With the tests carried out, it can be concluded that the insertion of z-pins promotes a change in the stiffness of the material and, consequently, generates changes in the modal responses. It was also found that the natural frequency and the damping factor are significantly dependent on both the size and the insertion density of the z-pins and that the maximum amplitude of vibration depends exclusively on the size of the z-pins, however there is a significant interaction between size and insertion density. Through the RSM meta-model, it was possible to optimize both mono and multi-objectives of the composites manufacturing process (ideal size and insertion density of the z-pins). The behavior and results obtained in this study of composites reinforced through thickness are in agreement with the results obtained by other, although not many, studies already carried out and indicate that there is the possibility of manual application of reinforcements in composite laminates.

Mode II fracture toughness analysis for the reinforced composites manufactured with PS drilled mold:

- The maximum (G_{IIc}) value achieved for the Non-precracked (NPC) step was for a small z-pin with a high pin density insertion, which was 2 times greater than the unpinned specimen, according to the experimental data. In addition, as compared to non-reinforced specimens, the thicker pins showed good responsiveness and high (G_{IIc}) values. The thinnest pin thus improved the crack by approximately two times, but it did not have the same effect in the Precracked (PC) step. The thicker z-pin

functioned as a beneficial influence in the PC stage, reducing delamination and achieving higher (G_{IIc}) values than the unpinned specimen. In addition, small z-pins with high areal density have a better behavior than unpinned, with a higher improvement in the (G_{IIc}) value. The results were confirmed by the response surface model and analysis of variance, which also showed that for the NPC case, increasing pin density always increases fracture toughness, and the contribution of pin size to increased fracture toughness is more pronounced in this case when the density is less than 1%. Increasing the pin's size has minimal effect in NPC after that. Apart from low pin density, increasing pin size reduces fracture resistance in the PC case. Furthermore, for the NPC situation, where model linearity is weaker than in the PC instance, the artificial neural network (ANN) trained with a portion of these experimental data demonstrated outstanding predictive capacity.

Modal Response analysis for the reinforced composites manufactured with PS drilled mold:

- In the free vibration testing, the z-pinned composites had a slightly increase in natural frequency, although four specimens had small reductions when compared to the non-reinforced counterparts. The reinforced composites showed larger decreases in amplitude for forced vibration compared to the unpinned specimen (reference), indicating a favorable influence of z-pins in this modal feature. Furthermore, when the experimental data was compared to the statistical results of analysis of variance (ANOVA), the z-pins design variables played a significant role in increasing and decreasing the modal properties natural frequency and forced vibration amplitude of z-pinned composites when compared to reinforced composites. Furthermore, using experimental testing carried out in this inquiry, the ANN trained with a portion of the experimental dataset demonstrated outstanding predictive capacity for forecasting modal response.

The project involved an original study and provided significant findings from analysis, offering new perspectives of an affordable z-pinning process with machined rectangular z-pins and VARTM infusion process. The acquired data allows to show the improvement in mode II fracture toughness and modal analysis and showed how the use of statistical (ANOVA) and computational tools (ANN) can work together with the experimental data achieved. Also important is to mention the use of DOE which improve the efficiency to

develop the testing selection and make the process manufacturing and tests faster and more affordable.

In this context, the z-pinning process, when is used in an optimized way, bring benefices regarding the assembling, manufacturing, and mechanical properties of through the thickness reinforced composites. When inserting few and calculated quantity of reinforcement (z-pins) there is a small gain in mass and a enhance in out of plane delamination properties such as the interlaminar fracture toughness in mode II.

Regarding the vibration properties, z-pin insertion in composites enhanced the natural frequency and reduced the vibration amplitude. Thus, for applications that a decrease in the amplitude vibration is needed and cannot have an increase in the composite mass system, an optimized z-pin insertion may generate a small gain in mass and increase the stiffness of the composite laminate.

Furthermore, more research may be required and beneficial to completely define and comprehend the impacts of in-house made rectangular z-pins on the interlaminar fracture toughness and vibration properties of 3D reinforced composites generated via VARTM. More research into the mechanical performance of Mode II and Modal Response in this type of approach, as well as the influence of pin size, density insertion, and composite laminate manufacturing process used and chosen in this work, may help to explain the resulting mechanisms responsible for the achieved results.

FUTURE WORKS

The main suggestions for future works are:

- Study the fractographic aspects of the fracture surfaces on mode II delamination;
- Make the composites manufacture process more robust;
- Improve and acquire more data to the ANN proposed in this work to predict the mechanical behavior in mode II fracture toughness and modal analysis;
- Fatigue analysis of the z-pinned composites with the same pin size and areal densities obtained from the DOE and used in this work;
- Study the Impact and Post-impact performance of composites reinforced through the thickness with machined rectangular z-pins using the same parameters of this doctoral thesis.

PUBLICATION

The papers below are resulting for this Doctoral Thesis activities.

Journal Paper Published:

BORTOLUZZI, D. B.; OLIVER, G. A.; ANCELOTTI JUNIOR, A. C.; GOMES, G. F. An experimental dynamic analysis of z-pinned unidirectional CFRP beams. ***Composites Structures***, v. 273, p. 114237, 2021.

Journal Papers Submitted in 2022:

BORTOLUZZI, D. B.; ANCELOTTI JUNIOR, A. C.; DINIZ, C. A.; RIBEIRO JUNIOR, F. R.; FRANCISCO, M. B.; GOMES, G. F. An experimental characterization on rectangular z-pinned parameters in the dynamic modal responses of reinforced composites. Submitted to ***Composites Structures.***

BORTOLUZZI, D. B.; DINIZ, C. A.; PEREIRA, J. L. J.; RIBEIRO JUNIOR, F. R.; GOMES, G. F.; ANCELOTTI JUNIOR, A. C. On the influence of rectangular z-pins parameters on mode II delamination resistance of through the thickness reinforced composites. Submitted to ***Composites Part B: Engineering.***

REFERENCES

ABDELLAH, M. Y.; MOHAMED, A. F.; HASAN, M. K. Characteristic analysis: Vibration behaviour of composite laminated structures compared to monotonic materials. **Int. J. Mech. Mechatron. Eng. IJMME-IJENS**, v. 19, p. 57-69, 2019.

ALLEGRI, G.; YASAEE, M.; PARTRIDGE, I. K.; & HALLETT, S. R. A novel model of delamination bridging via Z-pins in composite laminates. **International Journal of Solids and Structures**, v. 51, n. 19-20, p. 3314-3332, 2014.

ALMEIDA JR, J. H. S.; ANGRIZANI, C. C.; BOTELHO, E. C.; AMICO, S. C. Effect of fiber orientation on the shear behavior of glass fiber/epoxy composites. **Materials & Design**, v. 65, p. 789-795, 2015.

ASTM D7905/D7905M-19**. Standard Test Method for Determination of the Mode II Interlaminar Fracture Toughness of Unidirectional Fiber-Reinforced Polymer Matrix Composites.**

AVITABLE, P. Modal testing: a practitioner's guide. Hoboken, NJ: **John Wiley & Sons**, 2018.

BALCIOĞLU, H. E.; SEÇKIN, A. Ç. Comparison of machine learning methods and finite element analysis on the fracture behavior of polymer composites. **Archive of Applied Mechanics**, v. 9, n. 1, p. 223–239, 2020.

BARBOSA, L. C. M., BORTOLUZZI, D. B., & ANCELOTTI A. C. Analysis of fracture toughness in mode II and fractographic study of composites based on Elium® 150 thermoplastic matrix. **Composites Part B: Engineering**, v. 175, p. 107082, 2019a.

BARBOSA, L. C. M.; GOMES, G.; ANCELOTTI JR, A. C. Prediction of temperature-frequency-dependent mechanical properties of composites based on thermoplastic liquid resin reinforced with carbon fibers using artificial neural networks. **The International Journal of Advanced Manufacturing Technology**, v.105, n. 5, p. 2543-2556, 2019b.

BARRETT, David John. The mechanics of z-fiber reinforcement. **Composite structures**, v. 36, n. 1-2, p. 23-32, 1996.

BAYISSA, W. L.; HARITOS, N.7). Structural damage identification in plates using spectral strain energy analysis. **Journal of Sound and Vibration**, v. 307, n. 1-2, p. 226-249, 2007.

BHUDOLIA, S. K.; PERROTEY, P.; JOSHI, S. C. Enhanced vibration damping and dynamic mechanical characteristics of composites with novel pseudo-thermoset matrix system. **Composite Structures**, v. 179, p. 502-513, 2017.

BIANCHI, F.; ZHANG, X. A cohesive zone model for predicting delamination suppression in z-pinned laminates. **Composites Science and Technology**, v. 71, n. 16, p. 1898-1907, 2011.

BIANCHI, F. Numerical modelling of through-thickness reinforced structural joints. **PhD Thesis**, University of Cranfield, 2012.

BILISIK, K. Multiaxis 3D woven preform and properties of multiaxis 3D woven and 3D orthogonal woven carbon/epoxy composites. Journal of Reinforced Plastics and Composites, v. 29, n. 8, p. 1173-1186, 2010.

BORTOLUZZI, D. B.; GOMES, G. F.; HIRAYAMA, D.; & ANCELOTTI, A. C. Development of a 3D reinforcement by tufting in carbon fiber/epoxy composites. **The International Journal of Advanced Manufacturing Technology**, v. 100, n. 5-8, p. 1593-1605, 2019.

BORTOLUZZI, D. B.; OLIVER, G. A.; ANCELOTTI JUNIOR, A. C.; GOMES, G. F. An experimental dynamic analysis of Z-pinned unidirectional CFRP beams. **Composite Structures**, v. 273, p. 114237, 2021.

BRUNO, D., GRECO, F. Delamination in composite plates: influence of shear deformability on interfacial debonding. **Cement and Concrete Composites**, v. 23, n .1, p. 33-45, 2001a.

BRUNO, D., GRECO, F. Mixed mode delamination in plates: a refined approach. **International Journal of Solids and Structures**, v. 38, n .50-51, p. 9149-9177, 2001b.

BRUNO, D.; GRECO, F.; LONETTI, P. Dynamic mode I and mode II crack propagation in fiber reinforced composites. **Mechanics of Advanced Materials and Structures**, v. 16, n. 6, p. 442-455, 2009.

BUSCEMA, M. Back propagation neural networks. **Substance use & misuse**, v. 33, n. 2, p. 233-270, 1998.

CARTIE, D. D.; DELL'ANNO, G.; POULIN, E.; PARTRIDGE, I. K. 3D reinforcement of stiffener-to-skin T-joints by Z-pinning and tufting. **Engineering fracture mechanics**, v. 73, n. 16, p. 2532-2540, 2006a.

CARTIÉ, D. D.; TROULIS, M.; PARTRIDGE, I. K. Delamination of Z-pinned carbon fibre reinforced laminates. **Composites science and Technology**, v. 66, n. 6, p. 855-861, 2006b.

CHANDRASHEKHAR, M.; GANGULI, R. Nonlinear vibration analysis of composite laminated and sandwich plates with random material properties. **International Journal of Mechanical Sciences**, v. 52, n. 7, p. 874-891, 2010.

CHANG, P; MOURITZ, A. P.; COX, B. N. Flexural properties of z-pinned laminates. **Composites Part A: applied science and manufacturing**, v. 38, n. 2, p. 244-251, 2007.

CHENGHU, L. I.; YING, Y. A. N.; PING, W. A. N. G.; DESHENG, Q. I.; YONGHAI, W. E. N. Study on compressive properties of Z-pinned laminates in RTD and hygrothermal environment. **Chinese Journal of Aeronautics**, v. 25, n. 1, p. 64-70, 2012.

CHONG, E. K.; ZAK, S. H. An introduction to optimization. **John Wiley & Sons**, 2004

CUI, H.; LI, Y.; KOUSSIOS, S.; ZU, L.; BEUKERS, A. Bridging micromechanisms of Z-pin in mixed mode delamination. **Composite Structures**, v. 93, n. 11, p. 2685-2695, 2011.

CUI, H.; YASAEE, M.; MELRO, A. R. Dynamic inter-fibre failure of unidirectional composite laminates with through-thickness reinforcement. **Composites Science and Technology**, v. 176, p. 64-71, 2019a.

CUI, H.; MAHADIK, Y.; HALLETT, S. R.; PARTRIDGE, I. K.; ALLEGRI, G.; PONNUSAMI, S. A.; PETRINIC, N. Coupon scale Z-pinned IM7/8552 delamination tests under dynamic loading. **Composites Part A: Applied Science and Manufacturing**, v. 125, p. 105565, 2019b.

DANTULURI, V.; MAITI, S.; GEUBELLE, P. H.; PATEL, R.; KILIC, H. Cohesive modeling of delamination in Z-pin reinforced composite laminates. **Composites science and technology**, v. 67, n. 3-4, p. 616-631, 2007.

DAVIES, P.; BLACKMAN, B. R. K.; BRUNNER, A. J. Mode II delamination. **In: Moore, D. R., Williams, J. G., Pavan, A. Fracture mechanics testing methods for polymers, adhesives and composites**. Elsevier, 2001.

DE BORBÓN, F.; AMBROSINI, D.; CURADELLI, O. Damping response of composites beams with carbon nanotubes. **Composites Part B: Enngineering**, v. 60, p. 106-110, 2014.

DECONINCK, P.; CAPELLE, J.; BOUCHART, V.; CHEVRIER, P.; RAVAILLER, F. Delamination propagation analysis in tufted carbon fibre-reinforced plastic composites subjected to high-velocity impact. **Journal of Reinforced Plastics and Composites**, v. 33, n. 14, p. 1353-1363, 2014.

DI BENEDETTO, R. M., BOTELHO, E. C., JANOTTI, A., JUNIOR, A. A., & GOMES, G. F. (2021). Development of an artificial neural network for predicting energy absorption capability of thermoplastic commingled composites. Composite Structures, 257, 113131.

DINIZ, C. A.; DA CUNHA, S. S.; GOMES, G. F.; ANCELOTTI, A. C. Optimization of the layers of composite materials from neural networks with Tsai–Wu failure criterion. **Journal of Failure Analysis and Prevention**, v. 19, n. 3, p. 709-715, 2019.

EWINS, D. J. Modal testing: Theory and practice. Baldock, **England: Research Studies Press**, 2000.

EWINS, D. J. Modal testing: theory, practice and application. **John Wiley & Sons**, 2009

FAN, W.; DONG, J.; WEI, B.; ZHI, C.; YU, L.; XUE, L.; LI, L. Fast and accurate bending modulus prediction of 3D woven composites via experimental modal analysis. **Polymer Testing**, v. 78, p. 105938, 2019.

FEI, S.; WANG, W.; WANG, H.; YANG, D.; DING, H.; WANG, H.; KE, Y. Effect of Ø 0.11 mm Z-pinning on the properties of composite laminates via an ultrasound guided insertion process. **Composites Science and Technology**, p. 108906, 2021.

FERT, M. M. An investigation of the mechanical performance of Z-pin reinforced composites. **PhD Thesis**, Imperial College London, 2016.

FOUAD, H.; MOURAD, A. H. I.; ALSHAMMARI, B. A.; HASSAN, M. K.; ABDALLAH, M. Y.; HASHEM, M. Fracture toughness, vibration modal analysis and viscoelastic behavior of Kevlar, glass, and carbon fiber/epoxy composites for dental-post applications. **Journal of the mechanical behavior of biomedical materials**, v. 101, p. 103456, 2020.

FU, Z. F.; HE, J. Modal analysis**. Elsevier**, 2001

FRANCESCONI, L.; AYMERICH, F. Effect of Z-pinning on the impact resistance of composite laminates with different layups. **Composites Part A: Applied Science and Manufacturing**, v. 114, p. 136-148, 2018.

FUNARI, M. F.; GRECO, F.; LONETTI, P. A cohesive finite element model-based ALE formulation for z-pins reinforced multilayered composite beams. **Procedia Structural Integrity**, v.2, p. 452-459, 2016.

GNABA, I.; WANG, P.; LEGRAND, X.; SOULAT, D. Evaluation of the mechanical behaviour of tufted preforms. **In IOP Conference Series: Materials Science and Engineering**, v. 406, n. 1, p. 12019, 2018.

GOMES, G. F.; DE ALMEIDA, F. A.; DA CUNHA, S. S.; ANCELOTTI, A. C. (2018a). An estimate of the location of multiple delaminations on aeronautical CFRP plates using modal data inverse problem. **The International Journal of Advanced Manufacturing Technology**, v. 99, n.5, p. 1155-1174, 2018a.

GOMES, G. F.; MENDÉZ, Y. A. D.; ALEXANDRINO, P. S. L.; DA CUNHA, S. S.; ANCELOTTI, A. C. (2018b). The use of intelligent computational tools for damage detection and identification with an emphasis on composites – A review. **Composite Structures**, v. 196, p. 44-54, 2018b.

GRECO, F.; LONETTI, P.; ZINNO, R. An analytical delamination model for laminated plates including bridging effects. **International journal of solids and structures**, v. 39, n .9, p. 2435-2463, 2002.

GRIGORIOU, K.; LADANI, R. B.; MOURITZ, A. P. Electrical properties of multifunctional Z-pinned sandwich composites. **Composites Science and Technology**, v. 170, p. 60-69, 2019.

HAYKIN S. Neural networks. A comprehensive Foundation. **Prentice Hall**, New Jersey, 1994.

HAYKIN, S. S. Neural networks and learning machines. **Haykim**, 2009

HUANG, H. S.; WAAS, A. M. Compressive response of Z-pinned woven glass fiber textile composite laminates: Experiments. Composites Science and Technology, v. 69, n. 14, p. 2331-2337, 2009.

HUANG, H. S.; WAAS, A. M. Quasi-static mode II fracture tests and simulations of Z-pinned woven composites. **Engineering Fracture Mechanics**, v. 126, p. 155-165, 2014.

HENAO, A.; GUZMÁN DE VILLORIA, R.; CUARTERO, J.; CARRERA, M.; PICÓN, J.; MIRAVETE, A. (2015). Enhanced impact energy absorption characteristics of sandwich composites through tufting. **Mechanics of Advanced Materials and Structures**, v. 22, n. 12, p. 1016-1023, 2015.

HOFFMANN, J.; SCHARR, G. Mechanical properties of composite laminates reinforced with rectangular z-pins in monotonic and cyclic tension. **Composites Part A: Applied Science and Manufacturing**, v. 109, p. 163-170, 2018a.

HOFFMANN, J.; SCHARR, G. Pull-out performance of rectangular z-pins in hot-cured carbon fiber reinforced laminates. **Composite Structures**, v. 186, p. 62-67, 2018b.

HOFFMANN, J.; BRAST, A.; SCHARR, G. Z-pin insertion process for through-thickness reinforced thermoplastic composites. **Journal of Composite Materials**, v. 53, n. 2, p. 173-181, 2019.

IBRAHIM, Y.; MELENKA, G. W.; KEMPERS, R. Flexural properties of three-dimensional printed continuous wire polymer composites. **Materials Science and Technology**, v. 35, n. 12, p. 1471-1482, 2019.

INMAN, D. J. Engineering vibration. **Boston Pearson,** 2014.

KANNINEN, M. F.; POPELAR, C. L. Advanced fracture mechanics, **Oxford University Press**, New York, 1985.

KHATIR, S.; TIACHACHT, S.; LE THANH, C.; GHANDOURAH, E.; MIRJALILI, S.; WAHAB, M. A. An improved Artificial Neural Network using Arithmetic Optimization

Algorithm for damage assessment in FGM composite plates. **Composite Structures**, v. 273, p. 114287, 2021.

KOH, T. M.; ISA, M. D.; FEIH, S.; MOURITZ, A. P. Experimental assessment of the damage tolerance of z-pinned T-stiffened composite panels. **Composites Part B: Engineering**, v. 44, n. 1, p. 620-627, 2013.

KNAUPP, M.; BAUDACH, F.; FRANCK, J.; SCHARR, G. Impact and post-impact properties of CFRP laminates reinforced with rectangular z-pins. **Composites science and technology**, v. 87, p. 218-223, 2013.

KNAUPP, M., BAUDACH, F., FRANCK, J., & SCHARR, G. Mode I and pull-out tests of composite laminates reinforced with rectangular z-pins. Journal of Composite Materials, v. 48, n. 23, p. 2925-2932, 2014a.

KNAUPP, M.; SCHARR, G. Manufacturing process and performance of dry carbon fabrics reinforced with rectangular and circular z-pins. **Journal of Composite Materials**, v. 48, n. 17, p. 2163-2172, 2014b.

KNOPP, A.; SCHARR, G. Tensile Properties of Z-Pin Reinforced Laminates with Circumferentially Notched Z-Pins. **Journal of Composites Science**, v. 4, n. 2, p.78, 2020.

KNOPP, A.; FUNCK, E.; HOLTZ, A.; SCHARR, G. Delamination and compression-after-impact properties of z-pinned composite laminates reinforced with circumferentially notched z-pins. **Composite Structures**, p. 115188, 2022.

KOSTOPOULOS, V.; SARANTINOS, N.; TSANTZALIS, S. Review of Through-the-Thickness Reinforced z-Pinned Composites. Journal of Composites Science, v. 4, n. 1, p. 31, 2020.

KOVÀCS, Z. L. Redes neurais artificiais. **Editora Livraria da Fisica**, 2002.

KUMAR, N. J.; BABU, P. R. Analysis of mode I and mode II crack growth arrest mechanism with Z-fibre pins in composite laminated joint. **Applied Composite Materials**, v. 25, n. 2, p. 365-379, 2018.

LADANI, R. B.; RAVINDRAN, A. R.; WU, S.; PINGKARAWAT, K.; KINLOCH, A. J.; MOURITZ, A. P.; WANG, C. H. Multi-scale toughening of fibre composites using carbon nanofibres and z-pins. **Composites Science and Technology**, v. 131, p. 98-109, 2016.

LEPŠÍK, P.; KULHAVÝ, P. Design Optimization of Composite Parts Using Doe Method. **In: 58th ICMD 2017**, p. 200-205, 2017

LI, M.; CHEN, P. A new FE model for predicting the bridging micromechanisms of a Z-pin. **Composite Structures**, v. 223, p. 110957, 2019.

LI, M.; CHEN, P. FE parametric study on the longitudinal tensile strength and damage mechanism of Z-pinned laminates. **Polymer Composites**, v. 41, n. 2, p. 585-599, 2020.

LIAN, B.; SUN, T.; SONG, Y. Parameter sensitivity analysis of a 5-DoF parallel manipulator. **Robotics and Computer-Integrated Manufacturing**, v. 46, p. 1-14, 2017.

LIAO, B.; ZHANG, Z.; SUN, L.; ZHOU, J.; WANG, P.; LIN, Y.; & FANG, D. Experimental investigation on the double-position impact responses and damage mechanism for Z-pinned composite laminates. **Composite Structures**, v. 259, p. 113463, 2021.

LIU, J.; ZHANG, T.; JIANG, W.; LIU, J. Mechanical response of a novel composite Y-frame core sandwich panel under shear loading. **Composite Structures**, v. 224, p. 111064, 2019.

LOH, T. W.; LADANI, R. B.; RAVINDRAN, A.; DAS, R.; KANDARE, E.; MOURITZ, A. P. Z-Pinned composites with combined delamination toughness and delamination Self-Repair properties. **Composites Part A: Applied Science and Manufacturing**, v. 149, p. 106566, 2021.

MARTINS, A. T. Analysis of damage mechanisms in composite structures reinforced by tufting. **PhD Thesis**, Technology University of Compiègne, (2018)

MAURYA, M.; SADARANG, J.; PANIGRAHI, I.; DASH, D. Detection of delamination in carbon fibre reinforced composite using vibration analysis and artificial neural network. **Materials Today: Proceedings**, v. 49, p. 517-522, 2022;

MISHRA, I.; SAHU, S. K. Modal analysis of woven fiber composite plates with different boundary conditions. **International Journal of Structural Stability and Dynamics**, v. 15, n. 1, p. 1540001, 2015.

MILLS, A. R.; JONES, J. Investigation, manufacture, and testing of damage-resistant airframe structures using low-cost carbon fibre composite materials and manufacturing technology. **Proceedings of the Institution of Mechanical Engineers, Part G: Journal of Aerospace Engineering**, v. 224, n. 4, p. 489-497, 2010.

M'MEMBE, B.; GANNON, S.; YASAEE, M.; HALLETT, S. R.; PARTRIDGE, I. K. Mode II delamination resistance of composites reinforced with inclined Z-pins. **Materials & Design**, v. 94, p. 565-572, 2016.

M'MEMBE, B.; YASAEE, M.; HALLETT, S. R.; PARTRIDGE, I. K. (2019). Effective use of metallic Z-pins for composites' through-thickness reinforcement. **Composites Science and Technology**, v. 175, p. 77-84, 2019.

MOHAMED, G.; ALLEGRI, G.; YASAEE, M.; HALLETT, S. R. Cohesive element formulation for z-pin delamination bridging in fibre reinforced laminates. **International Journal of Solids and Structures**, v. 132, p. 232-244, 2018.

MONTGOMERY, D.C.; RUNGER, G.C. Applied Statistics and Probability for Engineers. 3rd Edition, **John Wiley & Son**, Inc., Hoboken, 2003.

MONTGOMERY, D. C.; RUNGER, G. C. Applied statistics and probability for engineers. **John Wiley & Sons,** 2010.

MONTGOMERY, D. C.; PECK, E. A.; VINING, G. G. Introduction to linear regression analysis, v. 821. **John Wiley & Sons**, 2012.

MONTGOMERY, D. C. Design and Analysis of experiments. **John Wiley & Sons**, 2017.

MOURITZ, A. P. Review of z-pinned composite laminates. **Composites Part A: applied science and manufacturing**, v. 38, n. 12, p. 2383-2397, 2007.

MOURITZ, A. P.; CHANG, P. Tension fatigue of fibre-dominated and matrix-dominated laminates reinforced with z-pins. **International Journal of Fatigue**, v. 32, n. 4, p. 650-658, 2010.

MOURITZ, A. P.; CHANG, P.; ISA, M. D. Z-pin composites: Aerospace structural design considerations. **Journal of Aerospace Engineering,** v. 24, n. 4, p. 425-432, 2011.

MOURITZ, A. P. Delamination properties of z-pinned composites in hot–wet environment. **Composites Part A: Applied Science and Manufacturing**, v. 52, p. 134-142, 2013.

MOURITZ, A. P.; KOH, T. M. Re-evaluation of mode I bridging traction modelling for z-pinned laminates based on experimental analysis. **Composites Part B: Engineering**, v. 56, p. 797-807, 2014.

MOURITZ, A. P. Review of z-pinned laminates and sandwich composites**. Composites Part A: Applied Science and Manufacturing**, v. 139, p. 106128, 2020.

OSMIANI, C.; MOHAMED, G.; TREIBER, J. W. G.; ALLEGRI, G.; PARTRIDGE, I. K. Exploring the influence of micro-structure on the mechanical properties and crack bridging mechanisms of fibrous tufts. **Composites Part A: Applied Science and Manufacturing**, v. 91, p. 409-419, 2016.

PARDINI, L. C. Preformas para compósitos estruturais. Polímeros, v. 10, p. 100-109, 2000.

PARIKH, H. H.; GOHIL, P. P. Experimental determination of tribo behavior of fiber-reinforced composites and its prediction with artificial neural networks. **In: Durability and Life Prediction in Biocomposites, Fibre-Reinforced Composites and Hybrid Composites**, p. 301-320, Woodhead Publishing, 2019.

PARTRIDGE, I. K.; CARTIÉ, D. D. Delamination resistant laminates by Z-Fiber® pinning: Part I manufacture and fracture performance. **Composites Part A: applied science and manufacturing**, v. 36, n. 1, p. 55-64, 2005.

PARTRIDGE, I. K.; YASAEE, M.; ALLEGRI, G.; LANDER, J. K. Damage-tolerant composite structures by Z-pinning. **In Toughening mechanisms in composite materials**, p. 161-189. **Woodhead Publishing**, 2015.

PARTRIDGE, I. K.; HALLETT, S. R. Use of microfasteners to produce damage tolerant composite structures. **Philosophical Transactions of the Royal Society A: Mathematical, Physical and Engineering Sciences**, v. 374, n. 2071, p. 20150277, 2016.

PEI, X.; LI, J.; CHEN, K.; DING, G. Vibration modal analysis of three-dimensional and four directional braided composites. **Composites Part B: Engineering**, v. 69, p. 212-221, 2015.

PEGORIN, F.; PINGKARAWAT, K.; DAYNES, S.; MOURITZ, A. P. Influence of z-pin length on the delamination fracture toughness and fatigue resistance of pinned composites. **Composites Part B: Engineering**, v. 78, p. 298-307, 2015.

PINGKARAWAT, K.; MOURITZ, A. P. Improving the mode I delamination fatigue resistance of composites using z-pins. **Composites Science and Technology**, v. 92, p. 70-76, 2014.

POURJABARI, A.; HAJILAK, Z. E.; MOHAMMADI, A.; HABIBI, M.; SAFARPOUR, H. Effect of porosity on free and forced vibration characteristics of the GPL reinforcement composite nanostructures. **Computers & Mathematics with Applications**, v. 77, n. 10, p. 2608-2626, 2019.

RAFIEE, M.; NITZSCHE, Fred; LABROSSE, M. R. Fabrication and experimental evaluation of vibration and damping in multiscale graphene/fiberglass/epoxy composites. **Journal of Composite Materials**, v. 53, n. 15, p. 2105-2118, 2019a.

RAFIEE, M.; NITZSCHE, F.; LABROSSE, M. R. Processing, manufacturing, and characterization of vibration damping in epoxy composites modified with graphene nanoplatelets. **Polymer Composites**, v. 40, n. 10, p. 3914-3922, 2019b.

RAHIMI, S.; MOHAMMADI, F.; YAVARI, Z. Removal of RR198 dye by TiO2/Fe3O4/persulfate nanoparticles under UV-LED irradiation and comparision of OFAT

and CCD experimental design in RSM modelling. **Indian Journal of Chemical Technology (IJCT)**, v. 27, n. 4, p. 283-293, 2020.

RAVINDRAN, A. R.; LADANI, R. B.; WANG, C. H.; MOURITZ, A. P. Synergistic mode II delamination toughening of composites using multi-scale carbon-based reinforcements. **Composites Part A: Applied Science and Manufacturing**, v. 117, p. 103-115, 2019a.

RAVINDRAN, A. R.; LADANI, R. B.; WANG, C. H.; & MOURITZ, A. P. Hierarchical mode I and mode II interlaminar toughening of Z-pinned composites using 1D and 2D carbon nanofillers. **Composites Part A: Applied Science and Manufacturing**, v. 124, p. 105470, 2019b.

RAVINDRAN, A. R.; LADANI, R. B.; WANG, C. H.; MOURITZ, A. P. Synergistic delamination toughening of composites using multi-scale carbon reinforcements. **Composites Part B: Engineering**, v. 161, p. 18-28, 2019c.

RAO, S.S.; GRIFFIN, P. Mechanical vibrations. **Harlow: Pearson**, 2018

RIBEIRO JUNIOR, F. R.; DE ALMEIDA, F. A.; GOMES, G. F. Fault classification in three-phase motors based on vibration signal analysis and artificial neural networks. **Neural Computing and Applications**, v. 32, n. 18, p. 15171-15189, 2020.

RIBEIRO JUNIOR, R. F.; METHODOLY, I. A. D. S. A.; CAMPOS, M. M.; TEIXEIRA, C. E.; DA SILVA, L. E. B.; GOMES, G. F. Fault detection and diagnosis in electric motors using 1d convolutional neural networks with multi-channel vibration signals. **Measurement**, p. 110759, 2022.

SHARIFPOUR, F.; MONTESANO, J.; TALREJA, R. Assessing the effects of ply constraints on local stress states in cross-ply laminates containing manufacturing induced defects. **Composites Part B: Engineering**, v. 199, p. 108227, 2020.

SINHA, L.; MISHRA, S. S.; NAYAK, A. N.; SAHU, S. K. Free vibration characteristics of laminated composite stiffened plates: **Experimental and numerical investigation.** Composite Structures, v. 233, p. 111557, 2020.

SOUZA ELOY, F.; GOMES, G. F.; ANCELOTTI JR, A. C.; DA CUNHA JR, S. S.; BOMBARD, A. J. F.; JUNQUEIRA, D. M. Experimental dynamic analysis of composite sandwich beams with magneto rheological honeycomb core. **Engineering Structures**, v. 176, p. 231-242, 2018.

SVOZIL, D.; KVASNICKA, V.; POSPICHAL, J. Introduction to multi-layer feed-forward neural networks. **Chemometrics and intelligent laboratory systems**, v. 39, n. 1, p. 43-62, 1997.

VAIDYA, U. K.; DUNCAN, B.; KOPACZ, J. Affordable processing and characterization of multi-functional z-pin reinforced VARTM composites. **Society of Manufacturing Engineers**, 2000.

VAZQUEZ, J. T.; CASTANIÉ, B.; BARRAU, J. J.; SWIERGIEL, N. Multi-level analysis of low-cost Z-pinned composite joints: Part 1: Single Z-pin behaviour. **Composites Part A: Applied Science and Manufacturing**, v. 42, n. 12, p. 2070-2081, 2011

WEI, X.; LI, D.; XIONG, J. Fabrication and mechanical behaviors of an all-composite sandwich structure with a hexagon honeycomb core based on the tailor-folding approach. **Composites Science and Technology**, v. 184, p. 107878, 2019.

WERDINE, D.; OLIVER, G. A.; DE ALMEIDA, F. A.; DE LOURDES NORONHA, M.; GOMES, G. F. Analysis of the properties of the self-compacting concrete mixed with tire rubber waste based on design of experiments. **In Structures**, v. 33, p. 3461-3474, 2021.

WISNOM, M. R. The role of delamination in failure of fibre-reinforced composites. **Phil. Trans. R. Soc. A**, vol. 370, p. 1850–1870, 2012.

YAN, W.; LIU, H. Y.; MAI, Y. W. Mode II delamination toughness of z-pinned laminates. **Composites Science and Technology**, v. 64, n. 13-14, p. 1937-1945, 2004.

YAN, S.; ZOU, X.; ILKHANI, M.; JONES, A. An efficient multiscale surrogate modelling framework for composite materials considering progressive damage based on artificial neural networks. **Composites Part B: Engineering**, v. 194, p. 108014, 2020.

YASAEE, M.; LANDER, J. K.; ALLEGRI, G.; HALLETT, S. R. Experimental characterization of mixed mode traction–displacement relationships for a single carbon composite Z-pin. **Composites Science and Technology**, v. 94, p. 123-131, 2014.

YASAEE, M.; MOHAMED, G.; HALLETT, S. R. Interaction of Z-pins with multiple mode II delaminations in composite laminates. **Experimental Mechanics**, v. 56, n.8, p. 1363-1372, 2016.

YASAEE, M.; MOHAMED, G.; PELLEGRINO, A.; PETRINIC, N.; HALLETT, S. R. Strain rate dependence of mode II delamination resistance in through thickness reinforced laminated composites. **International Journal of Impact Engineering**, v. 107, p. 1-11, 2017.

YEGNANARAYANA, B. Artificial Neural Networks. **Prentice-Hall of India Private Limited**, New Delhi, 2005.

ZENZEN, R.; KHATIR, S.; BELAIDI, I.; LE THANH, C.; WAHAB, M. A. A modified transmissibility indicator and Artificial Neural Network for damage identification and quantification in laminated composite structures. **Composite Structures**, v. 248, p. 112497, 2020.

ZHANG, Z.; FRIEDRICH, K. Artificial neural networks applied to polymer composites: a review. **Composites Science and technology**, v. 63, n. 14, 2029-2044, 2003.

ZHANG, X; HOUNSLOW, L; GRASSI, M. Improvement of low-velocity impact and compression-after-impact performance by z-fibre pinning. **Composites science and technology**, v. 66, n. 15, p. 2785-2794, 2006.

ZHANG, B.; ALLEGRI, G.; YASAEE, M.; HALLETT, S. R.; PARTRIDGE, I. K. On the delamination self-sensing function of Z-pinned composite laminates. **Composites Science and Technology**, v. 128, p. 138-146, 2016.

ZHANG, X.; LI, Y.; CHU, Q.; XIAO, J. Experimental study on the performance of twisted fiber reinforced composite z-pin. **In Proceedings of the 21th International Conference on Composite Materials**, Xi'an, China, p. 20-25, 2017.

ZHENG, X.; LI, Z; YANG, F. Experimental investigation on the fracture toughness of Z-pins reinforced composite laminates. **Acta Materiae Compositae Sinica**, v. 27, n. 4, p. 180-188, 2010.

APPENDIX A – RESIDUALS DATA

In this way, it is possible to analyze the standardized residual of the linear regression model for each of the answers and check if there is a normal distribution associated with the error term. In Figure A1 to Figure A3, it is possible to verify graphically that the characteristics of frequency, loss factor and amplitude, respectively, present residues normally distributed. These results can also be inferred through the Anderson-Darling normality test. It is important to note that the value residual is the difference between the observed and fitted values (Montgomery &Runger, 2003).

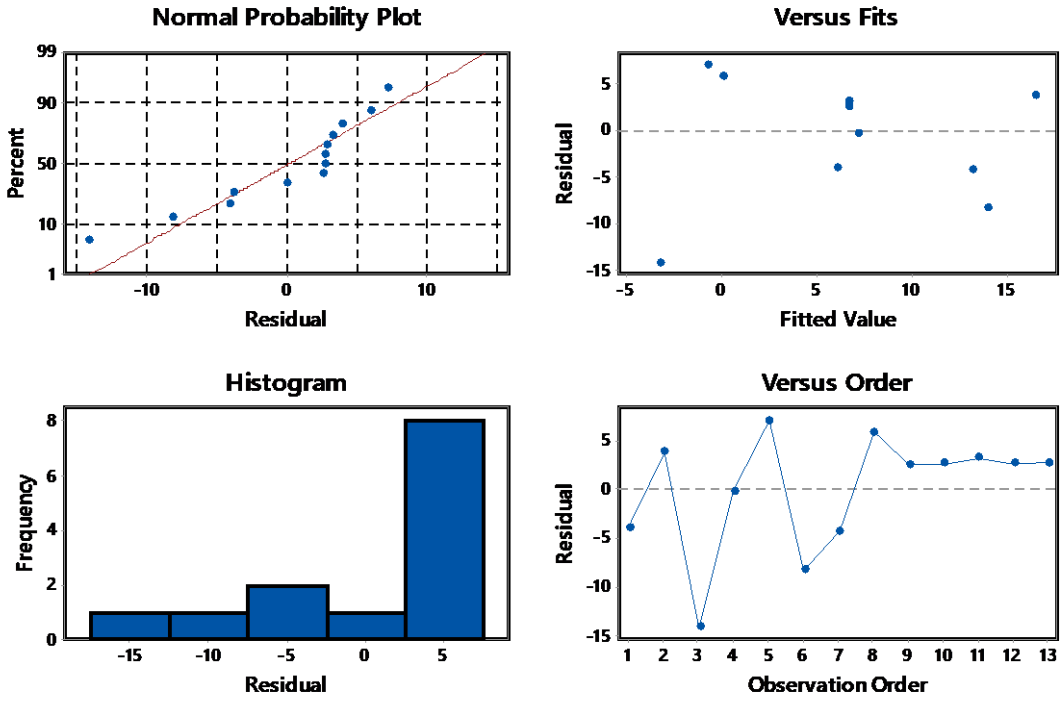

Figure A1 – Residual plots for natural frequency shift Δωn.

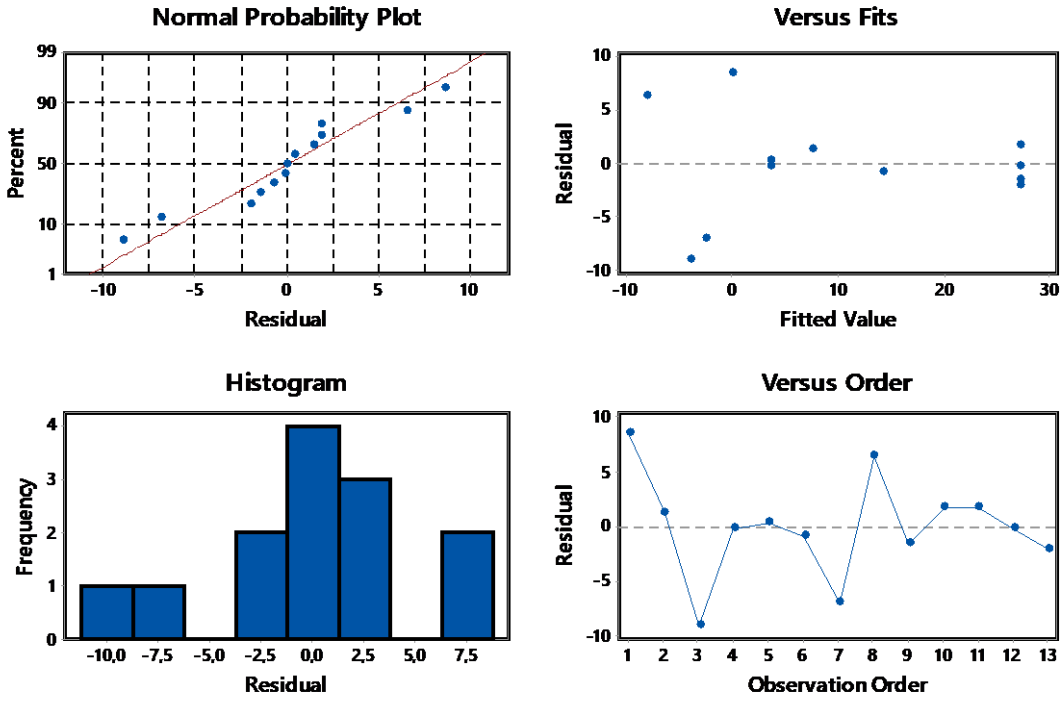

Figure A2 – Residual plots for loss factor shift Δη.

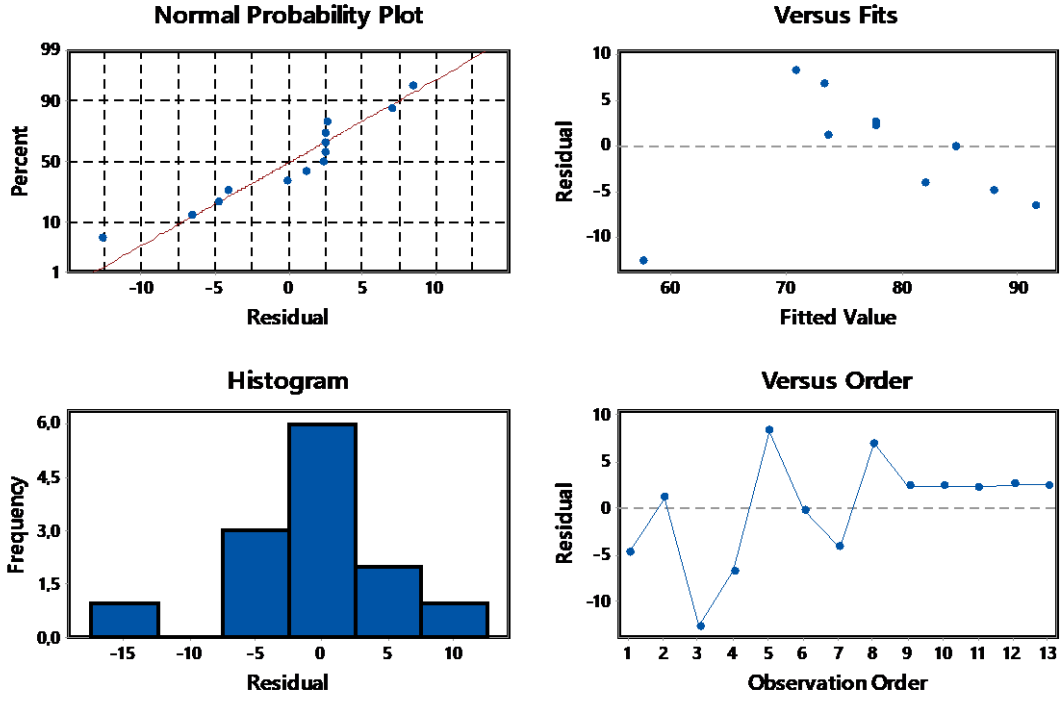

Figure A3 – Residual plots for forced vibration maximum amplitude shift ΔA.

APPENDIX B – Z-PINS MISALIGNMENT

During the VARTM process, when the vacuum is applied before the resin infusion, the compression of the dry plies and the excess of the inserted z-pins led to a misalignment of the z-pins. The Figure B1 represents the preform inside the vacuum bag and shows the inclined z-pins.

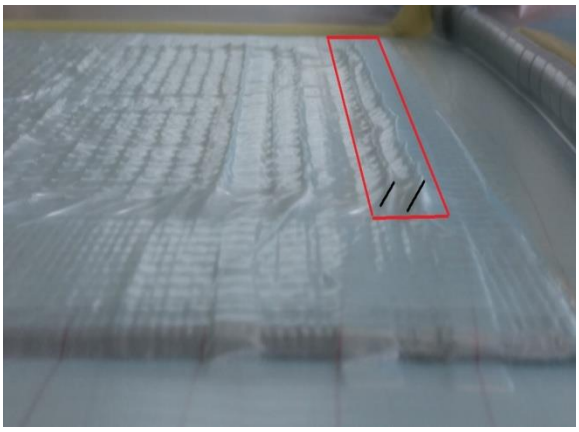

Figure B1 – Z-pins misalignment (red rectangle) in the perform prior to the resin infusion.

Different from Yasaee *et al*. (2014) that inspected the z-pins misalignment using a X-ray computer tomography (CT), in this work, to quantify and calculate the misalignment angle of the z-pins, stereo microscope images were taken from every specimen specification tested in this work (13 specimens reinforced through the thickness). In Figure B2 and Figure B3 it is possible to verify some examples of the inclined z-pins for different specimens.

Figure B2 – Z-pins misalignment in the specimen #6.

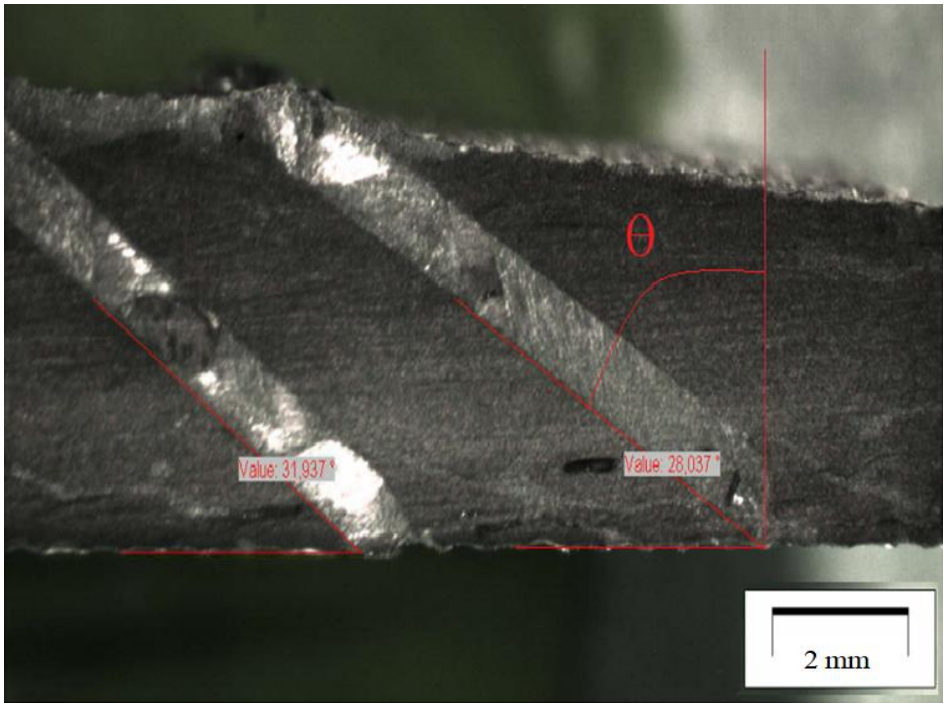

Figure B3 – Z-pins misalignment in the specimen #3.

The distribution of inclined angles follows a standard distribution bell curve with a mean value of 60,67º ± 3,91 and it is presented in the Figure B4.

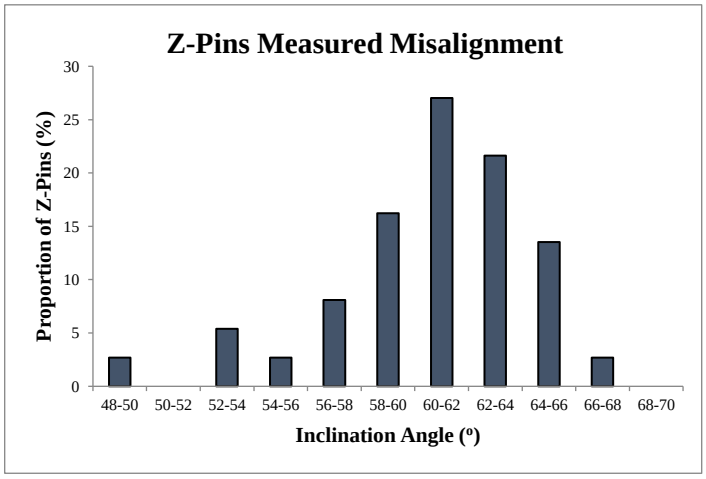

Figure B4 – Population of z-pins inclination angle (Θ) after the manufacturing process.